

APPLICATION OF THE THEORY OF ATOMS IN MOLECULES

By

Clement D.H. Lau, B.Sc.

A Thesis

Submitted to the School of Graduate Studies

in Partial Fulfilment of the Requirements

for the Degree

Doctor of Philosophy

McMaster University

APPLICATION OF THE THEORY OF ATOMS IN MOLECULES

DOCTOR OF PHILOSOPHY (1989)

(Chemistry)

McMASTER UNIVERSITY

Hamilton, Ontario

TITLE: Application of the Theory of Atoms in Molecules

AUTHOR: Clement D. H. Lau, B.Sc. (McMaster)

SUPERVISOR: Dr. R. F. W. Bader

NUMBER OF PAGES: xi,189

ABSTRACT

This thesis applies the theory of atoms in molecules to a series of hydrocarbon molecules. The atoms of theory are those that satisfy the quantum boundary condition. It is shown that regions of real space that obey this quantum boundary condition exist and the quantum mechanics which governs the total system also governs the atomic subsystems. These atoms of theory can be identified as the atoms of chemistry. An important result of this is that the total value of a property is a sum of the atomic contributions. Standard group energies can be defined. Using these facts, the additivity scheme for the homologous series of hydrocarbons, $\text{CH}_3(\text{CH}_2)_m\text{CH}_3$, starting at $m=0$ is recovered. The standard group energies are used in the prediction of strain energies. Finally it is shown that the Laplacian of the charge distribution is able to recover both the geometry model of Lewis and VSEPR theory as well as chemical reactivity.

Chapter I gives an overview of the basic theory itself while Chapter II examines the charge density for evidence of the atoms of theory. In Chapter III and IV a series of hydrocarbon molecules are investigated using the theory of atoms in molecules. Chapter V uses the Laplacian of the charge density to recover the Lewis and VESPR models and to provide a deeper understanding of the bridgehead bond of propellane molecules.

ACKNOWLEDGEMENTS

I wish to thank my supervisor, Richard Bader for his guidance and counsel over all the years. It certainly was a most memorable experience. I also wish to thank Tung Ngyen-Dang for sharing his insights and Friedrich Biegler-Konig for showing me the "right attitude" towards computational chemistry. Finally, I wish to thank Tom Slee for many philosophical discussions.

This thesis is dedicated to Kathy and my family who had the stamina to
endure this with me.

TABLE OF CONTENTS

	<u>PAGE</u>
Abstract	iii
Acknowledgements	iv
Table of Contents	vi
List of Figures	ix
List of Tables	xi
Chapter I. Review of the Theory of Atoms in Molecules	1
1. Introduction	1
2. The Quantum Mechanics of an Open system	4
A. The need for a quantum description of an open system	4
B. The action principle in quantum mechanics and Schwinger's principle of stationary action	5
C. Atomic Properties Defined	13
D. Energy of an Atom in a Molecule	14
CHAPTER II. Topological properties of the electronic charge distribution	19
1. Introduction	19
2. Topological Properties of the Charge Density	19
A. The Charge Density	19
B. The Dominant Form in the Charge Density	21
C. Critical Points	22
D. Critical points of Molecular Charge Distributions	27

TABLE OF CONTENTS(cont'd)

	<u>PAGE</u>
E. Gradient Vector Field of the Charge Density	29
F. Phase Portraits of the Gradient Vector Field	31
G. Elements of Molecular Structure	32
H. Chemical Bonds and Molecular Graphs	36
J. Rings and Cages	39
3. A Theory of Molecular Structure	41
CHAPTER III. Study of Hydrocarbons: Atoms, Bonds, Structure and	
Structural Stability	66
1. Introduction	66
2. Application of Theory	67
A. Atoms, Bonds and Structure	67
B. [1.1.1]Propellane as an Example	69
C. Bond Order	72
D. Bond Path Angle	74
E. Bond Ellipticity	76
F. Ellipticity and Ring Bond Rupture	78
CHAPTER IV. Study of Hydrocarbons: Group Properties	96
1. Introduction	96
2. Application of Theory	96
A. Atomic Properties	96
B. Atomic Populations	98
C. Electronegativity and Atomic Population	100
D. Geometric Strain and Electronegativity	102
E. Atomic Energies	106

TABLE OF CONTENTS(cont'd)

	<u>PAGE</u>
F. Group Additivity and the Acyclics	107
G. Strain Energy	114
H. Cyclic Molecules	115
J. The Bicyclic Molecules	119
K. Propellanes	127
3. Summary	131
Chapter V. Models of Molecular Geometry and Reactivity	145
1. Introduction	145
2. The role of the Laplacian of the charge density in the quantum theory of molecular structure	146
3. The Laplacian of the Charge Density and the Lewis Electron Pair Model	150
4. The characterization of atomic interactions	155
5. Characterization of bonds in Hydrocarbons and Strain Energy	158
6. Conclusions	173
References	189

LIST OF FIGURES

<u>FIGURE</u>	<u>PAGE</u>
II.1 Contour plots of the electronic charge distribution of ethylene, C_2H_4	46
II.2 Contour plots and gradient vector field displays of the charge distribution for two symmetry planes in cyclopropane, C_3H_6	48
II.3 Gradient vector field (a) and contour plot (b) of the electronic charge distribution in tetrahedrane, C_4H_4	50
II.4 Phase portraits of the gradient vector field illustrating the behaviour of gradients paths originating or terminating from critical points	52
II.5 Gradient vector field displays of ethylene, C_2H_4	54
II.6 Molecular graphs for a variety of molecules in the equilibrium geometries	56
II.7 Gradient vector fields along the reaction coordinate for the thermal isomerization of isocyanide, CNH	58
II.8 Molecular graphs of [1.1.1]propellane illustrating the bifurcation catastrophe	60
II.9 Profile of the charge distribution along the direction of approach of a ring critical point to a bond critical point leading to a bifurcation catastrophe	62
II.10 A two dimensional cross section of the structure diagram for an ABC system	64

LIST OF FIGURES (cont'd)

<u>FIGURE</u>	<u>PAGE</u>
III.1 Planar projections of molecular graphs generated from theoretical charge distributions	84
III.2 Relief maps of the charge density in the symmetry plane bisecting the bridgehead bond in the propellanes and the corresponding plane of the related bicyclic structures	86
III.3 Planar projections of the molecular graphs defining structures 1a, 1b and 1c of cyclopropylcarbinyl cation, $C_4H_7^+$	88
IV.1 Carbon skeletal structures of strained hydrocarbons showing net group charges and strain energies	135
V.1 Relief maps of Laplacian of the charge density for ClF_3	176
V.2 Contour maps of the Laplacian of the charge density with bond paths overlaid for cyclopropane and the symmetry plane containing the bridgehead bond in [1.1.1]propellane	178
V.3 Contour maps of the Laplacian of the charge density overlaid with bond paths for ethane, bicyclo[1.1.0]butane, distorted geometry of [1.1.1]propellane, [2.1.1]- [2.2.1]- and [2.2.2]propellane	180
V.4 Orbital energy level diagram for propellanes and bicyclobutane	182
V.5 Contour maps of the transition densities for the bridgehead bonds in [1.1.1]-, [2.2.2]propellane and corresponding bicyclic molecules	184
V.6 Relief maps of the lowest energy symmetric and antisymmetric transition densities for the propellanes	182

LIST OF TABLES

<u>TABLE</u>	<u>PAGE</u>
III.1 Bond Properties in Hydrocarbons 6-31G [*] /6-31G [*]	90
III.2 Geometry and Bond Path Angles	94
III.3 Bond Properties for C ₄ H ₇ ⁺ Structures: 6-31G [*] Basis	95
IV.1 Atomic Properties in Hydrocarbons	137
IV.2 Total Energies and Errors in Integrated Atomic Energies and Populations	141
IV.3 Effect of basis Set on Atomic Properties	142
IV.4 Net Charges on Methyl and Methylene Groups and Their Energies Relative to Standard Values 6-31G [*] /6-31G [*]	143
IV.5 Properties of H and C Atoms in CH ₃ Relative to CH ₃ in Hexane	144
V.1 Atomic Dipoles and Forces	188

Chapter I

Review of the Theory of Atoms in Molecules

1. Introduction

It is the primary purpose of this thesis to demonstrate that the atoms defined by the quantum theory of atoms in molecules can be identified with the atoms of chemistry. This is done by showing that the atoms of theory recover the experimentally measurable properties of atoms in molecules. The ability of the same theory to assign a unique structure to any system is utilized in a study of the structures and structural stabilities of a series of highly strained organic molecules. The thesis begins with a brief review of the generalization of quantum mechanics that leads to the definition of an open system that is identified as an atom in a molecule. A prediction of the properties of atoms in molecules is provided for by this theory. The generalization of quantum mechanics is accomplished through an extension of Schwinger's principle of stationary action (Schwinger 1951), an extension which is possible only if a certain boundary condition is satisfied. An atom in a molecule is an open system which is free to exchange charge and momentum with its neighbours. The boundary condition for an atom Ω demands that the flux in the gradient vector field of the charge density $\rho(\underline{r})$ vanish at every point of the surface $S(\Omega, \underline{r})$ which bounds an open system Ω . That is to say the surface is one of zero flux in $\nabla\rho$

$$\nabla\rho(\underline{r}) \cdot \underline{n}(\underline{r}) = 0 \quad \forall \underline{r} \in S(\Omega, \underline{r}) \quad (1)$$

As a consequence of the boundary being stated in terms of a property of the electronic charge density, quantum subsystems are defined in real

space. It is because of the dominant topological property of a molecular charge distribution, that it exhibits maxima at the position of the nuclei, the boundary condition leads to the partitioning of a molecular system into a set of disjoint spatial regions, each region containing in general a single nucleus. These are the regions which are identified with the chemical atoms. The properties of the gradient vector field also contain the information needed for a definition of molecular structure and its stability, using the mathematics of qualitative dynamics. The result is a theory of atoms, bonds, structure and structural stability.

A primary purpose of this thesis is to demonstrate that quantum mechanics predicts the properties of atoms in molecules just as it predicts the properties of the total system. Following the review of the generalization of quantum mechanics to an open system which yields a definition of an atom and its properties, examples of the application of the resulting theory of atoms in molecules to chemical problems are presented. These examples are chosen to illustrate the principal features of the theory:

a) The demonstration that each atom makes an additive contribution to the average value of every property of a molecular system. This is the principle underlying the cornerstone of chemistry which is that atoms and functional groupings of atoms make recognizable contributions to the total properties of a system. One predicts the properties of some total system in terms of the properties of the functional groups it contains. Conversely, one confirms the presence of a given group in a molecule through the observation of its characteristic properties. In those limiting situations where a functional group is essentially the same in two

different systems, one obtains a so called additivity scheme for the total properties. In this case the atomic contributions as well as being additive are transferable between molecules. It will be shown that the methyl group and methylene group as defined by the theory of atoms in molecules predict the additivity of the energy which is experimentally observed in normal hydrocarbons. The deviations in this additivity which are found for small cyclic molecules and which serve as the experimental definition of strain energy are also predicted by theory. It is the recovery of these experimentally measurable properties of atoms in molecules by the atoms of theory that confirms that these atoms of theory are indeed the atoms of chemistry.

b) The definition of bonds, molecular structure and structural stability as determined by the gradient vector field of the charge density is exemplified for hydrocarbon molecules which exhibit a wide range of structures. Included among these are the propellane molecules. These molecules have unusual structures as they exhibit an inverted tetrahedral geometry at the bridgehead carbon atoms.

Second only to the molecular structure hypothesis in the ordering of, understanding and prediction of chemical events is the Lewis model of the electron pair (Lewis 1916). This model and its associated models of molecular geometry and chemical reactivity find physical expression in the topological properties of the Laplacian of the electronic charge density. This scalar field, defined by the second derivatives of the electronic charge density, determines where electronic charge is locally concentrated and depleted. It plays a dominant role throughout the theory of atom in molecules. Therefore, this thesis also illustrates the following:

c) The recovery of the Lewis model of the electron pair in terms of the topological properties of the Laplacian of the charge density. The Laplacian of the charge density yields predictive models of molecular geometry and chemical reactivity.

d) The ability of the Laplacian of the charge density, when used in conjunction with the definition of a chemical bond and the local mechanics governing the charge density as provided by theory, to yield a classification of the atomic interactions. This classification scheme is directly applicable to experimentally measured charge distributions.

2. The Quantum Mechanics of an Open system

A. The need for a quantum description of an open system

It is a postulate of quantum mechanics that everything that can be known about a system is contained in the state function ψ . The value of a physical quantity is obtained through the action of a corresponding operator on ψ . Therefore, quantum mechanics is concerned with observables, the linear hermitian operators associated with the physical properties of a system and with their equations of motion. The theorems of quantum mechanics that yield relationships between various observables, such as the virial and Ehrenfest theorems, are derived from the Heisenberg equation of motion. Questions which can be raised about a quantum system are therefore answered in terms of the values and equations of motion for the relevant physical observables. These values and relationships refer to the total system. The use of the atomic concept in our attempts to understand and predict the properties of

molecules however, requires answers of a more regional nature. It would appear that to find chemistry within the framework of quantum mechanics one must find a way of determining the observables and their properties for portions of the system. How can these portions be chosen? Is there one or are there in fact many ways of partitioning a system into pieces in such a way that quantum mechanics predicts their properties? If indeed there is an answer to these questions then the necessary information must be contained in the state function ψ , for ψ contains all the information which can be known about a system.

The question "Are there atoms in molecules?" requires the asking of two equally important questions:

- (i) Does the state function ψ predict a unique partitioning of the system into subsystems?
- (ii) Does quantum mechanics then provide a complete description of the subsystems so defined?

To answer these questions one must turn to a development of physics that introduces the quantum observables and their equations of motion in a non-arbitrary way. Such is Schwinger's principle of stationary action. it replaces the conventional array of assumptions based on classical Hamiltonian dynamics and the correspondence principle with a single quantum dynamical principle. The approach is a very general one and allows one to pose and answer the questions outlined above.

B. The action principle in quantum mechanics and Schwinger's principle of stationary action

In Classical Mechanics, for a system of n particles with R degrees of freedom, the dynamical state of the system is defined by its coordinates (q_1, q_2, \dots, q_R) and its velocities $(\dot{q}_1, \dot{q}_2, \dots, \dot{q}_R)$. At each point in time, the configuration of the system can be represented by a point M in the R dimensional configuration space. A characteristic function of the system known as the Lagrangian can be denoted

$$L = L(q_1, q_2, \dots, q_R; \dot{q}_1, \dot{q}_2, \dots, \dot{q}_R; t) \quad (2)$$

The dynamics of the system now satisfy the following R differential equations:

$$d(\partial L / \partial \dot{q}_r) / dt - \partial L / \partial q_r = 0 \quad (r=1, 2, \dots, R) \quad (3)$$

These laws of motion are equally well expressed in the form of a variational principle. The system of Lagranges' equations is in fact equivalent to the principle of least action (Messiah 1958)

$$\delta \int_{t_1}^{t_2} L dt = 0; \delta M(t_1) = \delta M(t_2) = 0 \quad (4)$$

Let the action integral be denoted by

$$W = \int_{t_1}^{t_2} L dt \quad (5)$$

Many possible laws of motion can take a system from configuration M_1 at time t_1 to M_2 at time t_2 . The principle of least action identifies the law of motion which actually allows a system to pass from configuration M_1 at time t_1 to M_2 at time t_2 as the one which makes the integral $\int L dt$ stationary. One is now able to extend these ideas in quantum mechanics. Through a generalization of Schwinger's principle of stationary action one obtains the most general description of a quantum

system. The action integral for an isolated system is defined as

$$W_{12}[\psi] = \int_{t_1}^{t_2} dt \int L(\psi, \nabla\psi, \psi, t) d\tau = \int dt \mathcal{L}(\psi, t) \quad (6)$$

where the Lagrangian integral $\mathcal{L}(\psi, t)$ is defined in terms of the many particle Lagrangian density

$$L(\psi, \nabla\psi, \dot{\psi}, t) = (i\hbar/2)(\dot{\psi}^* \dot{\psi} - \dot{\psi} \dot{\psi}^*) - (\hbar^2/2m) \Sigma \nabla_i \psi^* \cdot \nabla_i \psi - \hat{V} \psi^* \psi \quad (7)$$

and where \hat{V} is the potential energy operator for the total system.

By requiring that $W_{12}[\psi]$ be stationary with respect to variations in ψ and ψ^* under the constraint that these variations vanish at the time end points, one obtains the Euler equations

$$i\hbar \dot{\psi} = \hat{H} \psi \text{ and } -i\hbar \dot{\psi}^* = \hat{H} \psi^* \quad (8)$$

which are Schroedinger's equations for a time dependent system. When these equations are satisfied, the average Lagrangian density $\mathcal{L}(\underline{r})$ reduces to (Bader and Nguyen-Dang 1981a)

$$\mathcal{L}(\underline{r}, t) = N \int d\tau^3 L = (-\hbar^2/4m) \nabla^2 \rho(\underline{r}, t) \quad (9)$$

where the symbol $\int d\tau$ denotes the same mode of integration as is used to define the electronic charge density

$$\begin{aligned} \rho(\underline{r}_j; \underline{X}, t) &= N \sum_{\text{spins}} \int \left\{ \prod_{j \neq i} d\underline{r}_j \right\} \psi^*(\underline{x}, \underline{X}, t) \psi(\underline{x}, \underline{X}, t) \\ &= N \int d\tau^3 \psi^*(\underline{x}, \underline{X}, t) \psi(\underline{x}, \underline{X}, t) \end{aligned} \quad (10)$$

where \underline{x} is the set of electronic space and spin coordinates, \underline{r}_j are

the space coordinates of a single electron, \underline{X} is the set of coordinates for a fixed nuclear configuration. Correspondingly, the Lagrangian integral for a many-particle system

$$\mathcal{L}[\psi, t] = \int d\underline{r} \int d\underline{r}' L(\psi, \nabla\psi, \dot{\psi}, t) \quad (11)$$

reduces to

$$\mathcal{L}[\psi, t] = \int d\underline{r} \mathcal{L}(\underline{r}, t) = (-\hbar^2/4m) \int d\underline{r} \nabla^2 \rho(\underline{r}, t) \quad (12)$$

Since

$$\int d\underline{r} \nabla^2 \rho(\underline{r}, t) = \oint dS(\underline{r}, t) \nabla \rho(\underline{r}, t) \cdot \underline{n}(\underline{r}, t) \quad (13)$$

and since the flux in $\nabla \rho$ vanishes at the boundary of an isolated system (where both ρ and $\nabla \rho$ are zero) its Lagrangian integral is zero. Therefore the Lagrangian integral $\mathcal{L}[\psi, t]$ for a closed quantum mechanical system is zero at each time t and correspondingly the action integral vanishes for any time interval Δt .

The atomic Lagrangian integral is defined to be

$$\mathcal{L}[\psi, \Omega, t] = \int_{\Omega} d\underline{r} \int d\underline{r}' L(\psi, \nabla\psi, \dot{\psi}, t) \quad (14)$$

where Ω denotes the atomic volume. The atomic action integral then is given by

$$W_{12}[\psi, \Omega] = \int_{t_1}^{t_2} dt \mathcal{L}[\psi, \Omega, t] \quad (15)$$

When ψ and ψ^* satisfy Schrodinger's equations, the atomic Lagrangian reduces to

$$\begin{aligned}\mathcal{L}[\psi, \Omega, t] &= (-\hbar^2/4m) \int_{\Omega} d\mathbf{r} \nabla^2 \rho(\mathbf{r}, t) \\ &= (-\hbar^2/4m) \oint dS(\mathbf{r}, t) \nabla \rho(\mathbf{r}, t) \cdot \mathbf{n}(\mathbf{r}, t)\end{aligned}\quad (16)$$

If the atomic region Ω is bounded by a surface which satisfies the zero flux boundary surface condition (equation 1), the atomic Lagrangian integral vanishes for each point in time t and the atomic action integral vanishes at each time interval Δt . This vanishing of the atomic Lagrangian integral occurs only for those atoms defined in the manner outlined above. In general this vanishing of the atomic Lagrangian will not be true for regions bounded by surfaces that do not satisfy the zero flux boundary condition. One may consider the vanishing of the action over the total system as being a consequence of the action vanishing separately over each atom.

As the system in any given quantum state changes and evolves with time, the atomic surfaces also evolve in a continuous manner. In this way the property of exhibiting zero flux surfaces is continuously maintained. Therefore, for any time interval the atomic action integral will always vanish,

$$W_{12}[\psi, \Omega] = (-\hbar^2/4m) \int_{t_1}^{t_2} dt \int_{\Omega} d\mathbf{r} \nabla^2 \psi(\mathbf{r}, t) = 0 \quad (17)$$

This condition is the quantum definition of an atom.

Schwinger demonstrated that one can obtain a complete description of mechanics through a generalization of the requirement that W_{12} be stationary. This generalization corresponds to the removal of the

constraint that the variations vanish at the time end points together with the introduction of a variation of the time end points themselves. It is followed by the demonstration that these end point variations may be identified with the generators of infinitesimal canonical or unitary transformations. The implementation of these steps leads to the principle of stationary action which is stated as

$$\delta W_{12} = \hat{A}(t_2) - \hat{A}(t_1) \quad (18)$$

In general, it is found that the variational properties of energy and Lagrangian functionals defined for arbitrary regions of space do not correspond to those exhibited by the same functionals defined for the total system. In the variation of the atomic action integral one obtains variations of ψ at the finite boundaries of the atom Ω . One is then forced to generalise the variational procedure and remove the constraint that the $\delta\psi$ vanish at the time end points. The variation of the atomic action integral $W_{12}[\psi, \Omega]$ where Ω is arbitrary does not satisfy the principle of stationary action. However, if the additional variational constraint that the region Ω be bounded by surfaces of zero flux in $\nabla\rho$ at all points of the variation then the resulting expression for $\delta W_{12}[\psi, \Omega]$ is identical in form and content to the corresponding expression for the total system. One imposes this constraint by requiring that

$$I_\Phi = \int_{\Omega(\phi, t)} \nabla^2 \rho_\phi \, d\underline{r} = 0 \quad (19)$$

for all admissible trial functions ϕ and for all t . This implies that

$$\delta I_\psi = \delta \left\{ \int \Omega(t) d\mathbf{r} \nabla^2 \rho(\mathbf{r}, t) \right\} = 0 \quad (20)$$

The expression of the principle of stationary action in operator form is

$$\delta W_{12} = \int_{t_1}^{t_2} dt \{ d\hat{A}/dt \} = \int_{t_1}^{t_2} dt \{ (i/\hbar) [\hat{H}, \hat{A}] \} \quad (21)$$

A comparison of the above with the atomic expression, which in the Schroedinger representation is

$$\delta W_{12}[\psi, \Omega] = \int_{t_1}^{t_2} dt \{ (i/\hbar) \langle [\hat{H}, \hat{A}] \rangle_\Omega + \text{c.c.} \} / 2 \quad (22)$$

demonstrates the equivalence of these variational expressions. In both the above equations, H is the Hamiltonian operator of the system and \hat{A} is the generator of an infinitesimal unitary transformation causing the change in the system. The commutator average in equation (22) is explicitly

$$\langle [\hat{H}, \hat{A}] \rangle_\Omega = N \int_\Omega d\mathbf{r} \int d\mathbf{r}' \psi^* [\hat{H}, \hat{A}] \psi \quad (23)$$

which involves an initial sum over all the spins and an integration over the coordinates of all the electrons but one, followed by an integration over the space of the atom Ω . In equation (22) the region Ω may be bounded by any surface that satisfies the condition of zero flux in $\nabla \rho$. Therefore, it applies equally well to the total system as

it does to an atom within that system. With this equation, one now has atoms that obey the same quantum mechanical laws as does the total system. In other words, the atoms are quantum subsystems.

The principle of stationary action for a subsystem can be expressed for an infinitesimal time interval in terms of a variation of the Lagrangian integral as given by equation (12) for the total system. For the atomic Lagrangian this statement is

$$\delta\mathcal{L}[\Psi, \Omega, t] = (1/2)\{ (i/\hbar) \langle [\hat{H}, \hat{A}] \rangle_{\Omega} + \text{c.c.} \} \quad (24)$$

For a stationary state, the Lagrangian integral, apart from the presence of a Lagrange multiplier to insure normalization of ψ , reduces to the energy functional used by Schroedinger (Schroedinger 1927) in the derivation of the stationary wave equation. For an atom in a molecule in a stationary state, this energy functional is

$$E[\psi, \Omega] = \int \Omega d\mathbf{r} \int d\mathbf{r}' \{ (\hbar^2/2m) \nabla_i \psi^* \cdot \nabla_i \psi + (\hat{V} + \lambda) \psi^* \psi \} \quad (25)$$

where V denotes the full many-electron potential energy operator, and λ the variational constraint on the normalization of ψ is identified with $-E$, the negative of the total energy. The atomic statement of the principle of stationary action in terms of this functional is

$$\delta E[\psi, \Omega] = -(\epsilon/2) \{ (i/\hbar) \langle [\hat{H}, \hat{A}] \rangle_{\Omega} + \text{c.c.} \} \quad (26)$$

The derivation of the principle of stationary action for an atom in

a molecule in the time dependent case or in a stationary state yields (i) the corresponding Schrodinger equation of motion for the total system, (ii) identifies the observables with the variations of the state function, (iii) defines their average values of the observables and (iv) gives their equations of motion. The statements of the atomic principle of stationary action as expressed in terms of variations in $\mathcal{L}[\psi, \Omega]$ and $E[\psi, \Omega]$ are variational statements of Heisenberg's equation of motion and of the hypervirial theorem for a generator \hat{A} respectively. They yield the theorems and relations governing the mechanics of an atom in a molecule.

C. Atomic Properties Defined

The atomic average of the property A associated with the operator \hat{A} must satisfy the atomic statement of the Heisenberg relation (Bader and Nguyen-Dang 1981a):

$$\begin{aligned} dA(\Omega, t)/dt = N/2 \{ (i/\hbar) \langle [\hat{H}, \hat{A}] \rangle_{\Omega} + \text{c.c.} \} + \int dS(\underline{r}) \{ (\partial S(\underline{r})/\partial t) \rho_A \\ - (\underline{J}_A \cdot \underline{n}(\underline{r})) + \text{c.c.} \} \end{aligned} \quad (27)$$

Therefore $A(\Omega, t)$ must be given by

$$A(\Omega, t) = \int_{\Omega} d\underline{r} \rho_A(\underline{r}) \quad (28)$$

where

$$\begin{aligned} \rho_A(\underline{r}) &= N \int d\underline{r}' (1/2) \{ \psi^* \hat{A} \psi + \text{c.c.} \} \\ &= N \int d\underline{r}' (1/2) \{ \psi^* [\hat{H}, \hat{A}] \psi + \text{c.c.} \} \end{aligned} \quad (29)$$

The atomic average of the property A is simply N times the value obtained for any single electron in the system.

Atomic properties have the necessary property of yielding the value of A for the total system when summed over all the atoms in the system,

$$\langle A \rangle = \sum A(\Omega) \quad (30)$$

The above equation states that each atom makes an additive contribution to the value of every property for a total system. This is the principle underlying the cornerstone of chemistry, that atoms and functional groups of atoms make recognizable contributions to the total properties of a system. In practice, one recognizes a group and predicts its effect on the static and reactive properties of a system in terms of a set of properties assigned to that group. In the limiting case of a group being essentially the same in two different systems, one obtains a so called additivity scheme for the total properties since in this case the atomic contributions in addition to being additive in the sense of equation (30) above are also transferable between molecules.

D. Energy of an Atom in a Molecule

The energy of an atom in a molecule is an atomic property that deserves special comment. Before deriving an expression for the energy of an atom in a molecule, an expression governing the average force acting on an atom in a molecule, the Ehrenfest force, is derived. In this case, the generator \hat{A} in equation (26) is set equal to

$$\hat{A} = -\epsilon \cdot \underline{p} \quad (31)$$

where \underline{p} denotes the conjugate momentum associated with the electron whose coordinate, \underline{r} , is integrated over the atomic volume Ω , one obtains (Bader 1980, Bader and Nguyen-Dang 1981a). The commutator of H and \underline{p} is the force operator $-\nabla_{\underline{r}} \hat{V}$ and according to equation (29) the average of this commutator defines the force acting on the electrons in the atom region Ω

$$\underline{E}(\Omega) = N \int_{\Omega} d\underline{r} \int d\underline{r}' (1/2) \{ \psi^* [\hat{H}, \hat{\underline{p}}] \psi + \text{c.c.} \} \quad (32)$$

$$= N \int_{\Omega} d\underline{r} \int d\underline{r}' \psi^* (-\nabla_{\underline{r}} \hat{V}) \psi \quad (33)$$

The variation in $E[\psi, \Omega]$ for this generator is determined to be (Bader and Nguyen-Dang 1981a)

$$\delta E[\psi, \Omega] = -\epsilon \oint dS \vec{\sigma} \cdot \underline{n}(\underline{r}) \quad (34)$$

where σ is the quantum mechanical stress tensor. It can be expressed as a functional of the one-density matrix $\Gamma^{(1)}(\underline{r}, \underline{r}')$

$$\vec{\sigma}(\underline{r}) = (\hbar^2/4m) [(\nabla \nabla + \nabla' \nabla') - (\nabla \nabla' + \nabla' \nabla)] \Gamma^{(1)}(\underline{r}, \underline{r}')|_{\underline{r}=\underline{r}'} \quad (35)$$

Thus from equation (26), the force acting over the region of an atom Ω , $\underline{E}(\Omega)$ in equation (33), is determined entirely by the force exerted on its surface

$$\underline{E}(\Omega) = -\oint dS \vec{\sigma} \cdot \underline{n}(\underline{r}) \quad (36)$$

If one now sets

$$A = -\epsilon \mathbf{r} \cdot \mathbf{D} \quad (37)$$

in the atomic statement of the principle of stationary action (equation 26) one obtains the atomic virial theorem (Bader and Nguyen-Dang 1981a):

$$-2T(\Omega) = V(\Omega) \quad (38)$$

where $T(\Omega)$ is the average electronic kinetic energy of the atom and $V(\Omega)$ is the virial of all the forces exerted on the atom Ω . For a stationary state $V(\Omega)$ can be expressed as

$$V(\Omega) = V_b(\Omega) + V_s(\Omega) \quad (39)$$

where

$$V_b(\Omega) = \int_{\Omega} d\mathbf{r} \int d\mathbf{r}' (-\mathbf{r} \cdot \nabla \hat{V}) \psi^* \psi \quad (40)$$

is the virial of the forces exerted over the basin of the atom (compare with equation (33)) and

$$V_s(\Omega) = \int dS(\mathbf{r}) \mathbf{r} \cdot \vec{\sigma}(\mathbf{r}) \cdot \mathbf{n}(\mathbf{r}) \quad (41)$$

is the virial of the forces exerted on the atomic surface (compare with equation (34)). The virial of the Ehrenfest forces acting on an atom $V(\Omega)$ in equation (39) defines the electronic potential energy.

The average electronic kinetic energy $T(\Omega)$ can be expressed in the

following two ways:

$$K(\Omega) = (-\hbar^2/4m)N \int_{\Omega} d\mathbf{r} \int d\mathbf{r}' \{ \psi^* \nabla^2 \psi + \psi \nabla^2 \psi^* \} \quad (42)$$

or

$$G(\Omega) = (\hbar^2/2m)N \int_{\Omega} d\mathbf{r} \int d\mathbf{r}' \nabla \psi^* \cdot \nabla \psi \quad (43)$$

In general $K(\Omega)$ differs from $G(\Omega)$ by,

$$K(\Omega) = G(\Omega) - (\hbar^2/4m) \int dS(\Omega) \nabla \rho \cdot \underline{n}(\mathbf{r}) \quad (44)$$

$$= G(\Omega) + L(\Omega) \quad (45)$$

However, as these atoms satisfy the zero flux boundary condition, equation (1), this difference $L(\Omega)$ vanishes and one has

$$T(\Omega) = K(\Omega) = G(\Omega) \quad (46)$$

The kinetic energy of an atom is well defined for atoms since they satisfy the quantum boundary condition. Thus the total electronic energy of an atom in a molecule defined in terms of the virial theorem is

$$E(\Omega) = T(\Omega) + V(\Omega) \quad (47)$$

or equivalently

$$E(\Omega) = -T(\Omega) = (1/2)V(\Omega) \quad (48)$$

The energies of the atoms in a molecule, like all atomic properties,

sum to give the total value. Specifically, for the total energy of an atom in a molecule

$$E_e = \sum_{\Omega} E(\Omega) \quad (49)$$

CHAPTER II

Topological properties of the electronic charge distribution

1. Introduction

The quantum mechanics for open subsystems was developed in Chapter I of this thesis. These open subsystems were found to obey the same quantum mechanics as the total system if they satisfied the zero flux boundary condition (equation 1)

$$\nabla\rho(\underline{r}) \cdot \underline{n}(\underline{r}) = 0$$

The question to be addressed now is whether or not regions of real space satisfying this quantum boundary condition actually exist. If such regions do exist, then they can be identified as the atoms of chemistry. To answer this question, one turns to examine the topology of the electronic charge density distribution.

2. Topological Properties of the Charge Density

A. The Charge Density

The state function ψ determines all of the information that can be known about a quantum system. If one desires a theory of molecular structure that is free of arbitrary or subjective assumptions, no information other than that contained in ψ should be used in its development. The state function for a molecular system is a function of the electronic and nuclear coordinates and also of the time t . One denotes this by $\psi(\underline{x}, \underline{X}, t)$ where \underline{x} is the set of electronic space and spin coordinates and \underline{X} the set of nuclear coordinates. While the general theory applies to the time dependent case, this thesis will primarily study

systems in a stationary state whose properties do not change with time. Denoting a solution to Schroedinger's stationary state equation for a fixed arrangement of nuclei by the symbol $\psi(\underline{x};\underline{X})$, the probability then of finding each one of the N electrons in a particular volume element

$$d\tau_i = dx_i dy_i dz_i \quad (50)$$

with spin coordinates σ_i (equal to either the α or β spin coordinate) for a given configuration of the nuclei \underline{X} is given by

$$\psi^*(\underline{x};\underline{X})\psi(\underline{x};\underline{X})dx_1dx_2....dx_N \quad (51)$$

where

$$dx_i = d\tau_i \sigma_i \quad (52)$$

The corresponding probability independent of spin is obtained by summing equation (51) over the over the spin coordinates. If the summing over all spins is followed by an integration over the spatial coordinates of all the electrons but one the resulting expression gives the probability of finding one electron in some elemental volume, independent of the positions of the other electrons. It does not matter which one of the electrons in particular is chosen to be excluded from the integration since ψ is an antisymmetrized function and therefore all the electrons are equivalent. This probability is expressed as

$$\begin{aligned} \text{probability of one electron being in volume } d\tau_1 = \\ \Sigma(\text{spins}) \{ \int d\tau_2 \int d\tau_3 \dots \int d\tau_N \psi^*(\underline{x};\underline{X})\psi(\underline{x};\underline{X}) d\tau_1 \end{aligned} \quad (53)$$

Multiplication of this probability by the total number of electrons N gives the probability of finding all of the electrons in the volume element $d\tau_i$. In other words the total probability of finding all of the electronic

charge in the elemental volume $d\mathbf{r}_1$. The corresponding probability density, the probability per unit volume, is called the electronic charge density and is denoted by the symbol $\rho(\mathbf{r};\mathbf{X})$. Here the space coordinate of the single electron, the one which was excluded from the integration, is denoted by

$$\mathbf{r} = ix + jy + kz \quad (54)$$

The charge density is to be discussed in more detail in this chapter and it can be written as

$$\rho(\mathbf{r};\mathbf{X}) = N \sum(\text{spins}) \left(\int d\mathbf{r}_2 \int d\mathbf{r}_3 \dots \int d\mathbf{r}_N \psi^*(\mathbf{x};\mathbf{X}) \psi(\mathbf{x};\mathbf{X}) \right) \quad (55)$$

The subscript 1 is suppressed in the above equation since the result refers to all the electrons but one. The form of the integration given in equation (55) which yields the density of charge in real space, recurs throughout the theory and is conveniently abbreviated in the following manner

$$\rho(\mathbf{r};\mathbf{X}) = N \int d\mathbf{r}' \psi^*(\mathbf{x};\mathbf{X}) \psi(\mathbf{x};\mathbf{X}) \quad (56)$$

where the mode of integration denoted here has previously been discussed in Chapter I.

B. The Dominant Form in the Charge Density

The local maxima in a charge distribution are illustrated in Figure II.1. The charge density in C_2H_4 is displayed in three planes as projections in the third dimension above the geometric plane, in other words as relief maps. The charge distribution exhibits a maximum at the position of each nucleus in Figure II.1a which shows the plane of the

nuclei. In Figure II.1b is shown a plane which contains the carbon-carbon nuclei but is perpendicular to that of Figure II.1a and is obtained by a rotation about the carbon-carbon axis. The charge density again exhibits maxima at the positions of the nuclei. The observation that a maximum in the charge distribution occurs at the nuclear positions is true when the distribution is viewed in any plane that contains the nuclei. It is this property that is classified as a local maximum in the charge density.

This behaviour of the charge distribution is to be contrasted with that displayed at the midpoint of the carbon-carbon axis, Figure II.1c. In the planes shown in Figure II.1a and II.1b the charge density has the appearance of a saddle at this midpoint. In the plane perpendicular to and bisecting the carbon-carbon axis the midpoint appears as a maximum. In this case the charge density is a maximum in only one particular plane. Knowledge of the behaviour of the charge density in one or two dimensions is insufficient to characterize its three-dimensional form. What is needed is a method of summarizing in a precise manner the principal topological features of a charge distribution. This can be accomplished by using the information provided by the curvatures of the charge density at its critical points.

C. Critical Points

Each topological feature of the charge distribution, whether it be a maximum, a minimum, or a saddle, has associated with it a point in space called a critical point, also known as an extremum. The properties of the charge distribution can be summarized in terms of its critical points

(Collard and Hall, 1977. Smith et al 1977). At the critical point, the first derivatives of the charge density function vanish. Therefore at each critical point \mathbf{r}_C ,

$$\nabla\rho(\mathbf{r}_C) = 0 \quad (57)$$

where $\nabla\rho$ denotes the operation

$$\nabla\rho = \mathbf{i}\partial\rho/\partial x + \mathbf{j}\partial\rho/\partial y + \mathbf{k}\partial\rho/\partial z \quad (58)$$

Whether a function is a maximum or a minimum at a critical point is determined by the sign of the second derivative or the curvature of the charge density at that point. The second derivative of a function $f(x)$ at x , for a one dimensional function, is the limiting difference between its two first derivatives which bracket the critical point

$$d^2f(x)/dx^2 =$$

$$\lim\{ [\lim((f(x+\Delta x)-f(x))/\Delta x) - \lim((f(x-\Delta x)-f(x))/\Delta x)]/\Delta x \} \quad (59)$$

At a point where $f(x)$ is a minimum, the second derivative is the difference between a positive and negative curvature and is therefore positive. On the other hand for a maximum of $f(x)$ the second derivative will be a difference between a negative and positive curvature which results in a value which is negative. For values of x lying between such extrema, both curvatures are either positive or negative and the resulting curvature can be either positive or negative depending upon whether x is in the region of a maximum or a minimum. At a point of inflection the second derivative has a value of zero and undergoes a change in sign. Clearly, from equation (59) above, when the curvature is negative at a point x , that is $f(x)$ is a maximum, the value of $f(x)$ is greater than the average of its values at neighboring points $x+\Delta x$ and $x-\Delta x$. The reverse is true when $f(x)$ is a minimum and the curvature at this point is positive.

In this case, the value of $f(x)$ will be less than the average value of the neighboring points $x+\Delta x$ and $x-\Delta x$. The curvature of a three dimensional function such as the charge density is completely analogous to the one dimensional case.

From examining Figure II.1a it is clear that the critical point between the two carbon nuclei has one positive curvature which is along the internuclear axis while in each of the two perpendicular planes it has a negative curvature. These central saddle points exhibits the positive curvature along the carbon-carbon axis and one of the negative curvatures in Figure II.1a and II.1b. The maximum observed in Figure II.1c is a display of both negative curvatures of this central saddle point.

In general, for an arbitrary choice of coordinate axes, one will encounter nine second derivatives of the form $\partial^2\rho/\partial x\partial y$ in the determination of the curvatures of the charge density at a point in space. Their ordered 3×3 array is called the Hessian matrix of the charge density, or simply the Hessian of ρ . This matrix is a real, symmetric matrix and as such, it can be diagonalized. The new coordinate axes are called the principal axes of curvature because the magnitudes of the three second derivatives of the charge density calculated with respect to these axes are extremized. The principal axes will correspond to the symmetry axes if the critical point is at the origin of such a set of axes. In the particular example of C_2H_4 discussed here, it happens to be the case. When this occurs, the corresponding curvatures are equal and any linear combination of the degenerate set of axes will serve as a principal axis of curvature. The trace of the Hessian matrix, the sum of its diagonal elements, is invariant to a rotation of the coordinate system. Therefore,

the value of the quantity $\nabla^2\rho$, also known as the Laplacian of the charge density, is given by

$$\nabla^2\rho = \nabla \cdot \nabla\rho = \partial^2\rho/\partial x^2 + \partial^2\rho/\partial y^2 + \partial^2\rho/\partial z^2 \quad (60)$$

and is invariant to the choice of coordinate system. The principal axes and their corresponding curvatures at a critical point in the charge distribution are obtained as the eigenvectors and corresponding eigenvalues in the diagonalization of the Hessian matrix. Therefore, the pairs of terms "curvature and eigenvalue" and "axes of curvature and eigenvector" can be used interchangeably in describing the properties of a critical point in the charge density.

While all of the eigenvalues of the Hessian matrix may be real, they may also equal zero. The rank of a critical point, denoted w , is equal to the number of non-zero eigenvalues or non-zero curvatures of the charge density at the critical point. The signature of the critical point, denoted σ , is simply the algebraic sum of the signs of the eigenvalues or curvatures of the charge distribution at the critical point. The critical point is labelled then by giving the two values as (rank,signature) or (w,σ) . Thus the central critical point of C_2H_4 with three non-zero curvatures, one positive and two negative is classified as a (3,-1) critical point.

With relatively few exceptions, the critical points of the charge distributions for molecules at or in the neighborhood of energetically stable geometric configurations of the nuclei are all of rank three. The near ubiquitous occurrence of critical points which have $w=3$ in such

cases is another general observation regarding the topological behaviour of molecular charge distributions. It is in terms of the properties of critical points with rank 3 that the elements of molecular structure are defined. A critical point which possess at least one zero curvature will have a rank less than 3 and is said to be a degenerate critical point. Such a critical point is unstable in the sense that a small change in the charge distribution as caused by the displacement of the nuclei will cause the degenerate critical point to either vanish or to bifurcate into a number of non-degenerate or stable critical points with rank 3. As structure is a generic property in the sense that a given structure or arrangement of bonds persists over a range of nuclear configurations, the observed limited occurrence of degenerate critical points is not surprising. One correctly anticipates the appearance of a degenerate critical point in a molecular charge distribution signifies the onset of structural change.

Only four possible signature values exist for critical points of rank 3. They are:

(3,-3) critical points where all three curvatures are negative and ρ is a local maximum at the point r_c

(3,-1) critical points where two curvatures are negative and ρ is a maximum in the plane defined by their corresponding axes. The remaining curvature is positive and ρ is a minimum at r_c along this third axis which is perpendicular to the previous plane.

(3,+1) critical point where two curvatures are positive and ρ is a minimum at r_c in the plane defined by their corresponding axes. The remaining curvature is negative and ρ is a maximum at r_c along this third axis which is perpendicular to the previous plane.

(3,+3) critical points where all the curvatures are positive and the charge density is a local minimum at r_c .

D. Critical points of Molecular Charge Distributions

The coulombic potential becomes infinitely negative when an electron and a nucleus coalesce therefore the state function for an atom or a molecule must exhibit a cusp at a nuclear position. While it is true that the charge density is a maximum at the position of the nucleus, this point is not a true critical point because $\nabla\rho$, like $\nabla\psi$, is discontinuous there. However, this is not a problem of practical importance and the nuclear positions behave topologically as do (3,-3) critical points in the charge distribution and hereafter, they will be referred as such.

All of the saddle points shown in Figure II.1a are of the (3,-1) type critical points. A (3,-1) critical point is found between every pair of nuclei which are considered to be linked by a chemical bond in the C_2H_4 molecule. In Figure II.2 is shown a representation of the charge distribution for two symmetry planes of the cyclopropane molecule. The topology of the charge distribution for the plane of the three carbon nuclei shown in Figure II.2a is clearly dominated by the maxima which occur at the positions of the nuclei. Between the three carbon nuclei are (3,-1) critical points which appear as saddles. In the centre of the ring

of carbons appears a minimum. Figure II.2b shows a symmetry plane that contains a single carbon nucleus and bisects the carbon-carbon axis opposite it in the ring. Here the carbon-carbon midpoint appears to be a maximum but this is the same behaviour of the (3,-1) critical point as displayed in Figure II.1b. The central critical point however now appears as a saddle. It is not until one examines the charge density along the direction of the C_3 axis of this molecule that one discovers the central critical point appears to be a maximum. Again, knowledge of the behaviour of the charge density in one or two dimensions is insufficient to characterize its three-dimensional form. This central critical point is in fact a (3,+1) critical point and appears in all molecules that form a ring.

The fourth and final kind of stable critical point is illustrated in Figure II.3 which gives representations of the charge distribution of the molecule tetrahedrane. The chemical structure assigned to this molecule is that of a cage. The critical point at the centre of the molecule appears as a minimum in the diagram and because of the symmetry possessed by this molecule this critical point will have the same appearance when viewed in any plane. It is therefore a (3,+3) critical point and the charge density is a local minimum at the centre of the cage structure. Each cage structure will display such a (3,+3) critical point.

The existence of a connection between the number and kind of critical points appearing in a charge distribution and its chemical structure has been demonstrated. It will now be shown that the qualitative associations of the topological features of the charge distribution with elements of

molecular structure can be replaced by a complete theory which recovers all of the elements of structure in a manner that is totally independent of any information other than that contained in the charge distribution itself (Bader et al 1981b). The underlying structure of the charge distribution is brought out most clearly by its associated gradient vector field. The boundary condition of a quantum subsystem is also stated in terms of this gradient vector field. It is the most remarkable coincidence of reasons for studying the gradient vector field, one from the quantum definition of a subsystem, the other from the independent demonstration that its form yields a mapping of the elements of molecular structure, that gives the theory of atoms in molecules its unified structure.

E. Gradient Vector Field of the Charge Density

The gradient vector field of the charge density is represented through a display of the trajectories traced out by the vector $\nabla\rho$. A trajectory of $\nabla\rho$, also called a gradient path, starting at some arbitrary point \mathbf{r}_0 is obtained by calculating $\nabla\rho(\mathbf{r}_0)$, moving a distance $\Delta\mathbf{r}$ away from this point in the direction indicated by $\nabla\rho(\mathbf{r}_0)$. This procedure is repeated until the path so generated terminates. This operation is the three-dimensional analogue of approximating a one-dimensional function $f(x)$ in terms of its tangent line at x

$$f(x+\Delta x) = f(x) + (df/dx)\Delta x \quad (61)$$

The above expression as a consequence of the definition of a derivative becomes exact in the limit $\Delta x = dx$.

Trajectories of $\nabla\rho$ possess the following properties:

- a) Since the gradient vector of a scalar function points in the direction

of steepest ascent, the trajectories of $\nabla\rho$ are perpendicular to lines of constant density. That is to say that the gradient vectors of the charge density will be perpendicular to contour lines of ρ .

b) The vector $\nabla\rho(\underline{r})$ is tangent to its trajectory at each point \underline{r} .

c) Every trajectory must originate or terminate at a point where $\nabla\rho(\underline{r})$ vanishes, that is at a critical point.

d) Trajectories cannot cross since $\nabla\rho(\underline{r})$ defines only one direction at each point \underline{r} .

The differential equation for $\nabla\rho(\underline{r})$ is

$$d\underline{r}(s)/ds = \nabla\rho(\underline{r}(s)) \quad (62)$$

where the notation $\underline{r}(s)$ implies that a point \underline{r} on a given trajectory is dependent upon a path parameter s . Equation (62) represents three first order differential equations and it yields unique solutions only when particular values are assigned to the three constants of integration. This corresponds to fixing some initial point on a trajectory at $s = s_1$ for example. Then every other point on the trajectory that passes through the point $\underline{r}(s_1)$ is obtained by integrating equation (62) with the three constants of the integration given by the components $\underline{r}(s_1)$

$$\underline{r}(s) = \underline{r}(s_1) + \int \nabla\rho(\underline{r}(t))dt \quad (63)$$

A trajectory of the gradient vector field of $\nabla\rho(\underline{r})$ is therefore a parameterized integral curve or solution curve, of the differential equation for $\nabla\rho(\underline{r})$. By fixing a point on a given trajectory all other points which lie on the same trajectory can be obtained by solving equation (61).

F. Phase Portraits of the Gradient Vector Field

An eigenvalue and its associated eigenvector of the Hessian of the charge distribution (a principal curvature and its associated axis) at a critical point define a one-dimensional system. If the eigenvalue or curvature is negative, then ρ is a maximum at the critical point on this axis and a gradient vector will approach and terminate at this point from both its left and right hand side as illustrated in Figure 11.4 for the case (1,-1) which is a system with rank 1 and signature -1. If the eigenvalue is positive then ρ is a minimum at the critical point on this axis and two gradient vectors will originate at this point as illustrated for the case (1,+1). In two dimensions, if both eigenvalues are negative then ρ is a maximum at the critical point and all trajectories of $\nabla\rho$ will terminate at the critical point as illustrated for the case (2,-2). This set of trajectories is defined by all possible linear combinations of the two associated eigenvectors which span the two dimensional space. Similarly if both eigenvalues are positive then ρ is a minimum at the critical point and all trajectories will originate at the critical point and again define a surface as illustrated for the case (2,+2). A more interesting situation is observed when the two eigenvalues are of opposite sign producing a signature of zero. The charge density in the two dimensional plane has the form of a saddle as illustrated for the case (2,0). In this situation the two trajectories associated with the axis of the negative curvature terminate at the critical point while the two associated with the positive curvature originate there. The trajectories formed by the linear combinations of the two associated eigenvectors neither terminate nor originate at the critical point but instead avoid

In three dimension, the pairs of eigenvectors associated with the two negative or two positive eigenvalues of a (3,-1) or (3,+1) critical point, respectively will again define a surface. Unlike the two dimensional examples discussed above, these surfaces will be planar only if the critical point r_c lies in a symmetry plane. If this is not the case, then the surface will be planar only in the immediate neighborhood of r_c and will in general be curved beyond this region but still defined by the unique set of trajectories which terminate at a (3,-1) critical point or originate from a (3,+1) critical point. In the final diagram in Figure II.4 is displayed of the three dimensional form of the phase portrait of a (3,-1) critical point. The unique pair of trajectories associated with the single positive eigenvalue originate at the critical point, as in the (1,+1) case illustrated above. The set of trajectories defined by the linear combinations of the pair of eigenvectors associated with the two negative eigenvalues terminate at the critical point and define a surface. The charge density is a maximum in the surface at the critical point and a minimum at this same point along the perpendicular axis. The behaviour of the charge density at a (3,+1) critical point is just the converse of that described for the (3,-1) case discussed above. Its phase portrait is obtained by simply reversing all the arrows in the phase portrait of the (3,-1) case.

G. Elements of Molecular Structure

The gradient vector field of the charge density in the plane containing the nuclei of the C_2H_4 molecule is illustrated in Figure II.5. A (3,-3) critical point, which occurs at the position of each nucleus, serves as the

terminus of all the paths starting from and contained in some neighborhood of the critical point. A (3,-3) critical point exhibits the property which defines a point attractor in the gradient vector field of the charge distribution: there exists an open neighborhood B of the attractor which is invariant to the flow of $\nabla\rho$ such that any trajectory originating in B terminates at the attractor. The largest neighborhood satisfying these conditions is called the basin of the attractor.

Since (3,-3) critical points in a many-electron charge distribution are generally found only at the positions of the nuclei, the nuclei act as the attractors of the gradient vector field of $\rho(\underline{r},\underline{X})$. The result of this identification is that the space of a molecular charge distribution, that is to say real space, is partitioned into disjoint regions or basins. Each of these regions contains one point attractor or nucleus. This fundamental topological property of a molecular charge distribution is illustrated in Figure II.5a which depicts only those gradient paths of the charge distribution which terminate at each of the nuclear attractors in the molecule. While Figure II.5a illustrates this property for only one plane, it is to be emphasized here that because the charge distribution is a local maximum at a nucleus, which is a (3,-3) critical point, the basin of an attractor is a region of three dimensional space and the partitioning which is so clearly indicated in Figure II.5a extends throughout all of space. An atom, free or bound, is defined as the union of an attractor and its associated basin.

Alternatively, an atom can be defined in terms of its boundary. The basin of the single nuclear attractor in an isolated atom covers the entire three dimensional space R^3 . For an atom in a molecule, the atomic basin

is an open subset of R^3 . It is separated from neighboring atoms by interatomic surfaces. The existence of an interatomic surface denoted as S_{AB} , signifies the presence of a (3,-1) critical point between neighboring atoms A and B. The presence of such a critical point between certain pairs of nuclei was noted above as being a general topological property of molecular charge distributions. Their presence now appears as providing the boundaries between the basins of neighboring atoms. As discussed above and illustrated in Figure II.4, the trajectories that terminate at a (3,-1) critical point define a surface, called the interatomic surface S_{AB} . In a sufficiently small neighborhood of the critical point at r_c , the interatomic surface coincides with its tangent plane at r_c which is linearly spanned by v_1 and v_2 which are the eigenvectors associated with the negative eigenvalues of the Hessian matrix of ρ at r_c . The entire interatomic surface can be obtained by solving differential equation (62) for initial conditions $r_0 = r(0)$, such that each r_0 belongs to the intersection of the surface with the above neighborhood of r_c and is thus expressible as a linear combination of v_1 and v_2 .

It was shown in Figure II.1c that the charge density is a maximum at a (3,-1) critical point in this surface. Figure II.5b shows in addition to the trajectories that terminate at each of the nuclei in C_2H_4 , the trajectories associated with each of the (3,-1) critical points. Two trajectories terminate at each such critical point in the plane of the diagram. They denote the intersection of the interatomic surfaces with this plane. It should be noted that each such pair of trajectories are but two of an infinity of gradient paths all of which terminate at a (3,-1) critical point. This set of gradient paths define a surface in three

dimensions as shown in Figure II.4. The atomic surface S_A of atom A is defined as the boundary of its basin. Generally this boundary comprises the union of a number of interatomic surfaces separating two neighboring basins and some portions which may be infinitely distant from the attractor. The atomic surface of a carbon atom in C_2H_4 as seen in Figure II.5 for example, consists of three interatomic surfaces, two with hydrogens and one with the other carbon atom.

Through a generalization of the quantum action principle a single variational that defines the observables, their equations of motion and their average values for the total system or for an atom within a system is obtained. This generalization to a subsystem of some total system only applies to a region that satisfies a particular constraint on the variation of its action integral. This constraint requires that the subsystem be bounded by a surface of zero flux in the gradient vector field of the charge density as stated in equation 1. In order for the scalar product of \underline{n} , the vector normal to the surface, with $\nabla\rho$ to vanish, it is necessary that the atomic surface not be crossed by any trajectories of $\nabla\rho$ and as such it is referred to as a zero flux surface. The state function ψ and $\nabla\psi\cdot\underline{n}$ where the gradient is taken with respect to the coordinates of any one of the electrons, vanish on the boundary of a bound system at infinity. Thus ρ and $\nabla\rho$ vanish there as well and a total isolated system is also bounded by a surface which satisfies equation 1. Since the generalized statement of the action principle applies to any region bounded by such a surface, the zero flux surface condition places the description of the total system and the atoms which comprise it on equal footing.

The interatomic surfaces along with those surfaces found at infinity are the only closed surfaces in R^3 which satisfy the zero flux condition of equation 1. This is a natural result of the property of an atomic basin as shown in Figure II.5a. All the trajectories in the vicinity of a given nucleus terminate at that nucleus and no trajectories cross from one basin to the other. Since trajectories of $\nabla\rho$ never cross, the zero flux surface condition follows directly from the definition of an interatomic surface in terms of the set of trajectories which terminate at a (3,-1) critical point. In terms of this same definition, it follows that the vector $\nabla\rho(\underline{r})$ will be tangent to the surface $S(\underline{r})$ of an atom at every point \underline{r} .

II. Chemical Bonds and Molecular Graphs

Figure II.5b shows the pairs of gradient paths which originate at each (3,-1) critical point and terminate at the neighboring attractors. As previously discussed and illustrated in Figure II.4, each such pair of trajectories is defined by the eigenvector associated with the unique positive eigenvalue of a (3,-1) critical point. These two unique gradient paths define a line through the charge density linking the neighboring nuclei along which the value of the charge density is a maximum with respect to any neighboring line. Such a line is found between every pair of nuclei whose atomic basins share a common interatomic surface. In the general case, this line is referred to as the atomic interaction line.

The existence of a (3,-1) critical point and its associated atomic interaction line indicates that electronic charge density is accumulated between the nuclei that are so linked. This is made clear by studying

the displays of the charge density for such a critical point, like those shown in Figure II.1 for example, particularly in Figure II.1c which shows that the charge density is a maximum in an interatomic surface at the position of the critical point. This is the point where the atomic interaction line intersects the interatomic surface and charge is so accumulated between the nuclei along the length of this line. Both theory and observation concur that the accumulation of electronic charge between a pair of nuclei is a necessary condition if two atoms are to be bonded to one another. This accumulation of charge is also a sufficient condition when the forces on the nuclei are balanced and the system possess a minimum energy equilibrium internuclear separation. The presence of the atomic interaction line therefore satisfies both the necessary and sufficient conditions that the atoms are bonded to one another. In this case the line of maximum charge density linking the nuclei is called a bond path (Bader 1975. Runtz et al 1977) and the associated (3,-1) critical point is referred to as a bond critical point.

For a given configuration \underline{X} of the nuclei, a molecular graph, is defined as the union of the closures of the bond paths or atomic interaction lines (Bader et al 1981b). Pictorially, the molecular graph is the network of bond paths linking pairs of neighboring nuclear attractors. The molecular graph isolates the pair-wise interactions present in an assembly of atoms which dominate and characterize the properties of the system be it at equilibrium or in a state of change.

A molecular graph is the direct result of the principal topological properties of a system's charge distribution: that the only local maxima, (3,-3) critical points, occur at the positions of the nuclei thereby

defining the atoms, and that (3,-1) critical points are found to link certain, but not all pairs of nuclei in a molecule. The network of bond paths thus obtained is found to coincide with the network generated by linking together those pairs of atoms which are assumed to be bonded to one another on the basis of chemical considerations. Molecular graphs for a sampling of molecules in equilibrium geometries with widely different bonding properties are illustrated in Figure II.6. The existence and position of a bond or (3,-1) critical point in this and other figures is indicated by a black dot.

The recovery of a chemical structure in terms of a property of the system's charge distribution is a most remarkable and important result. The representation of a chemical structure by an assumed network of lines has evolved through a synthesis of observations on elemental combination and models of how atoms combine, particularly models of chemical valency. This is a model which states that the ability of a given type of atom to form bonds, its valency, can be saturated and that valency is determined by the number of valence electrons. A great deal of chemical knowledge goes into the formulation of a chemical structure and, correspondingly, the same information is successfully and succinctly summarized by such structures. The demonstration that a molecular structure can be faithfully mapped onto a molecular graph imparts new information to them. The nuclei joined by a line in the structure are linked by a line through space along which electronic charge density, the glue of chemistry, is maximally accumulated. Finding the physical basis for a molecular structure also leads to a broadening of the concept which is that the dominant interactions between atoms, be they attractive or

repulsive, have a common physical representation. This is not an entirely surprising result since the ever present nuclear excursions from an equilibrium separation between a pair of atoms force a sampling of these same portions of a potential surface even though the atoms are considered to be bonded to one another. It is in answer to the closely related questions of what is meant by the making and breaking of chemical bonds that leads one to consider the most important extension of the molecular structure concept. The dynamic behaviour of the molecular graphs as caused by the relative motions of the nuclei forms the basis for the definition of structural stability and the analytical description of the mechanisms of structural change.

It is to be stressed that a bond path is not to be understood as representing a "bond". The presence of a bond path linking a pair of nuclei implies that the corresponding atoms are bonded to one another. As demonstrated later, the interaction can be characterized and classified in terms of the properties of the charge density at its associated (3,-1) critical point.

The agreement of structures predicted in this manner by quantum mechanics for a wide variety of systems with chemically accepted structures, shows that the many models which are used to rationalize the network of bonds in a molecule may be replaced with a single theory of molecular structure.

J. Rings and Cages

The remaining critical points of rank three occur as consequences of particular geometrical arrangements of bond paths and they define the

remaining elements of molecular structure, rings and cages. If the bond paths are linked so as to form a ring of bonded atoms, as in cyclopropane for example, then a (3,+1) critical point is found in the interior of the ring. As discussed above and illustrated in Figure II. 4, the eigenvectors associated with the two positive eigenvalues of the Hessian matrix of ρ at this critical point generate an infinite set of gradient paths which originate at the critical point and define a surface, called the ring surface. This behaviour is illustrated here by the gradient paths in the symmetry plane of the cyclopropane molecule as shown in Figure II.2. All of the trajectories which originate at the critical point at the centre of the ring of nuclei, the (3,+1) or ring critical point, terminate at the ring nuclei, but for the set of single trajectories each of which terminates at one of the bond critical points whose bond paths form the perimeter of the ring. These bond paths are noticeably inwardly curved away from the geometrical perimeter of the ring, a behaviour characteristic of systems which are electron deficient. The remaining eigenvector of a ring critical point, its single negative eigenvector, generates a pair of gradient paths which terminate at the critical point and define a unique axis perpendicular to the ring surface at the critical point. In cyclopropane this axis is perpendicular to the plane shown in Figure II.4. It represents the intersection of the boundaries of the basins of the hydrogen and carbon atoms forming the ring. A ring, as an element of structure, is defined as a part of a molecular graph which bounds a ring surface.

If the bond paths are so arranged as to enclose the interior of a molecule with ring surfaces then a (3,+3) or cage critical point is found

in the interior of the resulting cage. The charge density is a local minimum at a cage critical point. The phase portrait in the vicinity of a cage critical point is shown in Figure II.3a for tetrahedrane.

3. A Theory of Molecular Structure.

The ideas underlying the definition of structure and structural stability are first introduced in a qualitative manner with the aid of examples. The basic idea makes use of an equivalence relationship of gradient vector fields of the charge density as a function of nuclear configurations \underline{X} , equivalent vector fields possessing the same molecular graph.

Consider the thermal isomerization of HCN to the isocyanide, CNH. The gradient vector fields of the charge density, the fields $\nabla\rho(\underline{r};\underline{X})$ and the associated molecular graphs for points \underline{X} in nuclear configuration space along the reaction coordinate are illustrated in Figure II.7. The transition state occurs between values of the parameter $\theta = 72.1$ and 72.4 . The gradient vector fields of all configurations up to the transition state are equivalent, the gradient paths for one configuration \underline{X} can be mapped onto those for another, and they all have the same molecular graph corresponding to the structure H-C-N. This molecular graph is obtained for any and all arbitrary displacements of the nuclei in the vicinity of the equilibrium geometry of HCN. The structure denoted by one of the equivalent molecular graphs is a stable structure, as it occurs throughout an open region of nuclear configuration space. The gradient vector fields obtained after passage of the system through the transition state, while belonging to a single equivalence class, are not equivalent to

those which preceded the transition state. They correspond to the new structure C-N-H, which is also a stable structure, since it also persists for arbitrary nuclear motions. At some point in the neighborhood of the transition state, there is an abrupt and discontinuous change in structure, from H-C-N to C-N-H, as a result of the system passing through a configuration \underline{X}_C for which the gradient vector field and molecular graph are structurally unstable, that is, they exist for only one configuration on the reaction path. The structure corresponds to one in which the bond path from the hydrogen does not terminate at either the carbon or the nitrogen nucleus, but rather at the (3,-1) or bond critical point of the C-N bond path. This arrangement of bond paths is unstable as it corresponds to the two dimensional manifold of the bond critical point acting as an attractor in three-dimensional space. Such an intersection of manifolds of two (3,-1) critical points is mathematically unstable and is termed a conflict catastrophe, as the two attractors are in competition for a line of maximum charge density, the bond path to the proton.

The conflict mechanism represents one way in which a stable structure can be changed into another and it occurs by passage of the system through a catastrophe point \underline{X}_C , a configuration of the nuclei for which the associated gradient vector field of the charge density is unstable to nuclear motions. There is only one other type of possible instability of a gradient vector field, and it is termed a bifurcation catastrophe. It is illustrated by the transformation of the ring structure in [1.1.1]propellane into a cage structure, as shown in Figure II.8. The change in ρ which accompanies an extension of the bridgehead C-C bond causes the three (3,+1) or ring critical points to migrate towards the (3,-

1) or bond critical point of the bridgehead bond. The charge density in the plane of the ring has a positive curvature at each of the ring critical points and a negative curvature at the bond critical point, the axes for both curvatures lying along a common C_2 axis. For some particular extension of the C-C separation, the four critical points coalesce to form a single, new critical point and the gradient vector field undergoes an abrupt change into one which is no longer equivalent to those which preceded it. At coalescence, the original positive and negative curvatures lying on the C_2 axis must vanish and the result is a critical point of rank two, a degenerate critical point. Such a critical point is mathematically unstable with respect to the changes in ρ caused by nuclear motions. It exists only for this one configuration of the nuclei along the reaction coordinate. Further extension of the C-C separation causes the unstable critical point to vanish, the C-C bond has been broken and the ring structure has been transformed into the cage structure. These changes are summarized by the profiles of ρ along the direction of approach of the two critical points shown in Figure II.9.

The discussion so far has demonstrated that the definition of structure is inextricably bound up with the definition of structural stability. The result of applying the equivalence relationship to the field $\rho(\underline{r};\underline{X})$ is a partitioning of nuclear configuration space R^Q into a finite number of non-overlapping regions, each of which is characterized by a unique molecular structure (Bader et al 1981b). The structurally stable, open regions, called structural regions, are separated by boundaries, hypersurfaces in the space R^Q . A point on a boundary possesses a structure which is different from but transitional to the structures

characteristic of either of the regions it separates. Since a boundary is of dimension less than R^Q , arbitrary motions of the nuclei will carry a point on the boundary into neighboring stable structural regions and its structure will undergo corresponding changes. The boundaries are the loci of the structurally unstable configurations of a system. In general, the trajectory representing the motion of a system point in R^Q will carry it from one stable structural region through a boundary to a neighboring stable structural region. The result is an abrupt and discontinuous change in structure as illustrated in the above examples. A change in structure is catastrophic and for this reason the set of unstable structures is called the catastrophe set. A point in a structurally stable region of nuclear configuration space is termed a regular point, and a point on one of the structurally unstable boundaries is termed a catastrophe point.

A knowledge of the stable structural regions and their boundaries as defined by the catastrophe set enables one to construct a structure diagram, a diagram which determines all possible structures and all mechanisms of structural change for a given chemical system. Figure II.10 is a two-dimensional cross-section of the structure diagram for an ABC system. (The reason for the particular form shown there is justified in terms of catastrophe theory, (Thom 1975)). The letters may stand for atoms or functional groupings of atoms. The full lines, denoting the catastrophe set, partition nuclear configuration space into its structural regions. The hypocycloid portion denotes the loci of the bifurcation catastrophes, of the type illustrated in Figure II.8 and the three semi-axes, the loci of the conflict catastrophes, as illustrated in Figure II.7.

An equivalence relation for molecular graphs is defined as follows: two molecular graphs are equivalent if and only if they are associated with two points of the same structural region. An equivalence class of molecular graphs is called a molecular structure. It is then seen that a unique molecular structure is associated with a given structural region and that molecular structure, as defined above through the equivalence of molecular graphs, necessarily fulfills the requirement of being generic.

By appealing to the theorem of structural stability of Palis and Smale [41] one can show that only two kinds of structural instabilities or catastrophe points can arise and that there are therefore, only two basic mechanisms for structural change in a chemical system.

Palis and Smale's theorem of structural stability when used to describe structural changes in molecular system predicts a configuration $\underline{X} \in R^Q$ to be structurally stable if $\rho(r; \underline{X})$ has a finite number of critical points such that:

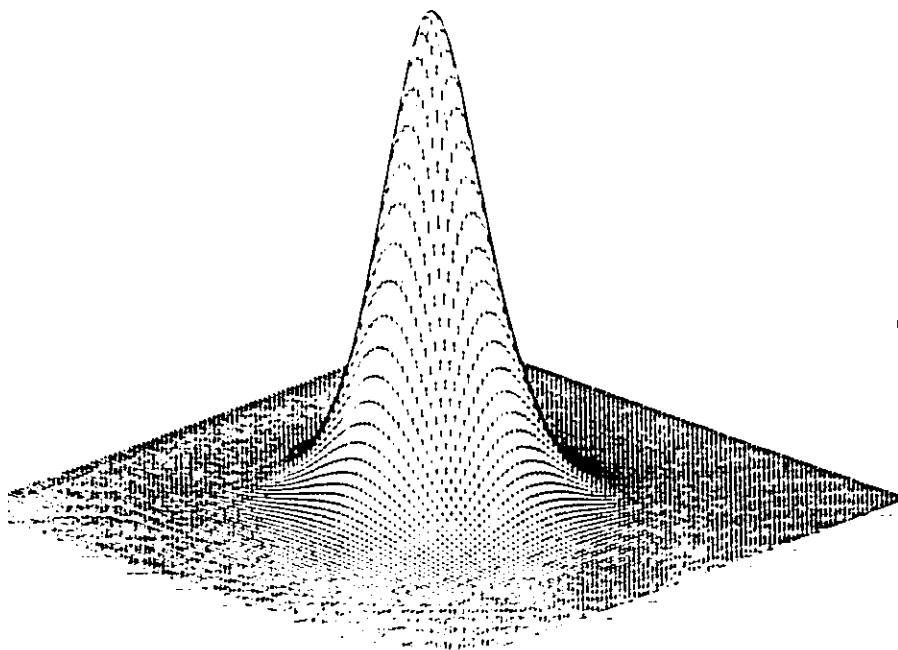
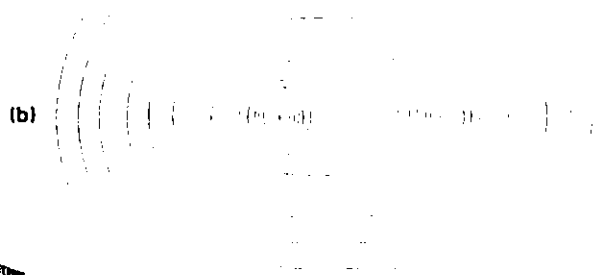
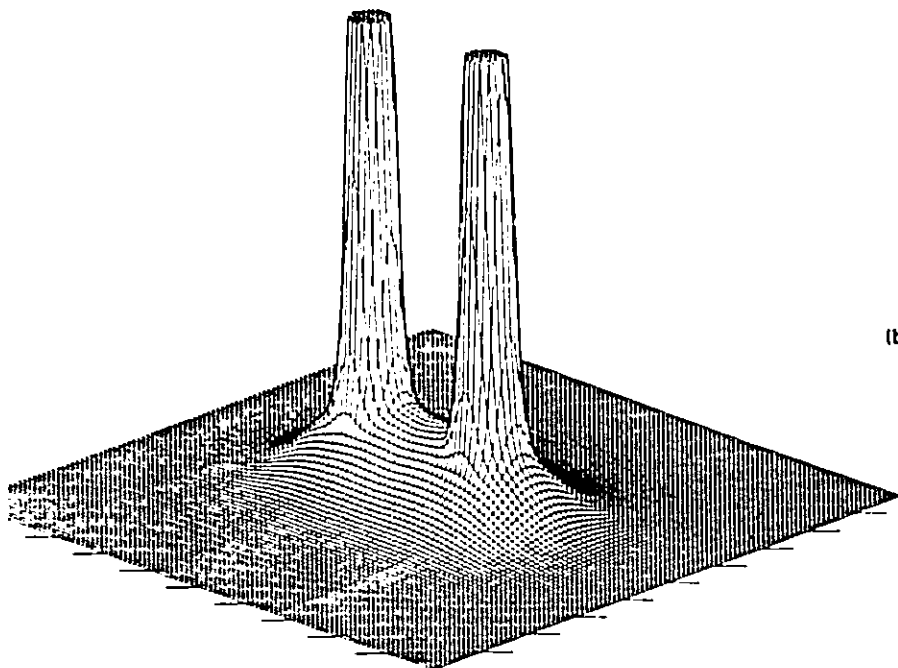
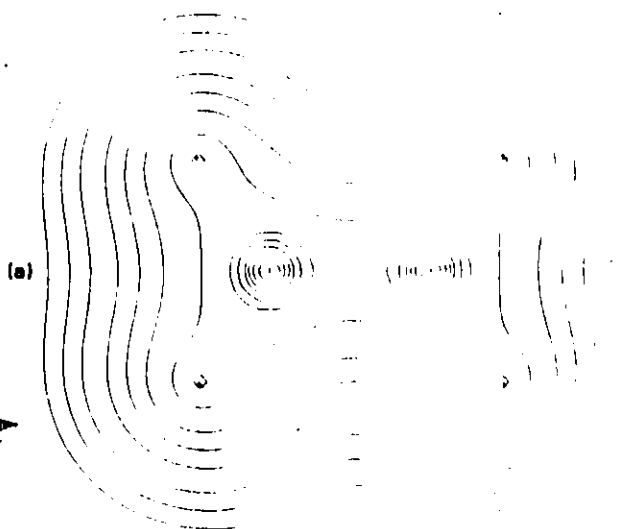
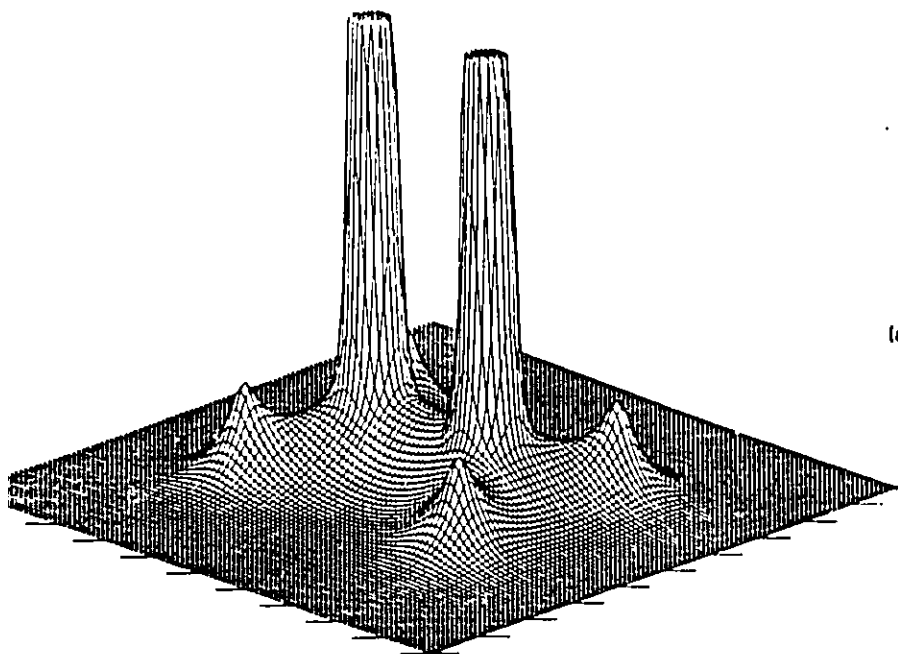
- (a) each critical point is non-degenerate, and
- (b) the stable and unstable manifolds of any pair of critical points intersect transversely.

The immediate consequence of the theorem is that a structural instability can be established through one of two possible mechanisms which correspond to the bifurcation and conflict catastrophes previously described. A change in molecular structure can only be caused by the formation of a degenerate critical point in the electronic charge distribution or by the attainment of an unstable intersection of the submanifolds of bond and ring critical points.

Figure II.1

Displays of the charge density in three planes of the ethylene molecule, C_2H_4 . On the left, the diagrams show the value of the charge density as a projection above the geometric plane called a relief map. On the right are the corresponding contour plots of the charge density.

- (a) The plane containing the nuclei.
- (b) The perpendicular plane containing only the carbon nuclei.
- (c) The perpendicular plane bisecting the carbon-carbon internuclear axis.



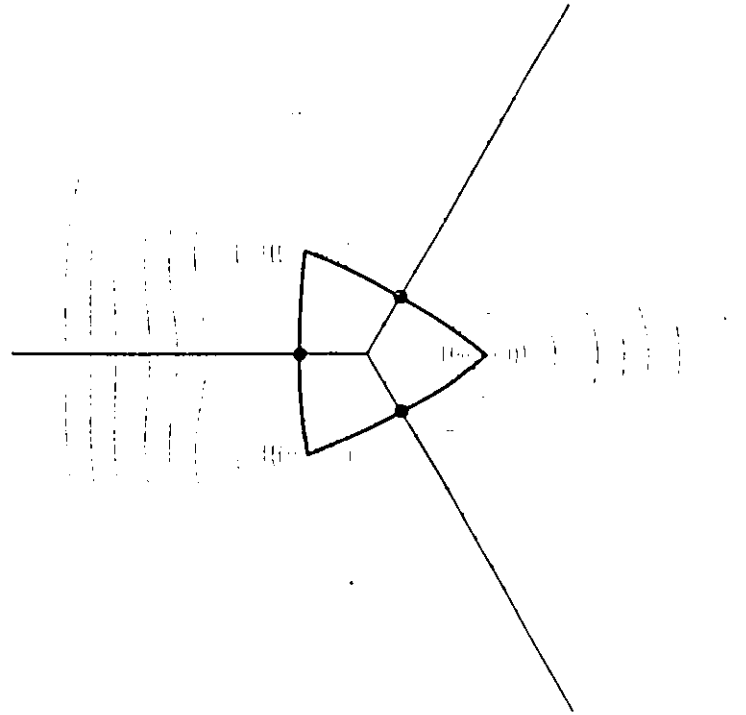
(c)

Figure II.2

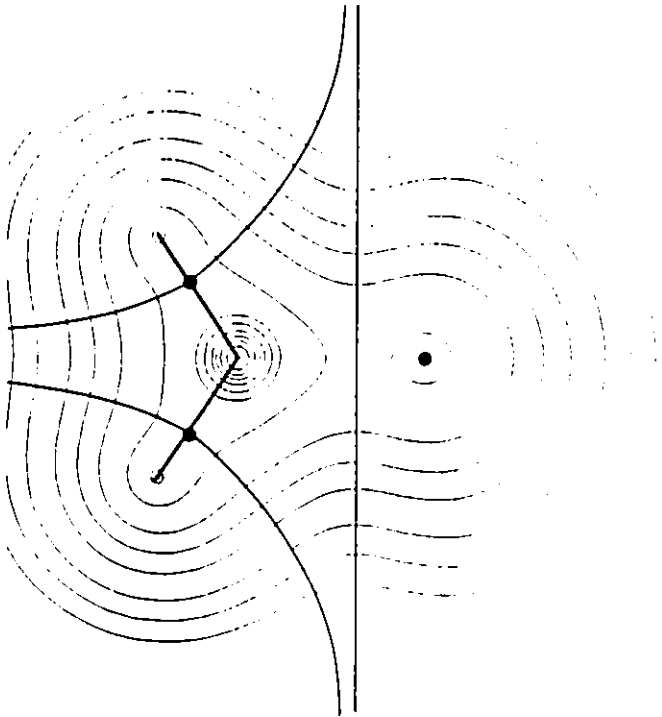
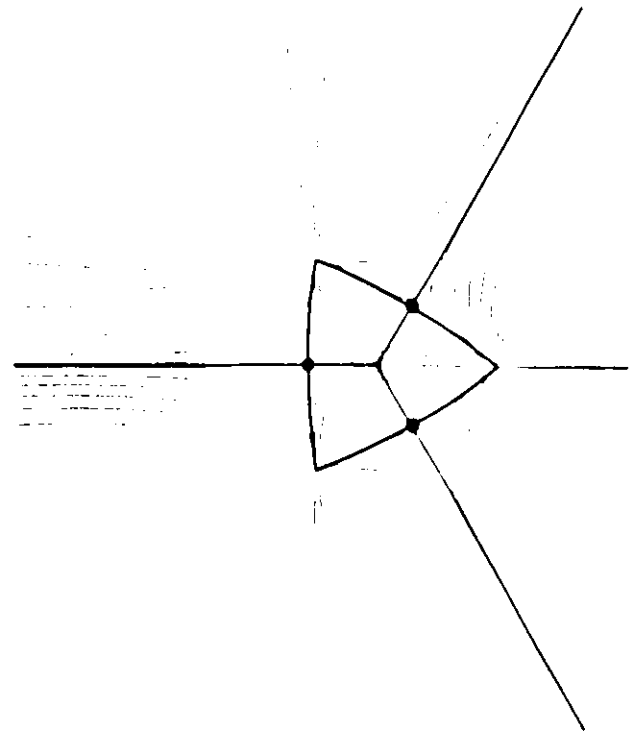
Contour plots and gradient vector field displays of the charge distribution for two symmetry planes in cyclopropane, C_3H_6 .

(a) The plane containing the three carbon nuclei. In the centre of the ring is a (3,+1) critical point. Black dots mark the positions of (3,-1) critical points.

(b) A σ_v symmetry plane containing a carbon nucleus and its associated protons. The lower (3,-1) critical point is the bond critical point between the two other out of plane carbon atoms.



(a)



(b)

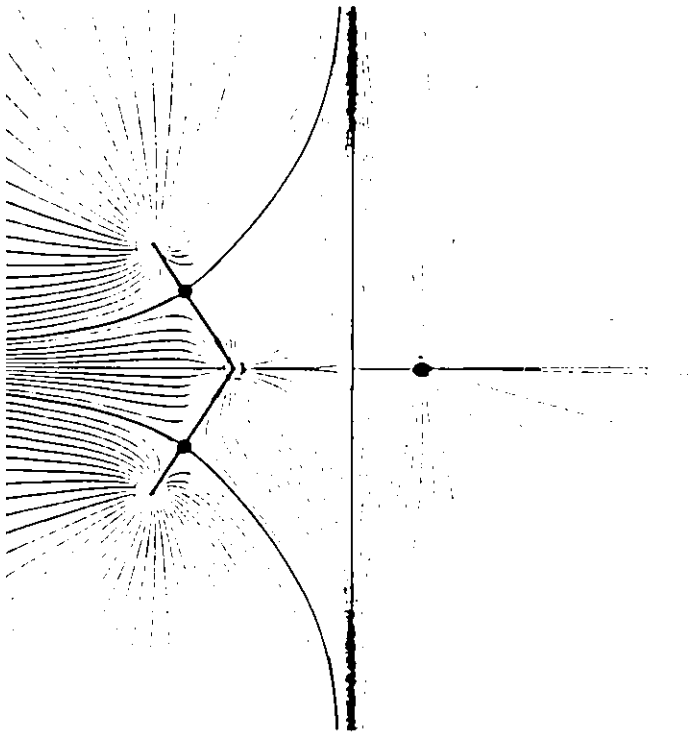


Figure II.3

Gradient vector field (a) and contour plot (b) of the electronic charge distribution in tetrahedrane, C_4H_4 . The critical point at the centre of the cage is a (3,+3) critical point which is common to all four carbon nuclei. The upper (3,-1) critical point is the bond critical point between the two out of plane carbon nuclei.

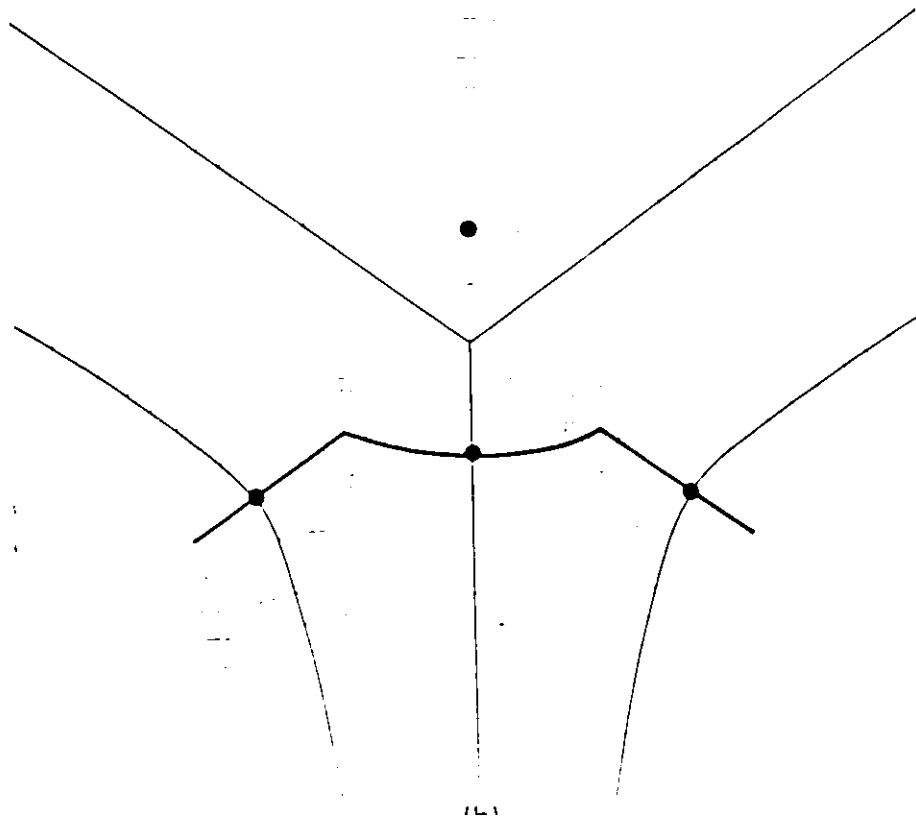
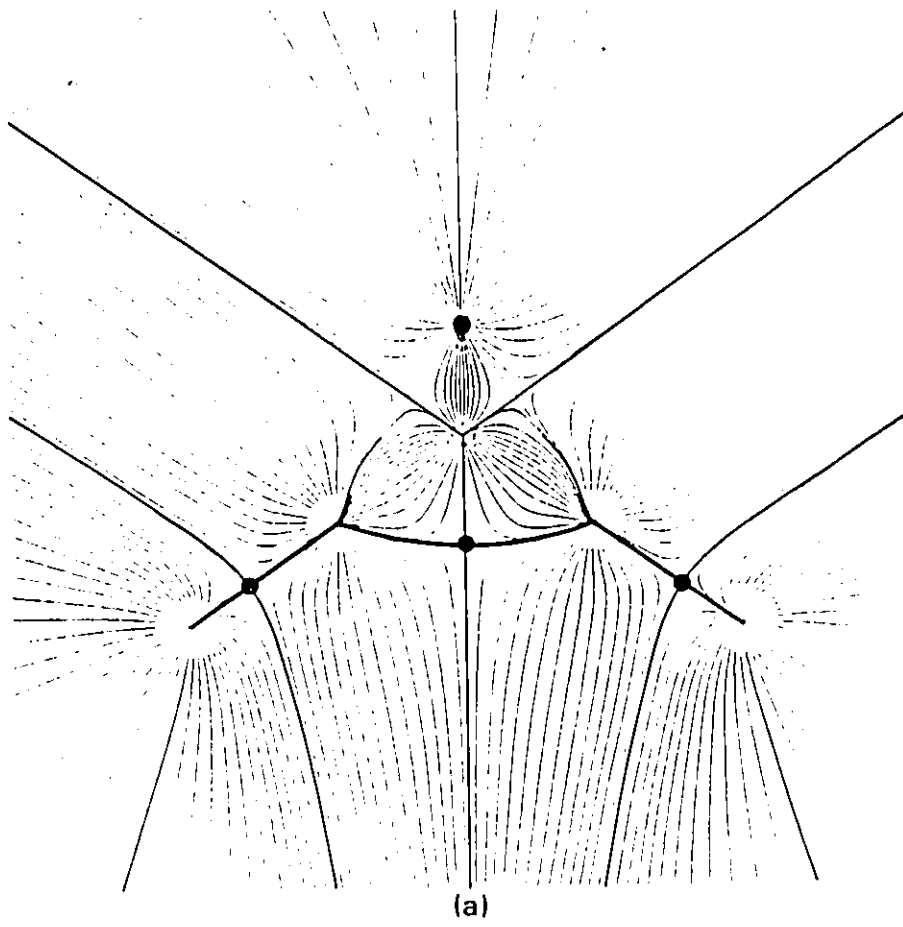
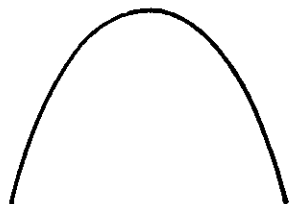
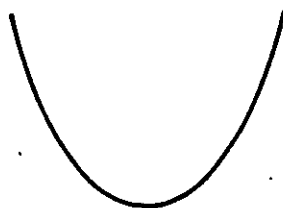


Figure II.4

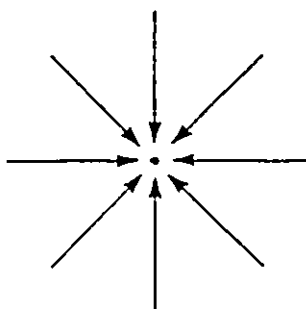
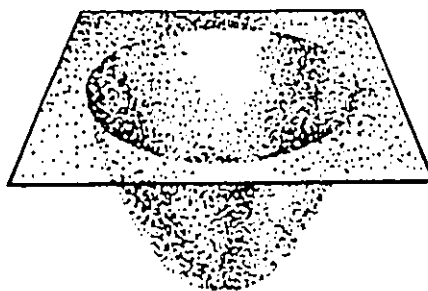
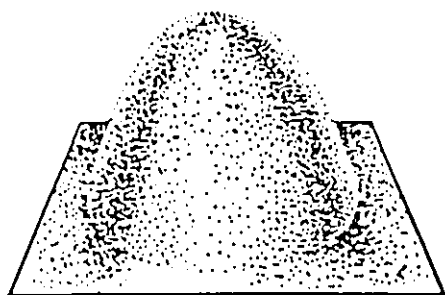
Phase portraits of the gradient vector field illustrating the behaviour of gradients paths originating or terminating from critical points. Direction of the gradient vectors are represented by the arrows. The dot surface representation above each phase portrait shows the appearance of the charge distribution itself.



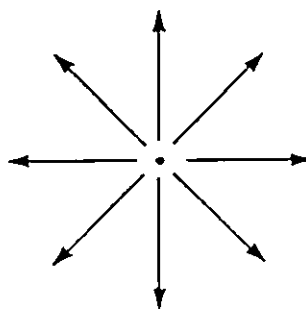
$(1, -1)$



$(1, +1)$



$(2, -2)$



$(2, +2)$

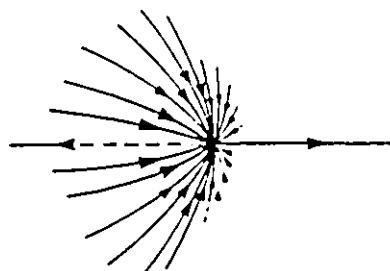
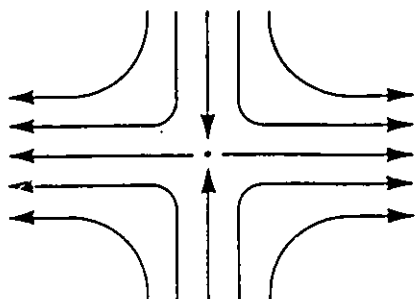


Figure II,5

Gradient vector field displays of ethylene, C_2H_4 .

- (a) Only trajectories that terminate at the positions of the nuclei are shown. The set of trajectories that terminate at a given nucleus or attractor defines the basin of that attractor.
- (b) Same as above but with trajectories which originate or terminate at the (3,-1) critical points included. The two trajectories that terminate at the (3,-1) critical points indicates the intersection of the interatomic surface with the plane displayed. Those gradient paths which originate from the (3,-1) critical point and terminate at a neighboring nucleus define the bond paths linking the nuclei.
- (c) Superposition of the trajectories originating or terminating at the (3,-1) critical points on a contour map of the charge distribution. These trajectories define the boundaries of the atoms and the molecular graph.

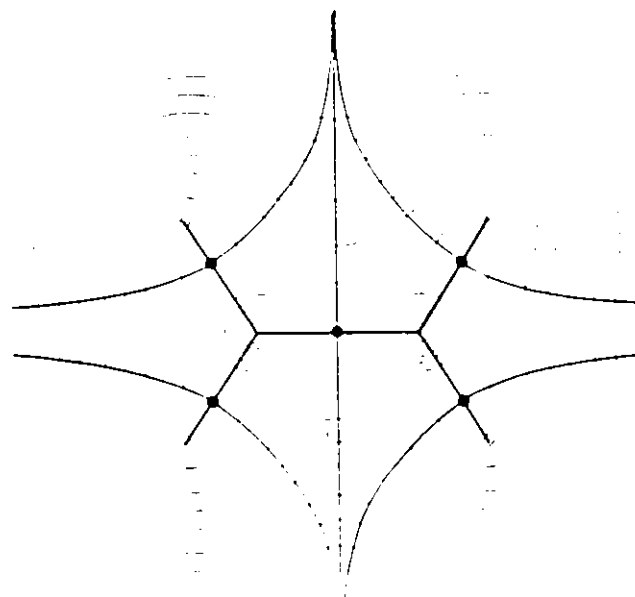
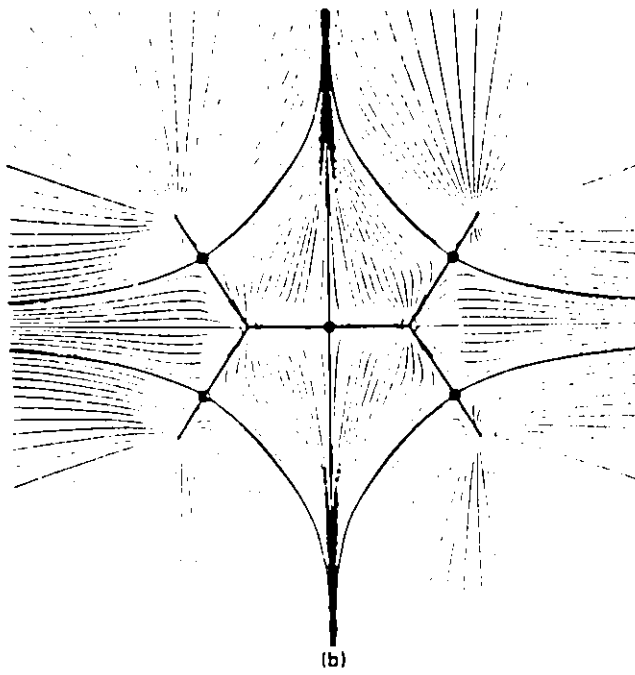
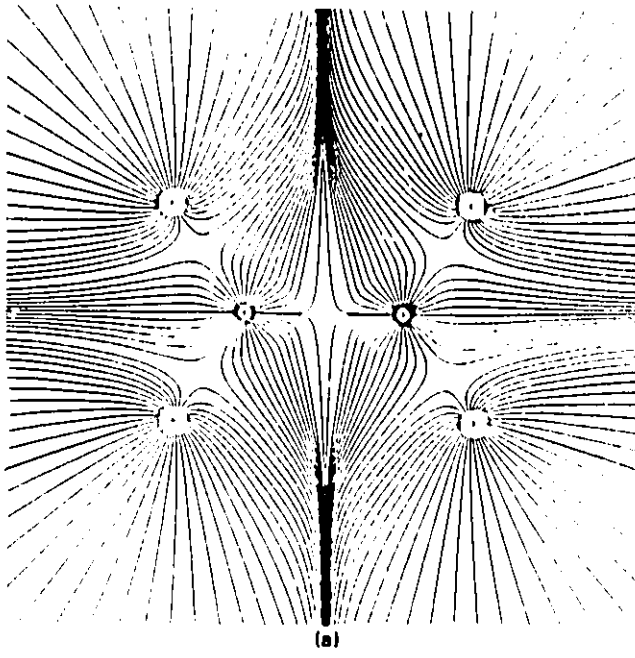


Figure 11.6

Molecular graphs for a variety of molecules in the equilibrium geometries.

Bond critical points are indicated by a black dot.

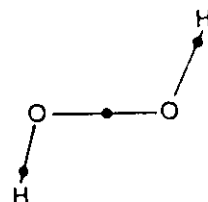
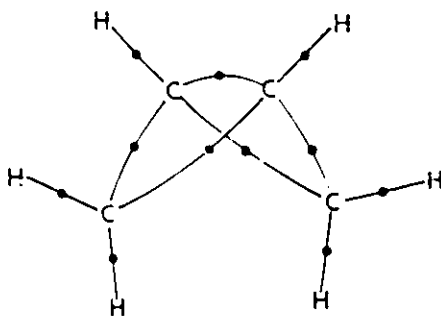
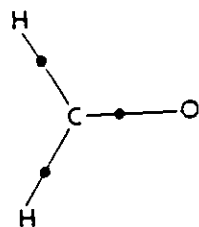
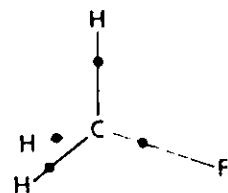
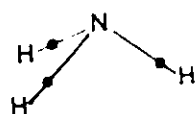
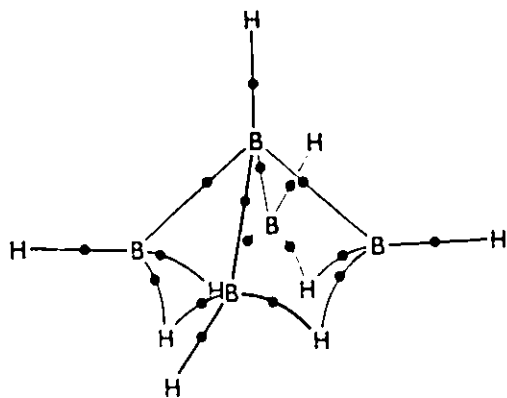
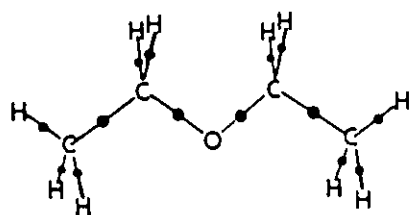
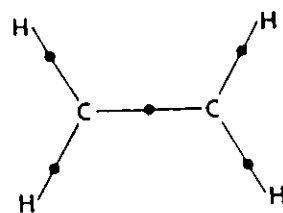
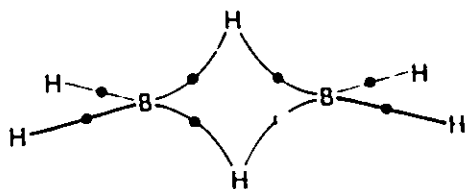
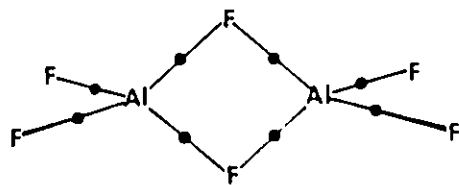
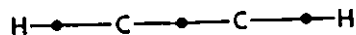
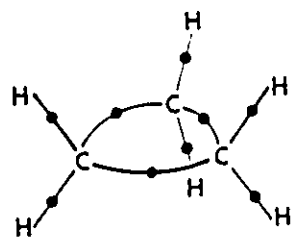
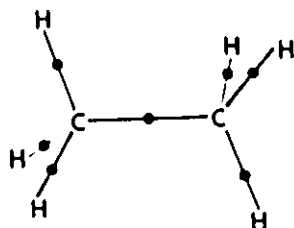
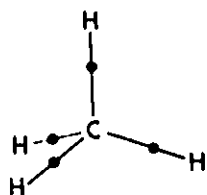
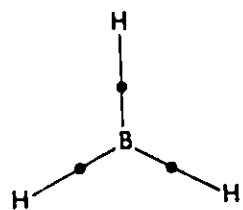
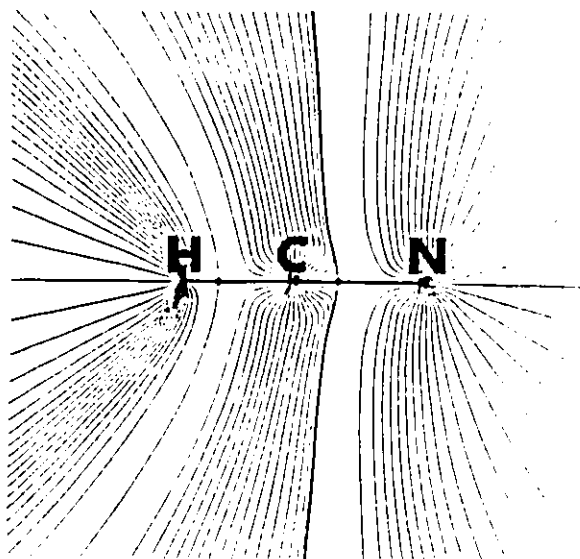
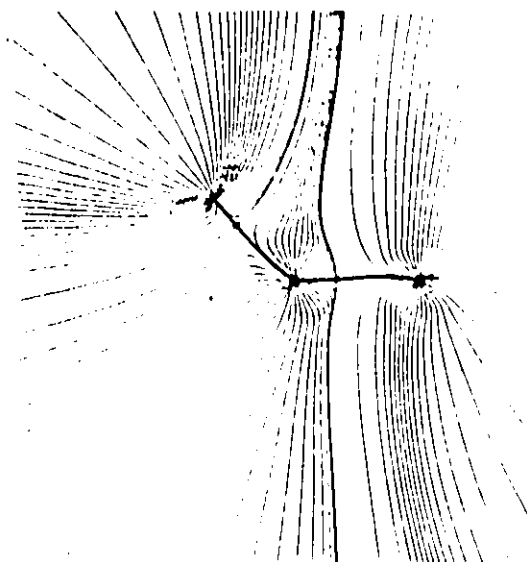


Figure II.7

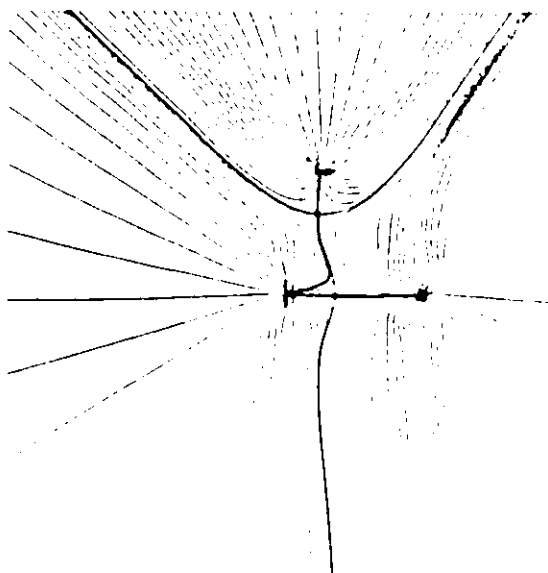
Gradient vector fields along the reaction coordinate for the thermal isomerization of isocyanide, CNH. Molecular graphs for each configuration are also shown. These molecular graphs illustrate one of two mechanisms for structural change, the conflict mechanism.



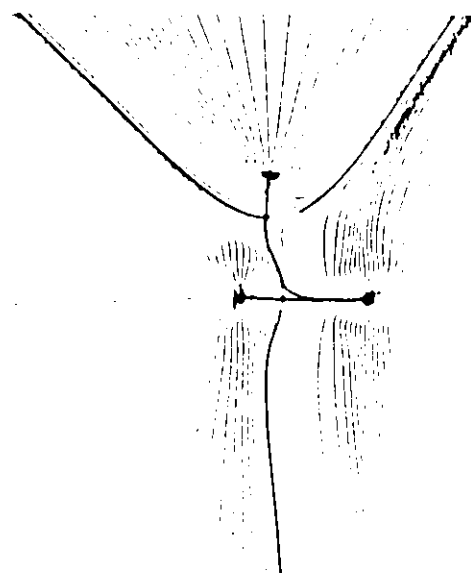
0.0



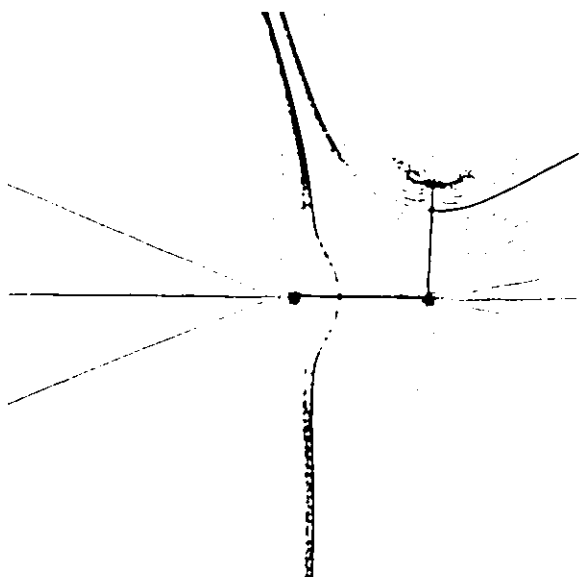
30.0



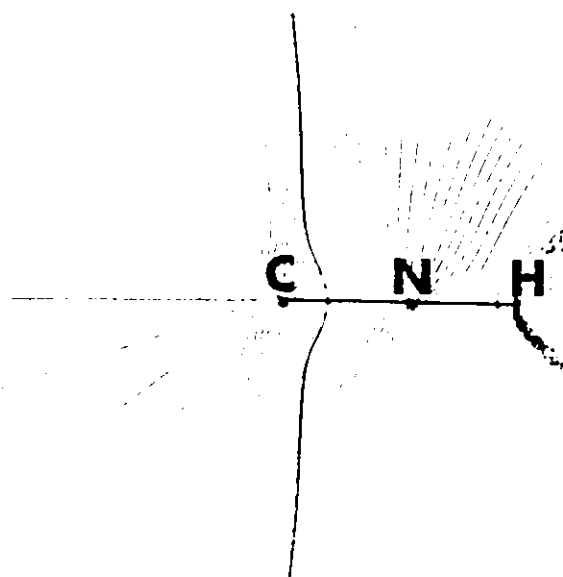
72.1



72.4



120.0



180.0

Figure 11.8

Molecular graphs, a-c, of three geometries of the [1.1.1]propellane molecule. Bond paths for the CH bonds are not shown. The dotted lines represent profiles of the ring surfaces.

- (a) The equilibrium geometry. Bond critical points are shown as black dots. The structure is three rings sharing a common bridgehead bond.
- (b) The bridgehead distance has been increased until the three ring critical points and the bridgehead bond critical point have coalesced, shown as a black square. This is an unstable structure as any motion of the carbon nuclei will change the structure.
- (c) On further increasing the CC bridgehead distance, the singularity bifurcates, forming three new ring critical points and a cage critical point.
- (d) Contour plot of the charge distribution for a symmetry plane of [1.1.1]propellane containing the bridgehead bond. The ring critical point is shown as a black triangle. Attention is drawn to the proximity of the ring critical point to the bridgehead bond critical point.
- (e) Contour plot of the symmetry plane in cyclopropane containing the three carbon nuclei. This plot is given for comparison with that in (d)

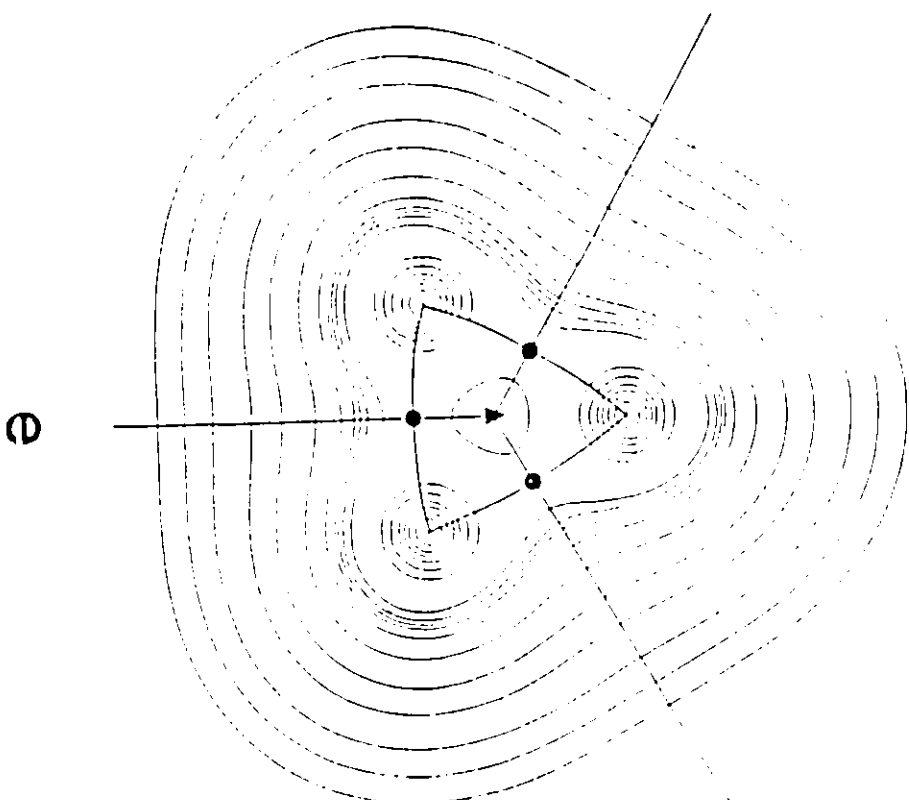
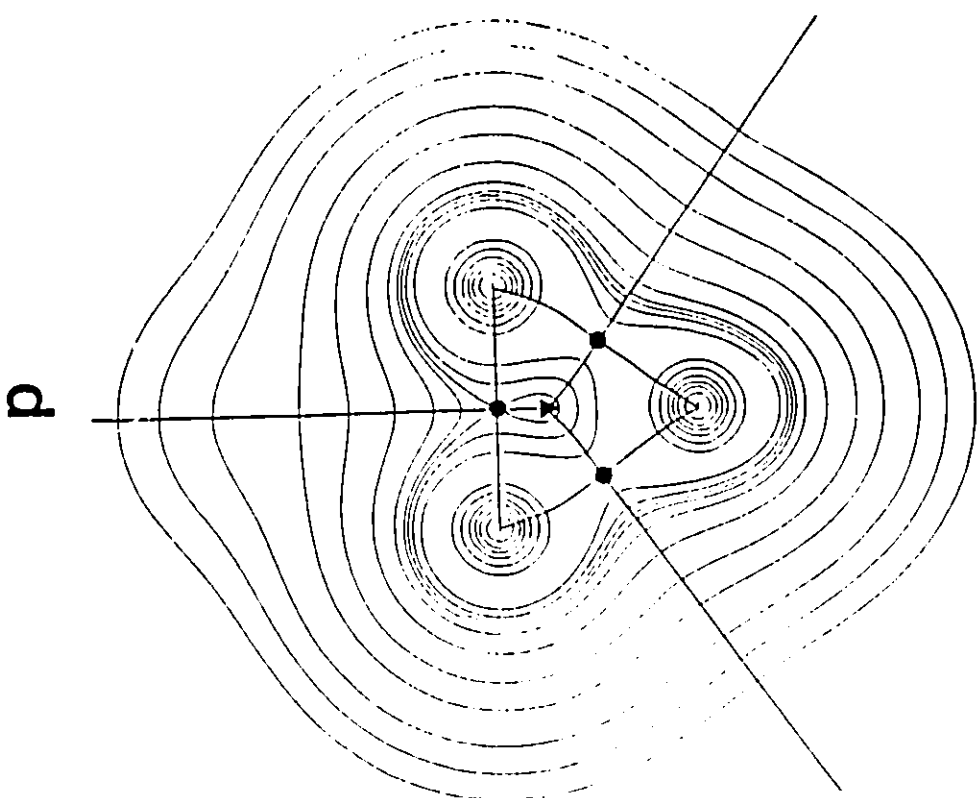
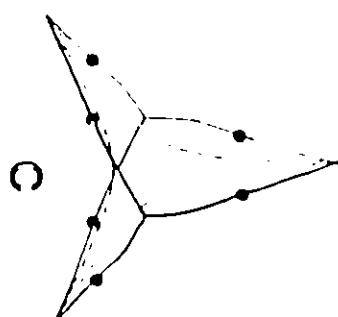
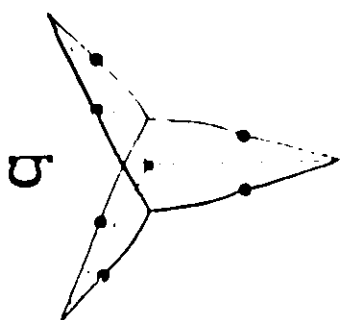
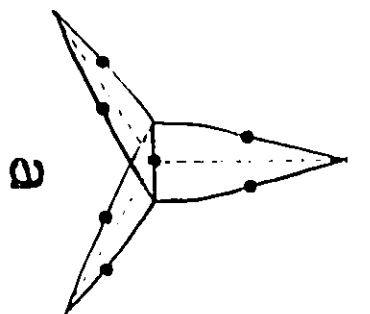


Figure II.9

Profile of the charge distribution along the direction of approach of a ring critical point to a bond critical point. This illustrates the second mechanism for structural change, the bifurcation mechanism.

- (a) Shortly after coalescence of the ring with the bond critical point.
- (b) At the point of coalescence of the ring and bond critical point. The new critical point formed is marked by a star.
- (c) Prior to coalescence. The ring critical point appears as a minimum while the bond critical point appears as a maximum.

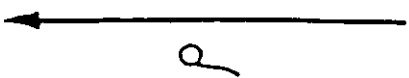
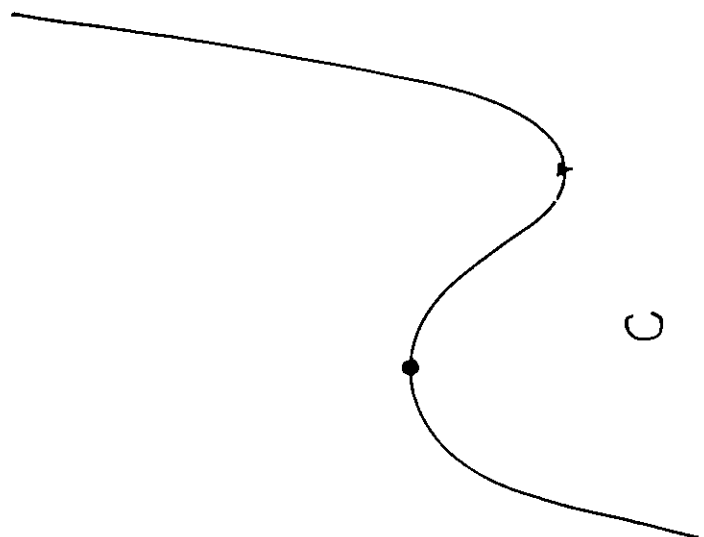
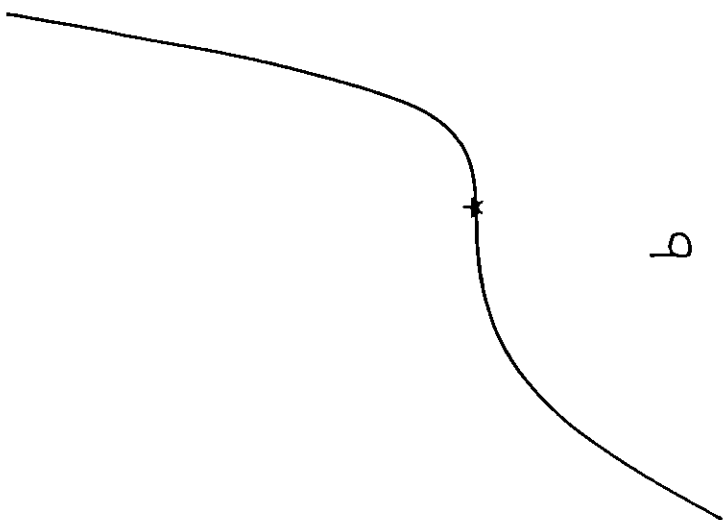
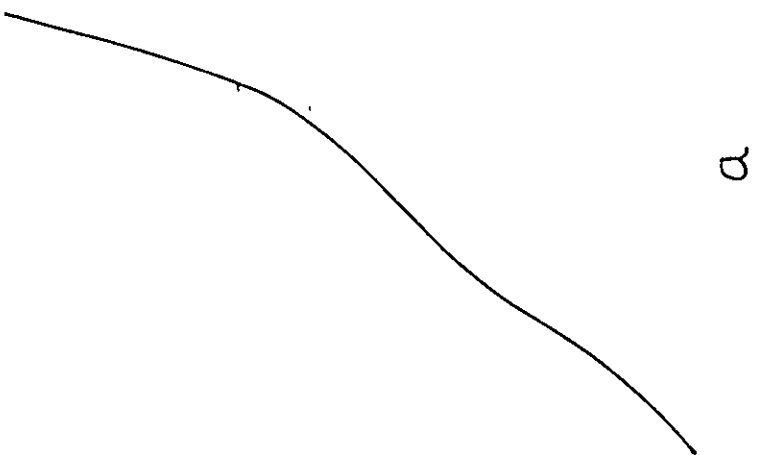
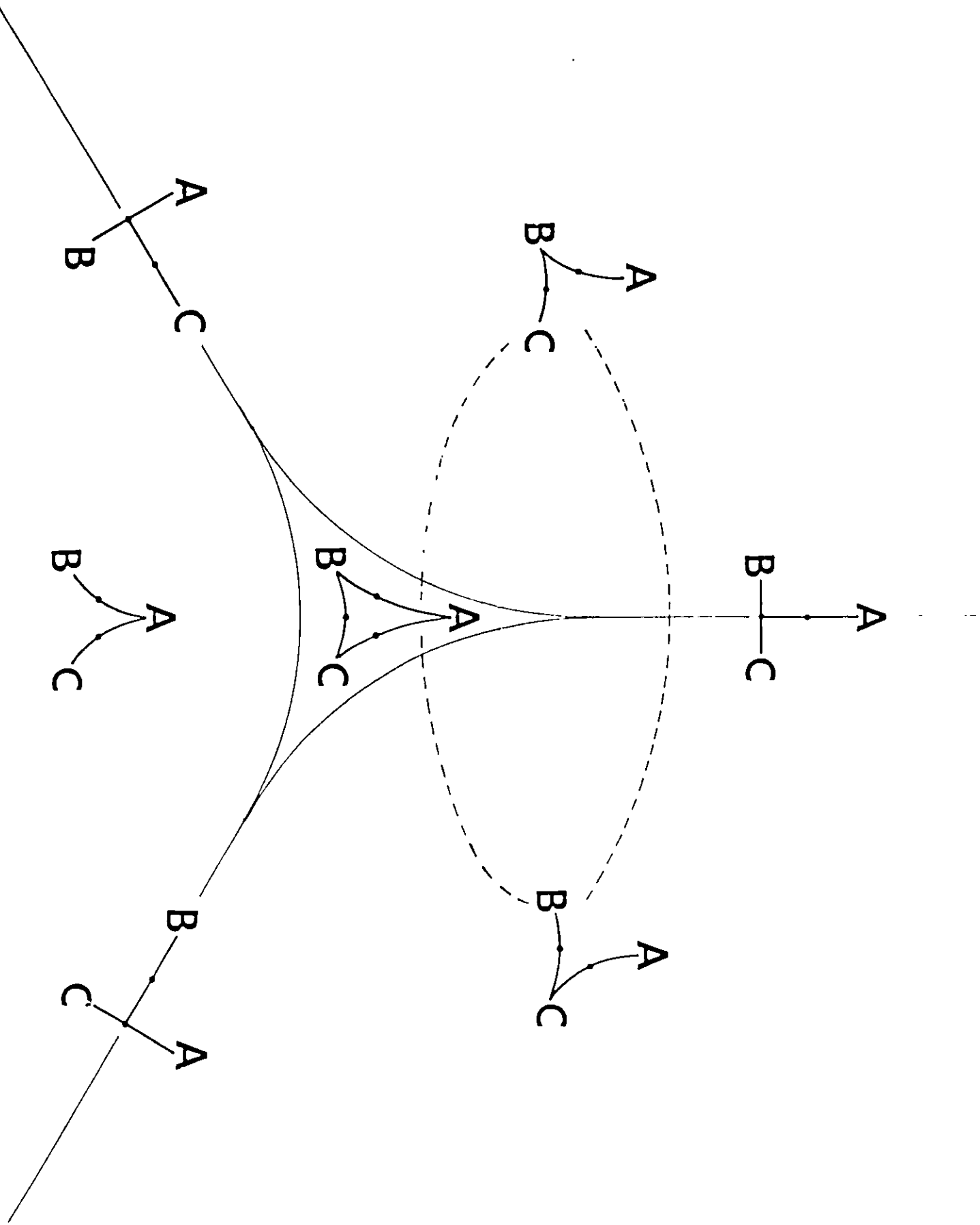


Figure II,10

A two dimensional cross section of the structure diagram for an ABC system. The full lines, denoting the catastrophe set, partition nuclear configuration space into its structural regions. The structure associated with each structural region is indicated by a representative molecular graph. The two dotted lines show the two possible mechanisms for structural change on going from the ABC structure to a BCA structure.



CHAPTER III

Study of Hydrocarbons: Atoms, Bonds, Structure and Structural Stability

1. Introduction

Chapter I outlined the quantum mechanical basis for the definition of atoms in molecules, structure and structural stability. Also defined were atomic properties, with special attention given to atomic energies. In this and subsequent chapters, a study of twenty six hydrocarbon molecules using these definitions will be discussed. This study will apply the concepts developed in the previous chapter to the understanding of bonding and structure in a number of hydrocarbon molecules. This group of molecules studied is comprised of eight normal alkanes, four cycloalkanes, seven bicyclic alkanes, four propellanes, tetrahedrane, spiropentane and cubane. The eight alkanes are methane, ethane, propane, butane, pentane, isopentane, neopentane and hexane. The four cycloalkanes are cyclopropane, cyclobutane, cyclopentane and cyclohexane while the seven bicyclic molecules studied are bicyclo[1.1.0]butane, bicyclo[2.1.0]pentane, bicyclo[2.2.0]hexane, bicyclo[1.1.1]pentane, bicyclo[2.1.1]hexane, bicyclo[2.2.1]heptane, bicyclo[2.2.2]octane. The propellanes studied are [1.1.1]propellane, [2.1.1]propellane, [2.2.1]propellane and [2.2.2]propellane. The distinguishing feature between the bicyclic compounds and their propellane counterparts is the presence or absence of the bridgehead bond. This feature will be examined closely and illustrated with [1.1.1]propellane and bicyclo[1.1.1]pentane.

2. Application of Theory

A. Atoms, Bonds and Structure

For each of the above molecules, wave functions were calculated using the computer program GAUSSIAN86. In most cases these wave functions were obtained by using the $6-31G^*$ basis set at the corresponding optimized geometry (Wiberg and Wendoloski 1982, Wiberg 1983, Wiberg et al 1983). These calculations are denoted $6-31G^*/6-31G^*$. In a few cases, namely for the molecules 11, 15, 17 and 22, the $6-31G^*$ basis was used at the $4-31G$ optimised geometry and these calculations are denoted $6-31G^*/4-31G$. The differences between the $6-31G^*$ and $4-31G$ geometries are generally quite small (Ibrahim and Schleyer 1985). A partial comparison is made between $6-31G^{**}/6-31G^*$ and $6-31G^*/6-31G^*$ results given in the following Chapter. All the critical points of each molecule can be quickly found using a computer program which searches the charge density for points \underline{r} that have $\nabla\rho(\underline{r}) = 0$. Upon locating these critical points, a full characterization is done. The rank and signature of the Hessian at each such point is determined so that the critical point can be classified by its type. The values of properties such as the charge density at this critical point are determined. Identification of the individual component atomic fragments that make up the particular molecule under study can then be done. All bond paths and atomic basins are identified. The structure of the molecule is now known.

The structures of the molecules studied here are shown by their molecular graphs which are displayed in Figure III.1. It is seen that the molecular graphs coincide in the most part with the traditional idea as to the "structures" of these molecules. Methane's structure is seen to

consist of the network of tetrahedrally arranged carbon to hydrogen bonds. The structures of the propellanes and their corresponding bicyclic compounds give examples of ring and cage structures. The structure of the propellanes studied here consist of a three rings which share a common bridgehead bond, each ring being either three or four membered. The three rings in the propellane structures share one common bond, namely the bridgehead bond. Addition of a molecule of hydrogen across this bond yields the corresponding bicyclic molecule. The structures of the carbon framework found in the bicyclic molecules ,16-19, differ from those of their propellane counterparts in a most important aspect, the absence of the bridgehead bond. It should be noted here that the theory determines the structure of a molecule and hence is able to discern between the structural differences occurring in any set of molecules.

A wider variety of structures are displayed by the bicyclic molecules. Whenever a set of rings enclose a region of space to form a closed or cage structure, a (3,+3) critical point is found inside this cage. Structures 16 and 19 are cage structures. The cage is bounded by three ring surfaces which are curved in these cases as the ring critical point is deflected away from the geometric surface defined by the nuclei making up the ring. These three rings enclose the cage critical point. As the signature of this critical point indicates, this point is a minimum in the charge density. All three orthogonal directions away from this cage critical point leads to an increasing charge density.

Structure 18 Bicyclo[2.2.1]heptane is an open structure, there are only two five membered rings sharing a common apex and there is no cage critical point for this molecule. Structure 17, Bicyclo[2.1.1]hexane,

exhibits two rings but is not an open structure as 18 is. Bicyclo[2.2.1]hexane, more commonly known as norbornane, is of C_{2v} symmetry and has two ring critical points along the two fold axis. The gradient vector field in the plane containing these two ring critical points shows that they are connected by a gradient vector. This situation is a topologically unstable one as any unsymmetrical motion of the carbon nuclei will change this structure into either a cage or open structure.

B. [1.1.1]Propellane as an Example

The propellanes and their bicyclic congeners exemplify the contrasting behaviour exhibited by the charge density between a pair of nuclei in situations where the atoms are and are not bonded to one another. Figure III.2 gives relief maps of the charge density in the plane which bisects and is perpendicular to the bridgehead internuclear axis for each propellane and its bicyclic analogue. Such a plane contains the critical point in the interatomic surface between the bridgehead atoms. It also contains the critical point in the interatomic surface between the methylenic carbon atoms linked by a peripheral bond and/or the C and H nuclei of a peripheral CH_2 group in the case of three-membered ring in a propellane or corresponding group in the bicyclic molecule. The charge density is a maximum at a bond critical point in the interatomic surface. Thus the diagrams for the [2.2.2]propellane and bicyclo[2.2.2]octane systems shown in Figure III.2a both exhibit three maxima in the charge density corresponding to the three peripheral bonds between the methylene groups. These maxima in bonded density are replaced by the nuclear maxima of a CH_2 group in [1.1.1]propellane. The purpose of the

diagram is to contrast the behaviour of the charge density at the bridgehead critical point for the propellanes with that found for the bicyclic molecules. In the propellanes which possess a bridgehead bond, the charge density is a maximum at this point, while in the bicyclic molecules which do not possess a bridgehead bond, the charge density is a minimum at this same point. In the propellane molecules there is a line of maximum charge density linking the nuclei. However, in the bicyclic molecules such a line is absent and the charge density is instead a local minimum at the central critical point. There is, therefore, an essential, qualitative difference in the manner in which electronic charge is distributed along a line linking a pair of bonded nuclei (as between the bridgehead nuclei in the propellanes) as compared to that linking two nuclei that are not bonded (as between the nuclei in the corresponding bicyclic structures).

In addition to the fundamental difference in the form of the bridgehead charge density between the two sets of molecules, there are also substantial quantitative differences in the values of ρ . The value of ρ at the bond critical in [1.1.1]propellane is 0.203 au, four-fifths the value of a normal C-C bond while the value of ρ at the corresponding cage critical point in the bicyclic molecule is 0.098 au. It is also clear from Figure III.2 that the values of ρ at the bond critical point and the three adjacent ring critical points are almost equal, giving rise to a very broad bonded maximum in ρ in the bridgehead interatomic surface in [1.1.1]propellane.

The fundamental difference in the manner in which electronic charge is distributed in the bridgehead internuclear region, between the

propellanes and the corresponding bicyclic molecules, is not made apparent in density difference maps (Dunitz et al 1983). Such deformation maps show a region of charge depletion between these nuclei for the propellanes as well as for the bicyclic molecules. First, there is no physical basis for demanding that a density difference map in polyatomic molecule show a charge buildup between a pair of nuclei if the nuclei are to be considered bonded to one another. Second, the reference density, in addition to being physically non-realizable, is arbitrary in its construction. Different results are obtained and different conclusions are reached depending on whether one uses spherical atom densities or densities of atoms in prepared valence states in the construction of the promolecule density. Third, in performing a comparison between density difference maps for pairs of molecules, [1.1.1]propellane and various cyclic and bicyclic molecules for example, one is actually comparing four different charge distributions. It is clear that the spherical atom promolecule density for bicyclo[1.1.1]pentane will, because of the larger bridgehead separation of 1.87Å, subtract considerably less charge from the bridgehead symmetry plane than will the corresponding promolecule density for the equilibrium geometry of [1.1.1]propeilane where the corresponding separation is calculated to be 1.54Å. Thus the observation of an "essential similarity" (Newton and Schulman 1972. Jackson and Allen 1984) in the deformation density distributions for these two molecules, in particular the lack of a charge buildup between the bridgehead nuclei, is an artifact of the promolecule distributions and is not a reflection of the relative properties of the two charge distributions of interest. Qualitatively and of fundamental

importance, the propellane molecule does accumulate charge at the bond midpoint and along the resultant bond path, while the bicyclic compound exhibits a local minimum in ρ in this same region. In addition, as demonstrated by a direct quantitative comparison of their charge distributions, the bicyclic molecule has significantly less charge in this region than does the propellane molecule. These essential observations are lost in a comparison of the deformation densities because the reference density for propellane removes more charge from the critical bridgehead region than does that for the bicyclic molecule. Why complicate a comparison of two distributions through the introduction of two more distributions which are arbitrary in their definition and are of no direct physical interest?

C. Bond Order

Properties of the charge density at the critical points are useful in characterizing the molecule. Using the value of charge density at the bond critical point, denoted ρ_b , it is possible to assign bond orders (Bader et al 1983). The empirical relationship between ρ_b and the bond path distance R_b has been found to be of the form (Bader et al 1983)

$$n = \exp\{A(\rho_b - B)\} \quad (64)$$

where the constants A and B are determined by a least squares analysis. These constants will be unique to the basis set used in a particular study as the actual value of $\rho(\underline{r})$ will vary from one basis set to another. This variation occurs in a very well behaved manner. Trends observed in one

basis set will still be observed at another basis. The bond order relationship for the 6-31G* basis set used in this investigation has constants $A=6.458$ and $B=0.2520$. This yields the equation:

$$n = \exp(6.458(\rho_b - 0.2520)) \quad (65)$$

where n is the bond order. This expression yields values of 1.00, 1.62, 2.05, 2.92 as values of n for the C-C bond in ethane, benzene, ethylene and acetylene respectively. Empirical bond orders so derived provide for a convenient measure of the extent to which charge is accumulated between pairs of bonded nuclei relative to standard values. The values of the properties of the charge density at the bond critical points for all the molecules studied are given in Table III.1. In the acyclic hydrocarbons, interior bonds and bonds in the branched structures have the highest bond orders with $n = 1.02$ to 1.03. Bond orders slightly less than unity are found for C-C bonds in the cyclic and bicyclic molecules. The smallest values for the bond order are found for the bridgehead bonds in [1.1.1] and [2.1.1]propellane. In [2.2.2]propellane the value for ρ_b is relatively high and yields a bond order of 1.26. There is not a simple correlation between bond order and bond length. A smaller bond length R_e does not necessarily imply a greater accumulation of charge along the bond path. Take a C-C bond in a branched alkane as an example. Although R_e is longer in the branched alkane than in ethane, the C-C bond has an order greater than unity. On the other hand, the C-C bonds in cyclopropane are shorter than that of ethane yet they are of order one.

The values of the charge density at the bond critical point, ρ_b , for the C-H bonds vary over a much smaller range of 0.2772 to 0.2790. They are formally all of order one but trends still exist. For instance, R_b increases in the order $\text{CH}_4 < \text{CH}_3^- < \text{CH}_2^- < \text{CH}^-$. Still larger values of ρ_b can be found for the C-H bonds in cyclopropane, but this value decreases as ring size increases. These values decrease to the extent that for cyclohexane, the value of ρ_b is in the acyclic range. The C-H stretching frequency in cyclopropane is larger than that of any acyclic alkane, reflecting the larger ρ_b . As anticipated, the decrease in the value of ρ_b as ring size increases from cyclopropane to cyclohexane is accompanied by the corresponding decrease in the C-H stretching frequency (Wong et al 1982).

D. Bond Path Angle

In structures where the geometry of the molecule precludes tetrahedrally directed bonds, the bond paths are noticeably curved. (Runtz et al 1977) The bond path angle α_b is the limiting value of the angle subtended at a nucleus by two bond paths. The geometrical angle α_e is the limiting value of the angle subtended at a nucleus by the straight lines joining the bonded nuclei. Define the difference in these angles $\Delta\alpha = \alpha_b - \alpha_e$. This value $\Delta\alpha$ is a measure of the degree of relaxation of the charge density away from geometrical constraints imposed by the nuclear framework. The length of the bond path, R_b , will also differ from the geometric distance R_e for these curved bond paths (Bader et al 1982). Values of α_e , α_b , $\Delta\alpha$ together with the strain energies (Wiberg 1986) as calculated using Franklin's group equivalents (Franklin 1949) are tabulated

in Table III.2 for the cyclic, bicyclic and propellane molecules under study. For most molecules, the value of $\Delta\alpha$ is positive, indicating that the bonds in these molecules are less strained than the geometric angle α_e suggests. In cyclopropane for example, $\Delta\alpha$ has a value of 18.8° and the deviation of the angle formed by the bond paths from the normal tetrahedral angle is correspondingly less, $\alpha_b = 78.84^\circ$ while $\alpha_e = 60.00^\circ$. As the ring size gets larger, this difference decreases. In cyclobutane, $\Delta\alpha = 6.1^\circ$ and becomes small and negative for five and six membered rings. There is a corresponding decrease in the value of the strain energy. Even though α_b for cyclopropane is smaller by almost 30° as compared to cyclobutane, both these molecules have similar strain energies. This similarity is accounted for in part by the much greater relaxation of angle strain between the bonds in cyclopropane and a more detailed discussion of bond energies will follow.

The value of $\Delta\alpha$ exceeds 10° only for three membered rings. Values of $\Delta\alpha$ are the largest in tetrahedrane, $\Delta\alpha = 21^\circ$, and in spiropentane where $\Delta\alpha$ for the angle formed by the bonds terminating at the central carbon has the value of 23° . Despite the large relaxations reflected by these large values of $\Delta\alpha$, the strain energies for these two molecules are large in comparison to cyclopropane as a prototype. In these two molecules, the carbon atoms making up the rings are common to two three membered rings in the case of the central carbon of spiropentane, or three rings as in tetrahedrane. These additional constraints result in an increase in the strain energy which can be observed to an even greater extent in bicyclo[1.1.0]butane as well as in the propellanes. When three rings are fused to a common bridgehead bond, the ability for relaxation of the

charge density to relieve geometric strain is inhibited. This inhibition decreases as ring size increases. Therefore, the apex angle of the three membered rings for [1.1.1]propellane exhibits a $\Delta\alpha$ that is small and negative while that for [2.1.1]propellane is small and positive. In [2.2.1]propellane there is observed a larger degree of relaxation as evidenced by the larger $\Delta\alpha$ for the apex angle of the three membered ring. For the angles made by the bond paths terminating at a bridgehead carbon, the value of $\Delta\alpha$ in both [1.1.1] and [2.1.1]propellane is quite large, resulting in these angles deviating only by 1° from the 109° tetrahedral angle. The corresponding bond paths forming these angles from three and four membered rings as in [2.2.1]propellane or from two four membered rings found in [2.2.2]propellane show a much smaller $\Delta\alpha$, indicating a lesser degree of relaxation in these two molecules. Values for $\Delta\alpha$ found in the propellanes can be compared to those found in their respective congeners. In bicyclo[1.1.1]pentane, the value of α_b is found to be 96° , giving a $\Delta\alpha$ of 8.65° which is larger than that found for [1.1.1]propellane and indicates that the degree of strain in these bonds is greater.

E. Bond Ellipticity

Another property of the charge density at the critical point is the ellipticity at that point. The bond ellipticity is defined to be

$$\epsilon = \lambda_1/\lambda_2 - 1 \quad (66)$$

where λ_1 and λ_2 are the two negative eigenvalues of the Hessian matrix,

with λ_2 being the smallest in magnitude. The ellipticity gives a measure of the preference for accumulation of charge in a given plane (Bader et al 1983). As charge is accumulated preferentially in a particular plane, the rate of decrease of the value of $\rho(r)$ in that plane is reduced, hence a lower magnitude of the eigenvalue associated with that eigenvector. The axis of the curvature λ_2 , the principle axis, determines the relative orientation of this plane within a molecule. In ethane for example, there is cylindrical symmetry and hence the ellipticity for the CC bond is 0 as the two eigenvalues are symmetrically equivalent. Ethylene on the other hand has a CC bond ellipticity of 0.45, reflecting the accumulation of charge in the perpendicular, or π , plane. For the basis set used in this study, namely the 6-31G* basis, the ellipticities of the C-C bonds in ethane, benzene and ethylene are 0.0, 0.23 and 0.45 respectively. In the latter two cases the principle axis is in the direction perpendicular to the molecular framework, as anticipated for these molecules with π bonding. The ellipticity is useful in understanding the chemistry of the three-membered ring. When comparing the values of the charge density, ρ , at a ring critical point, denoted ρ_r , to values of ρ at the bond critical point, ρ_b , one finds that these values are generally only slightly less than, and in some cases almost equal to ρ_b for the peripheral bonds in three-membered rings. These values are tabulated in Table III.1. As ring size increases, so does the difference between these two values. Since electronic charge is concentrated appreciably in the plane of the ring, the peripheral C-C bond critical points have large ellipticities and their principal axes lie in the plane of the ring. In hydrocarbons, this is a unique feature found only in three-membered rings. This accumulation of

charge over the entire surface of the ring accounts for the well documented ability of three-membered rings to act as an unsaturated system with π -like charge distribution in the plane of the ring that is able to conjugate with a neighboring unsaturated system (Capon and McManus 1976). Molecular orbital theory accounts for this behaviour by using arguments based on the Walsh orbitals (Walsh 1947,1949). The C-C bonds of cyclopropane exhibit a larger ellipticity than that for the double bond in ethylene. This indicates an even greater accumulation of charge in the plane of the ring in cyclopropane than in the π plane of ethylene. Large ellipticities are found for bonds of three-membered rings of the bicyclic and propellane molecules, the largest being that found in the bridgehead bond of [2.1.1]propellane. This very large value indicates a potentially unstable structure. The relationship between large values of the ellipticity and ease of bond rupture in three-membered rings is well illustrated by the propellanes in the following discussion.

F. Ellipticity and Ring Bond Rupture

The value of the charge density at a critical point, ρ_b , and of ρ_r for rings, together with the ellipticity of the bonds can help determine the structural stability of a compound, in particular three membered rings. When a bond in a three-membered ring is extended, the ring critical point migrates towards the bond critical point of the bond being extended. The gradient path connecting the bond critical point to the ring originates at the ring critical point and terminates at the bond. That is to say that the charge density has a positive curvature at the ring critical point and a negative curvature at the bond critical point in the direction of their

approach. Take [2.1.1]propellane as a specific example. The values of ρ at both the bond and ring critical points are $0.1971 \text{ e}/\text{\AA}^3$ and $0.1961 \text{ e}/\text{\AA}^3$ respectively. They are separated by only 0.25\AA . Consequently, due to the proximity of the ring critical point, the magnitude of the eigenvalue associated with the eigenvector in the direction of the ring is smaller than that of the other and the bridgehead bond has a large ellipticity. This accumulation of charge in the surface of the ring, indicated by this large ellipticity, facilitates migration of the ring critical point towards the bridgehead bond critical point. For some particular extension of the bridgehead bond, the ring and bond critical points will coalesce. At this point, the value of their curvatures must be equal. Since one is positive and the other negative, on coalescence, the new critical point formed must have one zero curvature. This critical point so formed will be unstable as it possess a zero curvature and the corresponding structure therefore persists only for this particular value of bond extension. The bridgehead bond is broken at this point. Further extension of the bridgehead nuclei will cause this unstable critical point to vanish and the ring structure is changed into an 'open' structure, corresponding to the loss of the ring and one bond critical point. This mechanism of ring bond opening is an example of one of two mechanism by which structural change can occur. In this particular instance, structural change occurs by a bifurcation mechanism. For the propellanes, this resulting 'open' structure is similar to the structure of the corresponding bicyclic congener. For this example, [2.1.1]propellane will, upon rupture of the bridgehead bond, attain a structure similar to that of [2.1.1]bicyclohexane.

Consider cyclopropylcarbinyl cation, $C_4H_7^+$ as another example, which is illustrated in Figure III.3. The charge distribution for the three structures illustrated were obtained from restricted Hartree-Fock calculations using the 6-31G* (Hariharan et al 1973) basis set for 4-31G optimised geometries (Levi et al 1979) and their bond properties are listed in Table III.3. Using the appropriate values A and B for the 6-31G* basis set, bond orders have been assigned. The most energetically stable geometry of $C_4H_7^+$ is the bisected one (Levi et al 1979) shown in Figure III.4a. However, the values of ρ_b of the C1-C2, C1-C3 bonds, and for the ring critical points only differ by 0.007A. The ellipticity of the two symmetrically equivalent C1-C2 and C1-C3 bonds is found to be quite extreme at 6.7. The negative curvature of ρ at the two bond critical points and the positive curvature at the ring in the direction of the bonds are small, -0.95A and 0.51A respectively (compared to 14.74A for the C1-C4 bond). The positive curvature of the two bond critical points, which point towards the nuclei, is much larger (6.19A) and hence there is a trough in the charge density linking these three critical points and migration of the critical points towards each other is extremely facile. These factors together, the small curvatures, the small difference in the values of $\rho(r)$ at the bond and ring critical points and the high ellipticities suggest a very labile structure. Indeed, there is a second energy minimum geometry only 0.5 kcal/mol higher in energy than the bisected geometry. The structure of this second geometry is shown in Figure III.4b. The structure 4b is an open structure, where one of the labile bonds has been annihilated with the ring critical point. The remaining bond is strengthened as evidenced by the increase in the bond

order to 0.9 but the ellipticity is still quite substantial and its principal axis is directed toward the region between C3 and C1. Therefore, ρ is still relatively flat along this line and close to forming a singularity and a weak unstable link between C1 and C3. The resulting structure would coincide with Winstein's suggestion (Winstein 1967) that $C_4H_7^+$ could exhibit homoconjugation and exist as the homoallyl cation.

Besides reforming the structure **4a** by linking C3 and C1, the structure **4b** can also form the puckered cyclobutyl cation **4c** by linking C3 to C4. The geometry of the resulting structure **4c** is energetically unstable, being some 10.9 kcal/mol (Levi et al 1979) above the energy for **4a** at the 4-31G level of approximation and 3.7 kcal/mol higher at the 6-31G* level. The ring critical point which is situated on the C3 side of the C2-C4 axis has a value of only 0.40\AA^{-3} less than that of the labile bonds. This is coupled with a very small curvature of ρ in the ring surface. Thus, these bonds are of low order and possess substantial ellipticities which indicates that this structure itself is also close to an instability. An opening of the long labile bonds which have $R_c=1.65\text{\AA}$ results in a scrambling of the methylene groups (Staral et al 1978).

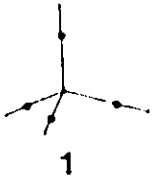
Of all the molecules under study here, the bridgehead bond of [2.1.1]propellane has the highest ellipticity and therefore has the highest potential for rupture. Examination of the properties of the bond critical point and the ring critical point (see Table III.1) reveals that λ_2 for the bond critical point is close to zero. As discussed above, on coalescence, the two critical points which merge must have the same values for their curvatures, and hence must reach a value of zero at the point of coalescence. A λ_2 value which is close to zero signals the onset

of coalescence. In this case λ_2 has a magnitude of 0.0347, as compared to 0.2820 for λ_1 . As has been previously demonstrated (Bader et al 1981b, 1982), extension of the bridgehead bond causes the ring and bridgehead bond to coalesce and form an unstable critical point which has two zero curvatures. Depending on the symmetry of the continued extension of the bridgehead bond, a number of stable structures can be formed, including a cage structure. In contrast to [2.1.1]propellane, [2.2.1]propellane having one fewer and [2.2.2]propellane no three-membered rings, exhibit a bridgehead bond with considerably reduced ellipticity. Naturally, both [1.1.1]propellane and [2.2.2]propellane are constrained by symmetry to have zero ellipticity in the bridgehead bond. However, in both these molecules, the value of ρ_r and ρ_b are not as close in magnitude as they are in [2.1.1]propellane. In fact, in [2.2.2]propellane which has only four-membered rings, the difference between ρ_r and ρ_b is quite large. On the other hand, [1.1.1]propellane exhibits ρ_r and ρ_b values of 0.1990 and 0.2030 e/a_0^3 respectively, which are quite similar in magnitude, yet through symmetrical constraint, the bridgehead bond shows no ellipticity. As suggested by their charge distributions, [2.1.1]- and [2.2.1]propellanes are relatively unstable and they are easily polymerized at 50° K. However, it is [1.1.1]propellane that is the most stable of these propellanes under study. Compared to [2.2.2]propellane, [1.1.1]propellane is more stable with respect to thermolysis (Eaton and Temme 1973). For [2.2.2]propellane it has been reported that $E_a = 22$ kcal/mol for the thermolysis of [2.2.2]propellane compared to 30 kcal/mol for [1.1.1]propellane. Stability of a molecule depends not only on the static properties of the charge distribution, but

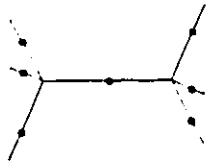
also on how the charge distribution changes with the possible nuclear motions. How the charge density changes with nuclear motion is discussed in a subsequent chapter.

Figure III.1

Planar projections of molecular graphs generated from theoretical charge distributions. Bond critical points are shown as black dots. Structures are numbered according to Table III.1.



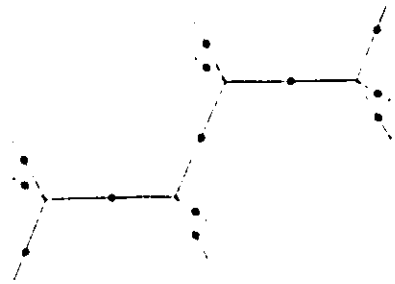
1



2



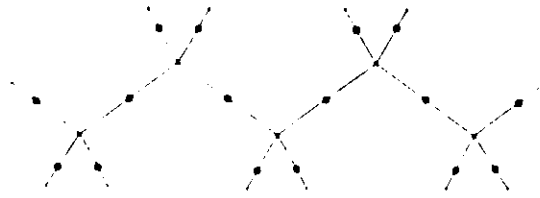
3



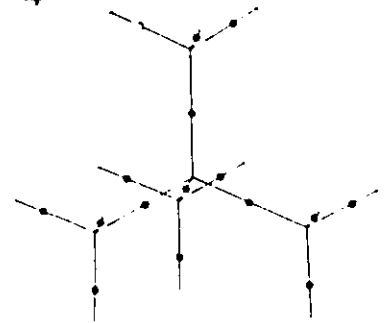
4



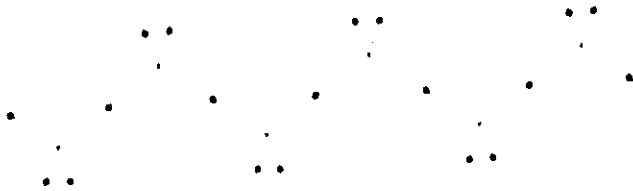
5



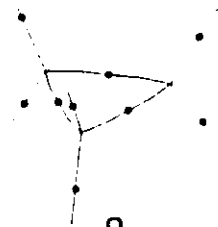
6



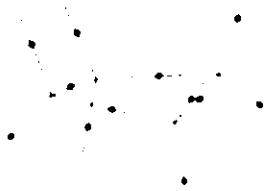
7



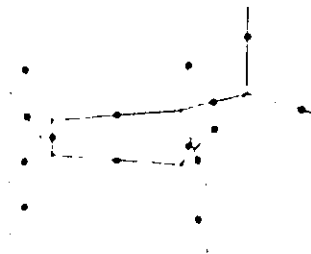
8



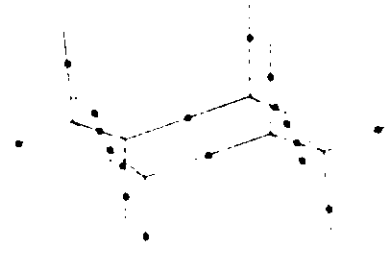
9



10



11



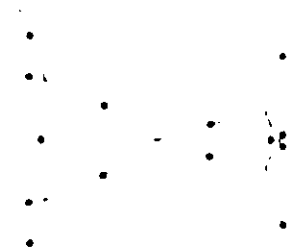
12



24



25



26

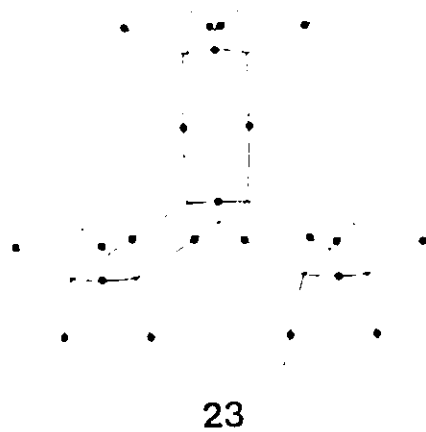
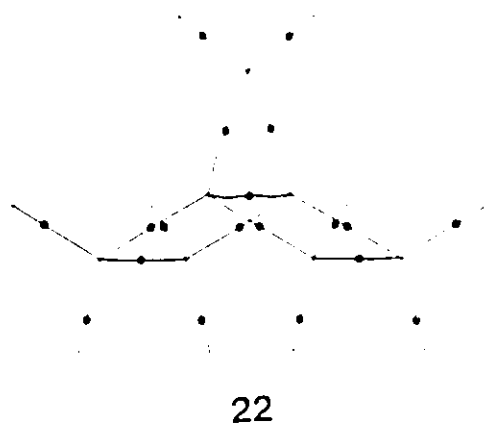
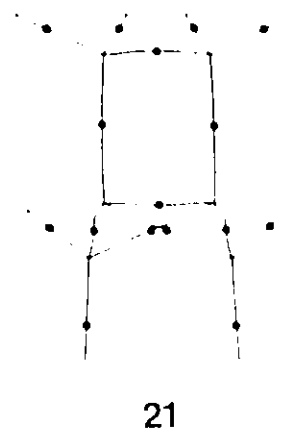
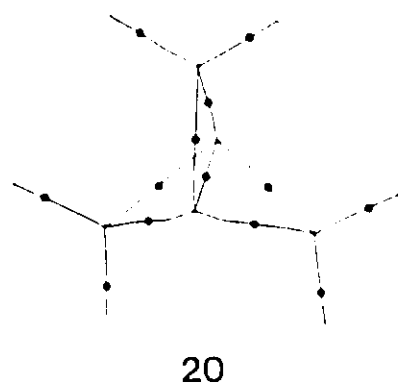
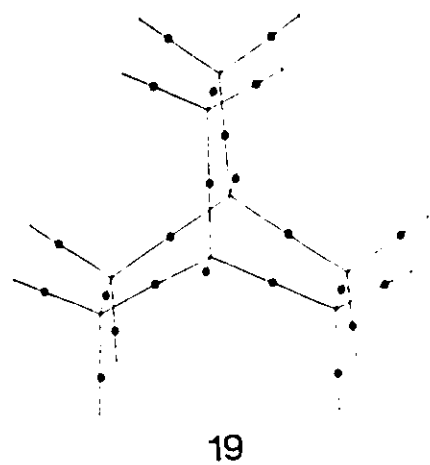
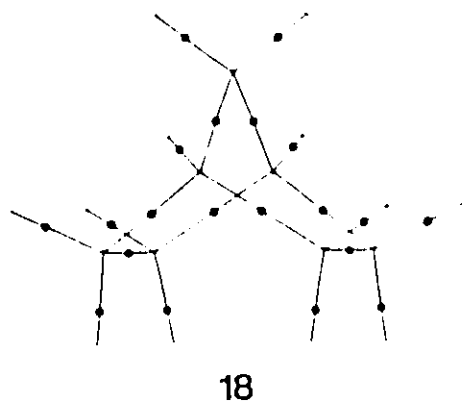
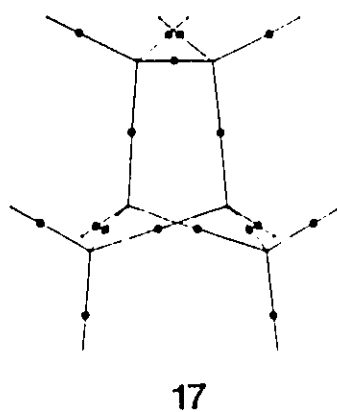
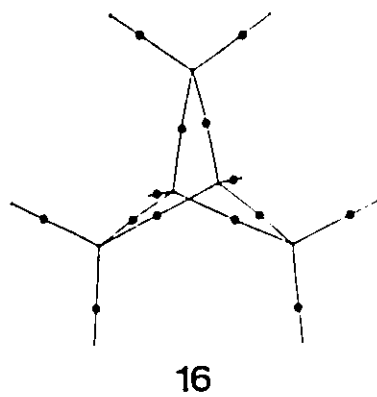
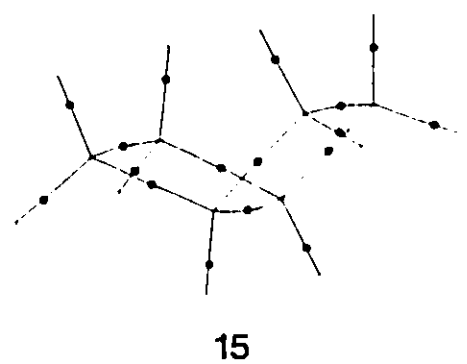
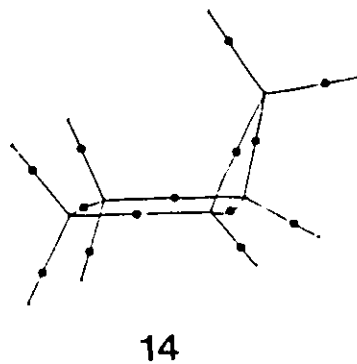
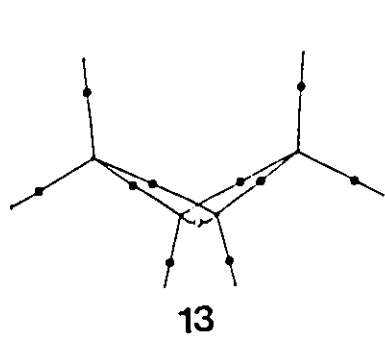
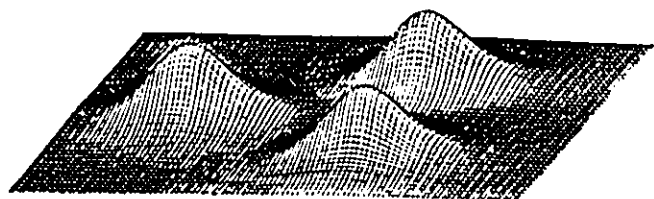


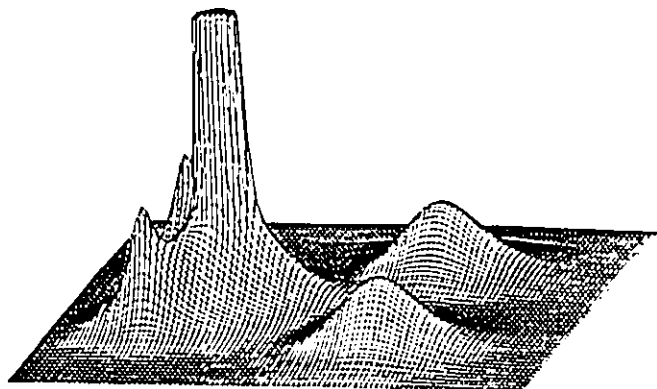
Figure III.2

Relief maps of the charge density in the symmetry plane bisecting the bridgehead bond in the propellanes on the right and the corresponding symmetry plane in each of the related bicyclic structures on the left.

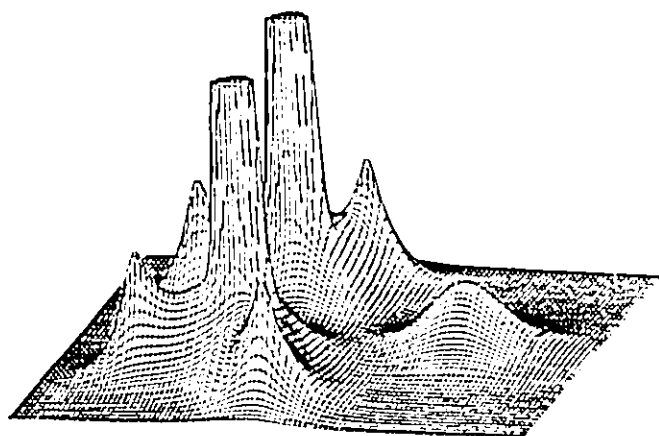
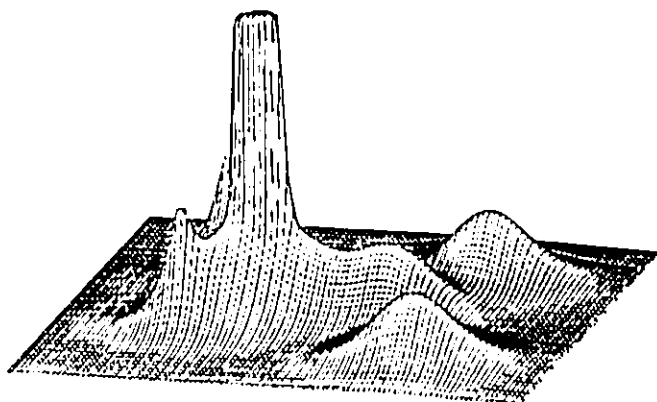
- (a) bicyclooctane and [2.2.2]propellane
- (b) norborane and [2.2.1]propellane
- (c) bicyclohexane and [2.1.1]propellane
- (d) bicyclopentane and [1.1.1]propellane



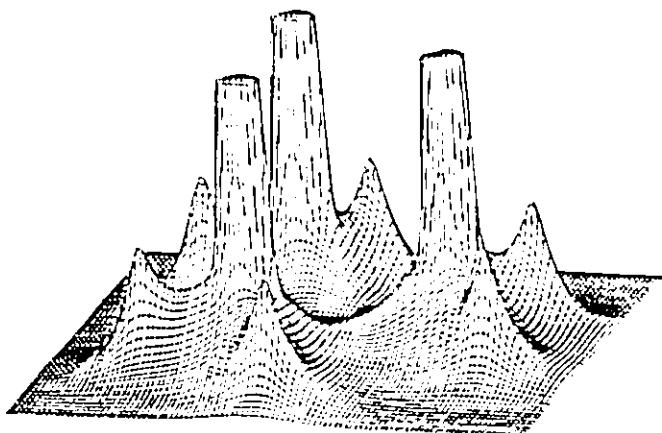
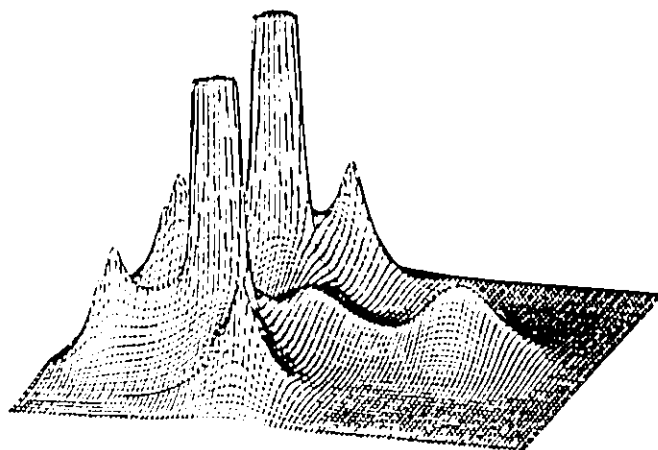
a



b



c



d

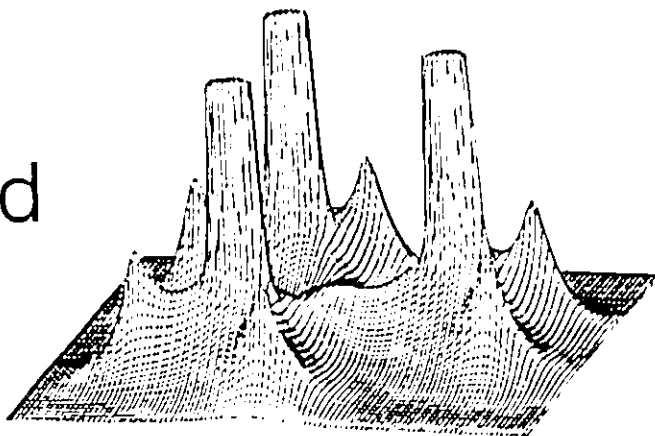
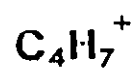
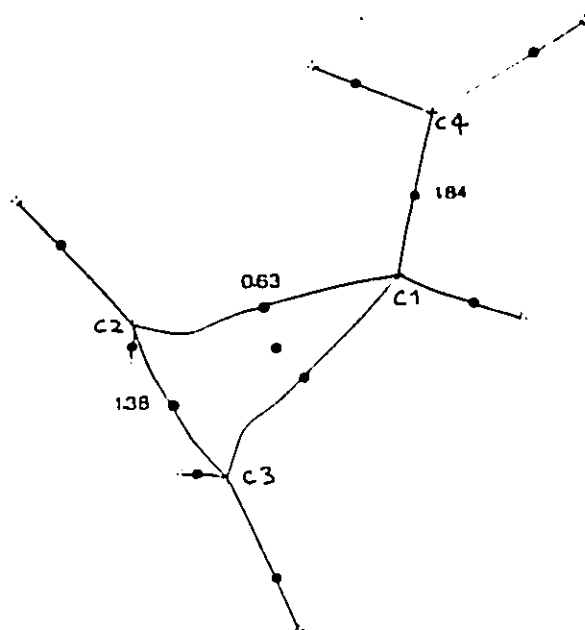


Figure III.3

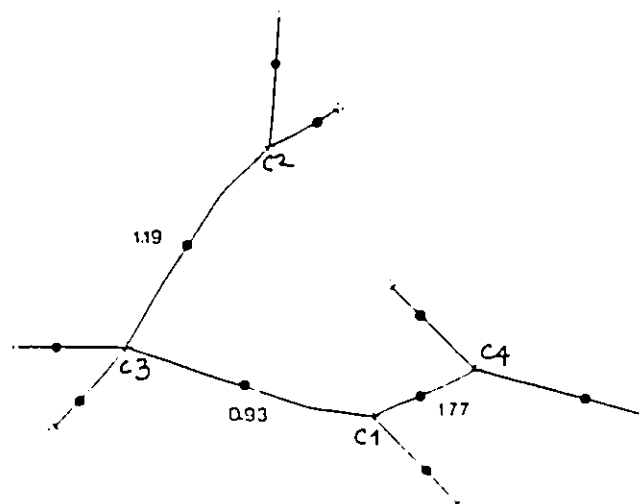
Planar projections of the molecular graphs defining structures 3a, 3b and 3c of cyclopropylcarbiny cation, $C_4H_7^+$. Bond critical points are shown as block dots. Bond orders have been assigned and are shown in the diagram.



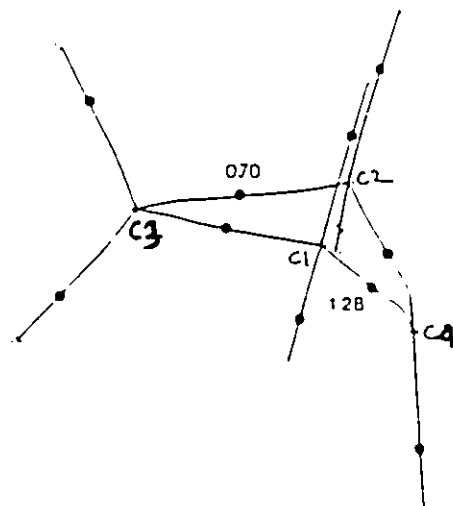
a





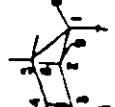
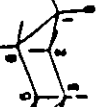
b



c



b. cyclic compounds

Formula	Structure	Bond	R_c	R_b	r_A	r_B	n	ρ_b (e/au ³)	$\nabla^2 \rho_b$ (e/au ³)	λ_1 (e/au ⁵)	λ_2 (e/au ⁵)	λ_3	ϵ	ρ_r and ρ_c (e/au ³)
C ₃ H ₆		C-C	1.4974	1.5069	0.7511	0.7511	0.98	0.2490	-0.5331	-0.4892	-0.3284	0.2845	0.4896	$\rho_r = 0.2044$
		C-H	1.0759		0.6802	0.3958		0.2849	-1.0383	-0.7604	-0.7412	0.4632	0.0260	
C ₄ H ₈		C-C	1.5485	1.5507	0.7751	0.7751	0.97	0.2467	-0.6269	-0.4616	-0.4610	0.2958	0.0014	$\rho_r = 0.0847$
		C1-H5	1.0418		0.6818	0.4030		0.2806	-1.0034	-0.7355	-0.7312	0.4633	0.0059	
		C1-H9	1.0418		0.6815	0.4034		0.2796	-0.9922	-0.7303	-0.7243	0.4624	0.0082	
C ₅ H ₁₀		C1-C2	1.5377		0.7688	0.7689	1.00	0.2517	-0.6504	-0.4755	-0.4730	0.2981	0.0053	$\rho_r = 0.0359$
		C2-C3	1.5439		0.7722	0.7728	0.97	0.2482	-0.6349	-0.4672	-0.4643	0.2966	0.0063	
		C3-C4	1.5515		0.7758	0.7768	0.96	0.2451	-0.6212	-0.4596	-0.4567	0.2952	0.0064	
		C1-H6	1.0836		0.6783	0.4053		0.2813	-1.0020	-0.7314	-0.7281	0.4575	0.0046	
		C1-H7	1.0841		0.6772	0.4070		0.2812	-0.9964	-0.7299	-0.7240	0.4575	0.0081	
		C2-H8	1.0839		0.6772	0.4067		0.2816	-0.9989	-0.7320	-0.7250	0.4581	0.0096	
		C2-H9	1.0826		0.6776	0.4050		0.2820	-1.0068	-0.7343	-0.7299	0.4575	0.0061	
		C3-H10	1.0832		0.6779	0.4053		0.2820	-1.0043	-0.7348	-0.7282	0.4587	0.0090	
		C3-H11	1.0838		0.6778	0.4059		0.2816	-1.0010	-0.7341	-0.7261	0.4592	0.0109	
C ₆ H ₁₂		C-C	1.5325		0.7663	0.7663	1.02	0.2510	-0.6673	-0.4837	-0.4807	0.2971	0.0062	$\rho_r = 0.0176$
		C1-H7	1.0870		0.6799	0.4071		0.2798	-0.9882	-0.7248	-0.7210	0.4576	0.0053	
		C1-H8	1.0892		0.6803	0.4090		0.2780	-0.9700	-0.7161	-0.7121	0.4582	0.0057	

formula	Structure	band	R_c	R_b	r_A	r_B	ρ	ρ_b	$\sigma^1 \rho_b$	λ_1	λ_2	λ_3	ϵ	ρ_r and ρ_c (e/au ³)
C_6H_6		C1-C3 C1-C2 C1-H5 C2-H6 C2-H7	1.4658 1.4826 1.0697 1.0781 1.0832	1.4819 1.4966 1.0697 1.0781 1.0832	0.7376 0.7538 0.6841 0.6826 0.6855	0.7376 0.7384 0.3856 0.3956 0.3977	0.98 1.01	0.2488 0.2541 0.2854 0.2854 0.2828	-0.3791 -0.5341 -1.0630 -0.7480 -1.0210	-0.3890 -0.4944 -0.7756 -0.7480 -0.7534	-0.2692 -0.3232 -0.7485 -0.7480 -0.7396	0.2792 0.2836 0.4611 0.4678 0.4719	0.4450 0.5295 0.0362 0.0270 0.0187	$\rho_r=0.2120$
C_7H_8		C1-C4 C1-C2 C1-C5 C2-C3 C1-H6 C3-H9 C3-H10 C5-H12 C5-H13	1.5129 1.5282 1.4935 1.5576 1.0753 1.0834 1.0856 1.0768 1.0795	1.5261 1.5304 1.5033 1.5501 1.0753 1.0834 1.0856 1.0768 1.0795	0.7602 0.7757 0.7456 0.7798 0.6812 0.6809 0.6821 0.6806 0.6814	0.7502 0.7542 0.7485 0.7798 0.3941 0.4025 0.4046 0.3962 0.3980	0.95 1.02 1.00 0.94	0.2440 0.2559 0.2528 0.2425 0.2849 0.2819 0.2805 0.2842 0.2833	-0.4877 -0.6668 -0.5472 -0.6100 -1.0451 -1.0094 -0.9984 -1.0341 -1.0162	-0.4748 -0.4935 -0.4973 -0.4600 -0.7656 -0.7368 -0.7352 -0.7594 -0.7480	-0.3059 -0.4746 -0.3348 -0.4478 -0.7421 -0.7349 -0.7282 -0.7360 -0.7312	0.2930 0.3012 0.2849 0.2979 0.4626 0.4623 0.4649 0.4614 0.4629	0.5523 0.0399 0.4856 0.0273 $\rho_r(3)=0.2063$ 0.0026 0.0096 0.0318 0.0229	
C_6H_{10}		C1-C4 C1-C2 C1-C6 C2-C3 C1-H7 C2-H8 C2-H9 C3-H10 C3-H11	1.5734 1.5493 1.5524 1.5600 1.0782 1.0817 1.0817 1.0814 1.0818	1.5965 1.5629 1.5545 1.5600 1.0782 1.0817 1.0817 1.0814 1.0818	0.7888 0.7761 0.7775 0.7807 0.6763 0.6782 0.6779 0.6781 0.6781	0.7888 0.7749 0.7766 0.7807 0.4014 0.4035 0.4038 0.4033 0.4037	0.92 0.97 0.96 0.94	0.2398 0.2479 0.2466 0.2418 0.2851 0.2822 0.2821 0.2824 0.2820	-0.5893 -0.6326 -0.6262 -0.6070 -1.0376 -1.0097 -1.0088 -1.0116 -1.0073	-0.4489 -0.4687 -0.4654 -0.4546 -0.7492 -0.7368 -0.7380 -0.7382 -0.7373	-0.4443 -0.4687 -0.4606 -0.4486 -0.7481 -0.7302 -0.7310 -0.7326 -0.7302	0.3040 0.3006 0.2998 0.2962 0.4597 0.4592 0.4602 0.4552 0.4602	0.0103 0.0091 0.0104 0.0133 0.0015 0.0066 0.0095 0.0077 0.0097	$\rho_r=0.0816$
C_7H_8		C-C C1-H6 C2-H7	1.5457 1.0823 1.0846	1.5507 1.0823 1.0846	0.7740 0.6839 0.6812	0.7757 0.3984 0.4034	0.96	0.2457 0.2826 0.2819	-0.5984 -1.0337 -1.0111	-0.4502 -0.7511 -0.7404	-0.4499 -0.7511 -0.7323	0.3017 0.4685 0.4616	0.0007 0.0000 0.0111	$\rho_r=0.1020$ $\rho_c=0.0983$
C_6H_{10}		C1-C5 C1-C2 C2-C3 C1-H7 C2-H8 C5-H13 C5-H14	1.5583 1.5418 1.5639 1.0770 1.0822 1.0816 1.0807	1.5615 1.5421 1.5641 1.0770 1.0822 1.0816 1.0807	0.7772 0.7741 0.7821 0.6775 0.6777 0.6772 0.6777	0.7837 0.7679 0.7821 0.3995 0.4045 0.4044 0.4045	0.94 1.00 0.92	0.2421 0.2517 0.2397 0.2865 0.2827 0.2826 0.2827	-0.5919 -0.6444 -0.5933 -1.0566 -1.0120 -1.0161 -1.0120	-0.4460 -0.4760 -0.4392 -0.7597 -0.7366 -0.7369 -0.7366	0.2982 0.2994 0.2929 0.4605 0.4583 0.4571 0.4583	0.0041 0.0178 0.0178 0.0031 0.0039 0.0007 0.0039	$\rho_r(5)=0.0418$	
C_7H_{12}		C1-C7 C1-C2 C2-C3 C1-H C7-H C2-H9 C2-H10	1.5392 1.5425 1.5577 1.0853 1.0869 1.0856 1.0853	1.5399 1.5427 1.5578 1.0853 1.0869 1.0856 1.0853	0.7656 0.7691 0.7789 0.6809 0.6801 0.6793 0.6794	0.7741 0.7735 0.7789 0.4044 0.4058 0.4053 0.4059	1.00 1.00 0.94	0.2525 0.2517 0.2424 0.2815 0.2789 0.2806 0.2806	-0.6454 -0.6481 -0.6071 -1.0080 -0.9839 -0.9930 -0.9931	-0.4737 -0.4753 -0.4478 -0.7336 -0.7202 -0.7278 -0.7278	0.3001 0.2990 0.2930 0.4582 0.4543 0.4582 0.4582	0.0038 0.0074 0.0103 0.0015 0.0030 0.0052 0.0058	$\rho_r=0.0216$	
C_8H_{14}		C1-C2 C2-C3 C1-H C2-H	1.5352 1.5510 1.0855 1.0857	1.5353 1.5511 1.0855 1.0857	0.7639 0.7755 0.6779 0.6783	0.7714 0.7755 0.4076 0.4074	1.02 0.96	0.2550 0.2450 0.2824 0.2806	-0.6672 -0.6236 -1.0052 -0.9900	-0.4839 -0.4580 -0.7310 -0.7264	-0.4820 -0.4576 -0.7310 -0.7205	0.2986 0.2921 0.4569 0.4569	0.0039 0.0008 0.0000 0.0082	$\rho_r=0.0216$ $\rho_c=0.0211$

4. propellanes and others

Formula	Structure	Bond	R_c	R_b	λ	r_0	r_b	n	ρ_b (e/au ³)	$\frac{v^2 \rho_b}{(e/au^3)}$	λ_1	λ_2	λ_3	ϵ	ρ_r and ρ_c (e/au ³)
C ₅ H ₆		C1-C3	1.5430			0.7715	0.7715	0.73	0.2030	+0.0253	-0.1089	-0.1089	0.2432	0.0000	$\rho = 0.1990$
		C1-C2	1.5020	1.5112		0.7398	0.7632	1.00	0.2515	-0.5248	-0.4914	-0.3176	0.2843	0.5472	
		C2-H	1.0750			0.6862	0.3808		0.2898	-1.0924	-0.7864	-0.7799	0.4739	0.0084	
C ₆ H ₈		C1-C4	1.5944	1.5955		0.7976	0.7976	0.70	0.1971	-0.0674	-0.2820	-0.0347	0.2493	7.1237	$\rho(3)=0.1961$
		C1-C2	1.5468	1.5483		0.7956	0.7522	0.96	0.2461	-0.6216	-0.4666	-0.4488	0.2938	0.0396	
		C1-C5	1.4926	1.5022		0.7382	0.7558	1.01	0.2530	-0.5355	-0.4975	-0.3176	0.2796	0.5664	
		C2-C3	1.5387	1.5413		0.7704	0.7704	1.00	0.2526	-0.6555	-0.4813	-0.4747	0.3006	0.0140	
		C2-H7	1.0820			0.6819	0.4001		0.2833	-1.0217	-0.7477	-0.7396	0.4656	0.0109	$\rho(4)=0.0883$
		C5-H12	1.0781			0.6877	0.3904		0.2874	-1.0685	-0.7747	-0.7690	0.4751	0.0075	
C ₇ H ₁₀		C5-H11	1.0775			0.6857	0.3918		0.2868	-1.0661	-0.7716	-0.7665	0.4721	0.0067	
		C1-C4	1.5343	1.5388		0.7673	0.7673	0.98	0.2482	-0.4922	-0.4914	-0.3013	0.3005	0.6312	$\rho(3)=0.2130$
		C1-C2	1.5452	1.5482		0.7874	0.7600	0.95	0.2438	-0.6033	-0.4625	-0.4344	0.2936	0.0647	
		C1-C7	1.4973	1.5049		0.7490	0.7508	0.97	0.2477	-0.4959	-0.4887	-0.2816	0.2744	0.7355	
		C2-C3	1.5808	1.5832		0.7914	0.7914	0.89	0.2341	-0.5720	-0.4376	-0.4283	0.2939	0.0217	
		C2-H8	1.0819			0.6911	0.4003		0.2834	-1.0234	-0.7505	-0.7387	0.4658	0.0161	$\rho(4)=0.0869$
		C2-H9	1.0804			0.6802	0.4003		0.2836	-1.0253	-0.7473	-0.7410	0.4630	0.0085	
C ₈ H ₁₂		C7-H	1.0714			0.6798	0.3916		0.2887	-1.0749	-0.7762	-0.7636	0.4648	0.0165	
		C1-C4	1.5122			0.7561	0.7561	1.26	0.2878	-0.8303	-0.5821	-0.5821	0.3339	0.0000	$\rho = 0.0861$
		C1-C2	1.5508	1.5545		0.7760	0.7758	0.95	0.2441	-0.6083	-0.4615	-0.4458	0.2978	0.0381	
		C2-C3	1.5745	1.5768		0.7883	0.7883	0.90	0.2360	-0.5810	-0.4393	-0.4353	0.2936	0.0090	
C ₉ H ₁₂		C-H	1.0859			0.6825	0.4034		0.2795	-0.9899	-0.7308	-0.7215	0.4624	0.0129	
		C-C	1.4634	1.4842		0.7378	0.7378	1.02	0.2551	-0.4672	-0.3813	-0.3733	0.2874	0.0213	$\rho = 0.2013$
C ₉ H ₁₄		C-H	1.0635			0.6850	0.3745		0.2852	-1.0965	-0.7747	-0.7747	0.4528	0.0000	$\rho = 0.1833$
		C-C	1.5632	1.5677		0.7834	0.7834	0.95	0.2440	-0.6079	-0.4571	-0.4546	0.3038	0.0057	$\rho = 0.0814$
C ₉ H ₁₆		C-H	1.0852			0.6858	0.3994		0.2786	-0.9989	-0.7307	-0.7307	0.4635	0.0000	$\rho = 0.0118$
		C1-C2	1.5127	1.5213		0.7586	0.7586	0.94	0.2425	-0.5005	-0.4722	-0.3138	0.2855	0.5049	$\rho = 0.2036$
		C1-C3	1.4789	1.4923		0.7369	0.7491	1.03	0.2571	-0.5719	-0.5027	-0.3623	0.2931	0.3874	
		C-H	1.0772			0.6817	0.3955		0.2839	-1.0322	-0.7578	-0.7394	0.4650	0.0249	

^a The data for structures marked with an "a" are from a 6-31G*/3-21G calculation.

TABLE III.2

Geometry and Bond Path Angles^a




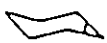



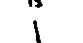




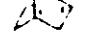

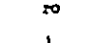
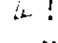


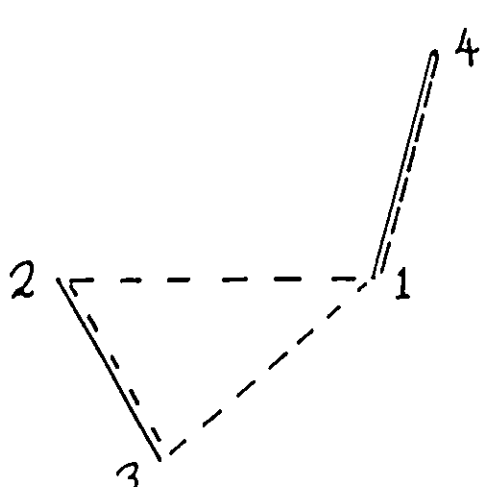
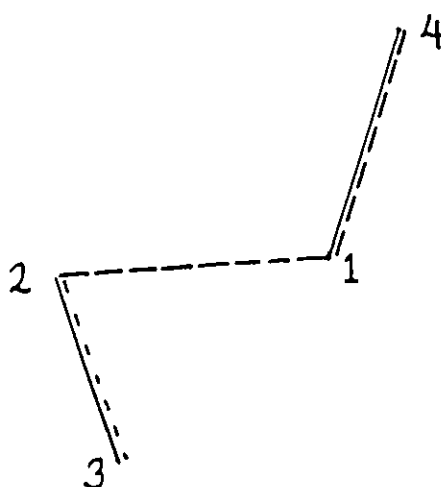
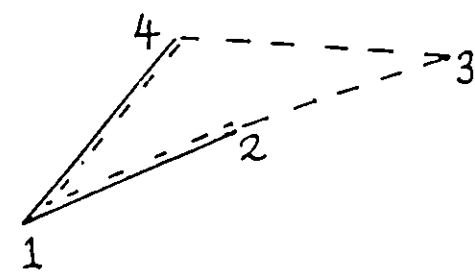
molecule		angle	geometric angle α_g	bond path angle α_b	$\Delta\alpha$ $\alpha_b - \alpha_g$	strain energy, kcal
cyclopropane		1	60.0	78.84	18.84	27.5
cyclobutane		1	89.01	95.73	6.72	26.5
cyclopentane		1	104.55	104.02	-0.53	6.2
		2	105.36	104.43	-0.93	
		3	106.50	105.03	-1.54	
cyclohexane		1	111.41	110.08	-1.34	0.0
bicyclo[1.1.0]butane		1	58.99	72.78	13.79	61.9
		2	60.50	76.62	16.12	
		3	97.91	105.07	7.16	
bicyclo[2.1.0]pentane		1	60.86	79.28	18.42	54.7
		2	59.57	78.30	18.72	
		3	90.84	96.76	5.92	
		4	89.16	95.77	6.61	
		5	110.03	109.72	-0.31	
bicyclo[2.2.0]hexane		1	90.17	97.01	6.85	51.8
		2	89.91	96.59	6.67	
		3	114.43	112.64	-1.79	
bicyclo[1.1.1]pentane		1	74.44	84.72	10.27	68.0
		2	87.20	95.85	8.65	
bicyclo[2.1.1]hexane		1	99.20	100.69	1.48	37.0
		2	101.77	103.46	1.69	
		3	86.11	94.21	8.10	
		4	82.60	90.95	8.35	
bicyclo[2.2.1]heptane		1	94.37	97.42	3.05	14.4
		2	101.51	102.90	1.39	
		3	108.43	108.69	0.26	
		4	103.13	103.57	0.44	
bicyclo[2.2.2]octane		1	109.30	108.68	-0.62	7.4
		2	109.64	108.56	-1.08	
[1.1.1]propellane		1	61.81	59.37	-2.44	98.0
		2	95.98	107.99	12.01	
		3	59.09	69.09	9.99	
[2.1.1]propellane		1	88.97	93.65	4.69	104.0
		2	91.03	97.91	6.88	
		3	112.30	116.3	4.00	
		4	57.72	67.96	10.25	
		5	97.27	111.45	14.18	
		6	64.57	65.27	0.71	
[2.2.1]propellane		1	59.18	75.40	16.22	105.0
		2	61.64	74.32	12.68	
		3	112.38	116.43	4.06	
		4	90.86	92.97	2.11	
		5	89.14	95.43	7.30	
		6	128.49	126.57	-1.91	
[2.2.2]propellane		1	91.15	97.05	5.90	89.0
		2	119.96	118.51	-1.44	
		3	88.85	96.81	7.97	
tetrahedrane		1	60.00	81.36	21.36	140.0
cubane		1	90.00	97.43	7.43	154.7
spiro[3.3]heptane		1	59.24	79.04	19.80	61.2
		2	61.51	84.84	23.33	
		3	137.5	123.02	-14.55	

Table III.3

Bond Properties for $C_4H_7^+$ Structures: 6-31G* Basis

Structure	Bond	$R(\text{\AA})^a$	$\rho_b(\text{\AA}^{-3})$	n	ϵ	$\nabla^2\rho(\text{\AA}^{-5})$
 <p>1a</p>	C1-C4	1.347	2.378	1.91	0.28	-28.68
	C1-C2	1.664	1.161	0.60	6.74	- 2.13
	C2-C3	1.412	2.067	1.42	0.18	-21.49
 <p>1b</p>	C1-C4	1.357	2.340	1.85	0.25	-27.60
	C1-C2	1.522	1.603	0.91	0.32	-12.76
	C3-C2	1.456	1.893	1.20	0.19	-18.42
 <p>1c</p>	C1-C2	1.435	1.984	1.31	0.16	-20.65
	C2-C3	1.650	1.271	0.66	0.36	- 7.51

^a Calculated at 4-31G geometries.

CHAPTER IV

Study of Hydrocarbons: Group Properties

I. Introduction

The theory of atoms in molecules has been outlined in previous chapters. Along with the ability to determine structure, it brings to the chemist the ability to study atomic properties, structural stability, means of structural change and reactivity. In this chapter the theory is applied to the molecules under study to provide further insight into the components that constitute the molecule, whether one chooses to study the atomic fragments or fragments consisting of several atoms as in a functional group.

II. Application of Theory

A. Atomic Properties

Atomic properties which one could wish to study can be expressed in terms of a corresponding three-dimensional density distribution which is then integrated over the basin of the atom to obtain its average value. For each property A , the value of A for the total system is given by equation (30)

$$A = \langle A \rangle = \sum A(\Omega) \quad (30)$$

A number of these properties, which include atomic populations and atomic energies are listed in Table IV.1. The average electron population of atom Ω , denoted $N(\Omega)$, is calculated by numerical integration of the

charge density over the basin of the atom Ω . A net charge on atom Ω , $q(\Omega)$, is calculated by subtracting $N(\Omega)$ from the nuclear charge.

$$q(\Omega) = Z_{\Omega} - N(\Omega) \quad (67)$$

With only a few exceptions, these integrations were performed over each distinct atom in each molecule studied here. The exceptions to this being the bridgehead carbon atoms in bicyclo[2.1.1]hexane where the structure of this molecule exhibits an unstable intersection of gradient paths associated with the two rings¹. The computer program PROAIM (Biegler-Konig et al 1982) used to perform the numerical integrations has not been programmed for such a situation. Populations and atomic energies for these atoms were obtained by difference. Overall the accuracies of the integrations can be measured by comparing the sums of the integrated atomic populations and energies and comparing them with the total number of electrons and the total computed energy respectively. These numbers are listed in Table IV.2. In general, the error in the total electron populations is less than $\pm 0.01e$ and the total energy being correct to $\pm 2.0 \text{ kcal/mol}$. Hydrogen atoms having a very simple atomic shape, as it were, with only a single interatomic surface composed of slowly curving trajectories in the surface lends itself to much higher accuracy in the integration process. Hydrogen atom populations are correct to $\pm 0.001e$. Carbon atoms with four interatomic surfaces and a much more rapidly

¹The gradient path associated with an eigenvector with a negative eigenvalue from one ring critical point is the same gradient vector associated with the eigenvector with a positive eigenvalue of the other ring critical point in this case. Such an intersection is known as an unstable one.

changing set of gradient vectors in the atomic basin are more difficult to integrate. Their individual accuracies can be judged by the value of the integral of $\nabla^2\rho$. The zero flux surface condition for the interatomic surface and Gauss' theorem together causes the value of the integral of $\nabla^2\rho$ to vanish. The extent to which this condition is satisfied is a test of how well the interatomic surface has been approximated.

The quantity $-(\hbar^2/4m)\nabla^2\rho$ is the local difference between two expressions for the kinetic energy density and appears in equation 42 of Chapter I. Its integrated value, listed as $L(\Omega)$ in Table IV.1, is a measure of the error in the average kinetic energy and the virial theorem as defined in equation (42). Generally, this value is less than 0.0001au or 0.06kcal/mol for a hydrogen atom. To obtain populations and energies that sum correctly to the total values, the carbon atom with the largest $L(\Omega)$ will have its populations and energies obtained by difference. These carbon atoms are marked by an asterisk in Table IV.1. These corrections will be equal to the differences between the totals and the sums of integrated values listed in Table IV.2 or will be less if that atom corrected is a member of a symmetric set.

B. Atomic Populations

As can be expected, the atomic populations exhibit a basis set dependence (Wiberg and Wendoloski 1981). Since atoms are defined in terms of properties of the charge density, changes in $N(\Omega)$ occur in an ordered and understandable way with changes in the basis set. Charge transfer between carbon and hydrogen in these molecules is small, so a minimal but balanced basis set yields populations similar to those obtained

by larger basis sets with polarizing functions. With this in mind, the STO-3G (Hehre et al 1969) and the 6-31G^{**} (Hariharan and Pople 1972) are equally balanced, the former having no polarizing functions, the latter having polarizing functions on both carbon and hydrogen. Table IV.3 lists the values of $q(\Omega)$ for carbon and hydrogen in a variety of saturated hydrocarbons obtained using the STO-3G, 6-31G^{**} and 6-31G^{*} (Hariharan 1972) basis sets. Between STO-3G and 6-31G^{**} the difference in hydrogen net charges are of the order of $0.003 \pm 0.001e$, the larger basis set yielding the larger charge. Corresponding to the larger charge on the carbon, the critical point between carbon and hydrogen is shifted closer to the hydrogen. The basis set used for this study is the 6-31G^{*} basis and is unbalanced in that polarization functions are included only for the carbon atoms. This shifts the CH bond critical point closer to the hydrogen by $0.0225 \pm 0.0007 \text{ \AA}$ as compared to results obtained by using the 6-31G^{**} basis set at the 6-31G^{*} geometry. Methane is the exception with the difference being only 0.0211 \AA . Although the absolute values of the charges obtained by the smaller 6-31G^{*} basis are smaller, the differences between the two sets of charges are remarkably constant. Hydrogen atom populations differ on average by $0.055 \pm 0.002e$ for the molecules listed in Table IV.3. This near consistency in the difference between the two sets of populations allows conversion of 6-31G^{*} results to 6-31G^{**} results simply by adding $0.055e$ to the hydrogen populations and making the appropriate accompanying adjustment to the carbon atoms.

As the changes that occur upon switching basis sets affects the position of the CH interatomic surface these changes affect populations in the functional groups alone. One now has the important result that

charges on the functional groups using either basis set are the same. Take for example the charges on the methyl group in the normal alkanes from propane to hexane. For the 6-31G** and 6-31G* basis sets the methyl group has a net charge of -0.018 and -0.017e respectively. The same result is obtained even for very strained systems. The net charge on a methylene group in [1.1.1]propellane differs only by 0.001e between the two basis sets and thus the bridgehead carbon in this molecule is assigned the same charge within integration error.

C. Electronegativity and Atomic Population

Results listed in Table IV.1 shows that hydrogen bears a negative charge. These results show that hydrogen is more electronegative than carbon in all of the acyclic hydrocarbons. Hydrogen has its most negative charge in the CH group of isobutane followed by its values in CH₂ and exhibits its least negative values in CH₃ of normal alkanes. Hydrogen becomes less electronegative than carbon however when the carbon experiences increasing geometric strain. In the series of molecules cyclopropane, bicyclobutane and tetrahedrane, the hydrogen atom has an increasing negative charge through the series. The values are 0.9949, 0.9463 and 0.8889 for the H in cyclopropane, the bridgehead hydrogen in bicyclo[1.1.0]butane and H in tetrahedrane respectively. Clearly as the geometric strain on the carbon atom is relieved, the more electronegative the hydrogen atom becomes. This trend is maintained in calculations using the 6-31G** basis set, but the actual values of the charges differ from those found with the 6-31G* basis because of the aforementioned constant 0.055e difference in populations found between the two basis

sets.

As hydrogen withdraws charge from carbon in the acyclic hydrocarbons, the relative group-electron-withdrawing ability is in the order $\text{CH}_3 > \text{CH}_2 > \text{CH} > \text{C}$. It is found however, that a methyl group attached to a methylene group withdraws an almost constant amount of charge. The results listed in Table IV.4 shows that in the series of propane to hexane, the methyl group has an almost constant charge, $q(\text{CH}_3)$, of $-0.0165 \pm 0.0005e$. The single methylene group found in propane bears a charge of $+0.034e$ while the methylene groups found in the series butane through hexane which are linked to a methyl and another methylene group bear a charge of $0.016e$. Within the integration error then, the methylene group in propane carries twice as much positive charge as compared to those which are linked to a methyl and another methylene found in butane through hexane. A methylene group linked only to other methylene groups bear no charge. Thus, the inductive transfer of charge from methylene to methyl is an almost constant quantity of $0.017e$ per methyl with the transfer damped by a single methylene group since a methylene group once removed has no charge.

The same constancy is observed with the net charges borne by the individual atoms that make up these groups. Hydrogen atoms in CH_3 groups that are in the plane of the carbon framework have a constant charge of $0.025e$, which is $0.003e$ smaller in magnitude than the other two hydrogens. Hydrogens in methylene groups linked to a single methyl group carry a charge of $-0.040e$ while hydrogen atoms on a carbon linked only to other methylenes have a charge of $-0.043e$. Values of the charge density at the positions of the nuclei are also listed in Table IV.1. These

values also reflect the constancy in the average populations observed for methyl and methylene groups in the normal alkanes. One could anticipate that these consistencies are a result of the essentially constant charge distribution over the corresponding atoms. Furthermore, this near constancy of the distribution of charge for the atoms in these functional groups leads to an anticipation that the contributions to the total energy by these groups will be nearly constant. The central methylene groups in both hexane and pentane have an essentially zero net charge and their energies are found to be equal to the additive contribution per methylene group in the energy additivity scheme for the normal alkanes. These methylene groups will be taken as the "standard" methylene group for comparison purposes with the methylene groups found in the cyclic and bicyclic hydrocarbons.

In cases where three methyls are attached to a single carbon as is the case in isobutane, each methyl group withdraws significantly more charge than when bonded to methylene. One notes that in neopentane, this effect is most dramatic. This is borne out by the net charge on the carbon atoms of CH_3 , CH_2 (linked only to methylenes), CH_2 (linked to one methyl), CH , and C fragments alone. These net charges are +0.065, +0.085, +0.097, +0.129 and +0.137e respectively.

D. Geometric Strain and Electronegativity

The cyclic hydrocarbons exhibit a different behaviour. When a carbon atom is subjected to geometric strain, it becomes more electronegative than a carbon in a geometrically unstrained environment. Decreases in the atomic populations of hydrogens bonded to geometrically strained

carbons is a direct result of the carbon atoms increased electronegativity. In Figure IV.1 is displayed the net atomic charges as well as the group charges for all of the cyclic molecules under investigation here. By symmetry, a CH_2 group of three-, four- and six-membered cyclic molecules bear a net zero charge, similar to the standard CH_2 group previously defined. Using the hydrogen atoms in the standard CH_2 group for comparison, the hydrogens of the methylene group in cyclopropane have 0.048 fewer electrons (this difference is 0.046e at the 6-31G** level of calculation). In cyclobutane, this difference drops to 0.014e and in cyclohexane, the average of the axial and equatorial hydrogen populations is only 0.003e less than hydrogen in the standard methylene group. Carbon atom populations increase accordingly with the decrease of the hydrogen atom populations as the amount of geometric strain increases. The net charge of the carbon atom in six-, five-, four- and three-membered rings are +0.086 to +0.077(average), +0.057 and -0.010e respectively. Increasing ring strain increases the carbon atom population. Cyclohexane, which may be considered strain free exhibits a carbon atom population which differs from the standard methylene group carbon atom by only 0.006e. Bridgehead carbons in bicyclo[1.1.0]butane and both [2.1.1]propellane and [2.2.1]propellane carry the largest negative charges. Even the order of electron withdrawing ability found in the unstrained acyclic hydrocarbons is reversed in the strained molecules. In the unstrained acyclics the order was found to be $\text{CH}_3 > \text{CH}_2 > \text{CH} > \text{C}$, however in the strained molecules CH and C groups withdraw charge from CH_2 groups. These observations indicate that carbon atoms become more electronegative with increasing geometric strain. This fact is of primary

importance in understanding the gross effects of geometrical constraints on the charge distribution and its energy.

One way of rationalizing this observation of the increase in electronegativity is to examine the explanation that can be offered by orbital theory. Orbital theories relate an increase in electronegativity of a carbon atom relative to that of a bonded hydrogen atom to an increase in the s character of its bonding orbital (Coulson, C.A. 1961). The decrease in bond length and pK_a accompanied by the increase in force constant and bond dissociation energy for C-H through the series cyclohexane, ethylene and acetylene is accounted for by a change in hybridization on the carbon from sp^3 to sp^2 to sp respectively. The increasing electron populations of these carbon atoms to yield charges of +0.080, -0.035 and -0.177e (see Table IV.3) respectively helps to quantify this accompanying increase in electronegativity. An empirical expression that relates the C-H coupling constant $J(^{13}C-H)$ to percent s character of the bond has been proposed (Scoolery 1959. Muller and Pritchard 1959). This relationship is given as

$$\%s = 0.2J(^{13}C-H) \quad (68)$$

The values of this coupling constant are 123, 156 and 249 Hz respectively (Levy et al 1980) and yield values of 25%, 31% and 50% for the s character.

This hybridization model also predicts that the smaller bond angles found in those systems with angular strain should result in an increase in the p character of the strained C-C bonds, thereby increasing the s

character of the associated C-H bond (Coulson and Moffitt 1949, Walsh 1947). In this way one can account for the increase in electronegativity of the carbon atom relative to the hydrogen atom as increasing geometric strain is introduced into the cyclic system. Coulson and Moffitt emphasize that the validity of this model is demonstrated by the observation that the properties of the CH₂ group in cyclopropane resemble those of ethylene. Both the observed and calculated (at the 6-31G* level) C-H bond lengths and HCH bond angles are similar for CH₂ groups in cyclopropane and ethylene. The actual observed values are 1.082 and 1.090Å and 116.6° and 116.5° respectively. This similarity extends even to the coupling constants for C-H bonds, the value for cyclopropane being 161Hz (March 1985) compared to that in ethylene of 156Hz. Even the C-H force constant, the bond dissociation energies as well as their pK_a values of 46 and 44, with ethylene being the more acidic (March 1985). In both of these molecules the carbon atom is negatively charged, with the carbon in ethylene being slightly more so. The properties for the bridgehead C-H group in bicyclo[1.1.0]butane approach those of the same group in acetylene. In both bicyclo[1.1.0]butane and acetylene, the carbon atoms have large negative charges, -0.121e and -0.177e respectively. The J(¹³C-H) coupling constant of 205Hz correlates to 41% s character. Although the C-H bond length of 1.070Å is longer than that of 1.057Å found in acetylene, it is shorter than the 1.090Å of ethylene. Since bicyclo[1.1.0]butane reacts with phenyllithium, (benzene pK_a is 43) the pK_a of this bicyclic molecule is probably less than 40, which makes it more acidic than ethylene or cyclopropane, but less acidic than acetylene itself which has a pK_a of 25. The ultimate argument for the increase in

electronegativity of the carbon atoms with increasing strain is of course one that relates this behaviour to the energy changes accompanying this increased strain. As the amount of strain increases for a C atom, the %s character of the C-H bond increases since the more tightly bound s electrons lowers the energy of the carbon atom thereby stabilizing it.

E. Atomic Energies

For a molecule in an equilibrium geometry, the energy $V(\Omega)$, the virial of the forces acting on the electrons, for an atom Ω is the potential energy of a molecule in the fixed nucleus approximation. Under these conditions, $V(\Omega)$ is the sum of the electron-nuclear energy V_{en} , the electron-electron energy V_{ee} , and the nuclear-nuclear energy V_{nn} . With these conditions the sum of the electronic energies $E(\Omega)$ gives the total energy of the molecule². The average kinetic energy of an atom is calculated by integrating the corresponding density over the basin of an atom. Application of the first of the two equations given in (43), one obtains the energy $E(\Omega)$. At the present level of calculation, namely the 6-31G* level, the virial theorem is not exactly satisfied. The ratio V/T , with V as defined above, is not exactly 2 as it should be. These values are listed in Table IV.2 as $\gamma-1$. To correct for this error in the virial, each atomic energy is multiplied by the factor $\gamma-1$ to obtain a set of corrected energies that now sum to the total energy of the molecule. From the values in Table IV.2, one finds that the correction factor $\gamma-1$ is close to unity, the value it should be at an equilibrium geometry.

²The electronic energy defined by the virial theorem equals the total energy of the system as usually defined plus the virial of the net forces exerted on the nuclei. At equilibrium geometries, these forces are zero, thus the electronic energy equals the usual total energy.

F. Group Additivity and the Acyclics

It is possible to fit the experimental heats of formation for the members of the homologous series $\text{CH}_3(\text{CH}_2)_m\text{CH}_3$, starting with $m=0$, with the expression $2A + mB$, where A is the contribution from the methyl group and B is the contribution from the methylene group (Prosen et al 1946). The generally accepted value for B at 25°C is -4.93 kcal/mol while A is -10.12 kcal/mol. It has been shown by Wiberg (Wiberg, K.B. 1984) that the correlation energy correction, the zero point energies and the change in ΔH_f on going from 298°K to 0°K are well represented by group equivalents. This is borne out by the calculated $6-31\text{G}^*$ energies at the $6-31\text{G}^*$ optimized geometries. These energies are calculated for the vibrationless molecule at 0°K . The calculated energies can be fitted to the expression $E = 2A + mB$ with $A = -39.61438\text{au}$ and $B = -39.03478\text{au}$ where $E(\text{CH}_3)$ in ethane is -39.61438au and $E(\text{CH}_2)$ of the standard CH_2 group is -39.03478au . Using these constants, one can reproduce all of the calculated energies within 0.05 kcal/mol. It has been shown that calculated energies without zero-point energy corrections (Schulman and Disch 1985) also satisfy the above expression for E . This result indicates that the calculated state functions, energies and charge density distribution contain the necessary information to account for the additivity observed in this homologous series of molecules.

Results listed in Table IV.4 shows that the group populations for the methyl fragment in ethane is not the same as that in another member of the homologous series. Similarly, the methylene group populations changes depending on whether it is bonded to a methyl or two

methylenes. These small differences are to be anticipated as the bonding environment for these fragments changes from one member to the other in the series. In ethane for example, the methyl is bonded to another methyl, but in any other member of the series, the methyl is bonded to a methylene. One recalls that the order of electron-withdrawing power for the acyclics is $\text{CH}_3 > \text{CH}_2 > \text{CH} > \text{C}$ so one anticipates that the population of the methyl group in say $\text{CH}_3(\text{CH}_2)_2\text{CH}_3$, butane, will be higher than found in ethane. Indeed the results listed in Table IV.4 show that the methyl group in ethane carries essentially zero charge while the same group in butane carries a slight negative charge of $-0.0170e$. The small changes in the populations of these groups reflect the small changes in the environments of these groups. In Table IV.4 are also listed the energies of the methyl group compared to the energy of a methyl group in ethane, the constant A. In the homologous series of molecules being discussed here, the energy of a methyl group other than in ethane itself is constant to within the error in integration. Similar behaviour is observed for the populations of these methyl groups. It is seen that the methyl group in those molecules other than ethane are more stable than the methyl group in ethane by $\Delta E = -10.7 \pm 0.9$ kcal/mol. The electron populations are increased by $\Delta N = 0.0165 \pm 0.0005e$. Using a $6-31\text{G}^{**}/6-31\text{G}^*$ level of approximation, the calculations yield identical behaviour with the energy and population differences being $\Delta E = -10.5 \pm 0.5$ kcal/mol and $\Delta N = 0.018 \pm 0.001e$ respectively. Examination of the results listed in Table IV.1 shows that the charge and energy gained by the methyl group is taken from the methylene groups. The energy gained by the methyl group is equal to that energy lost by the methylene groups. The increase

in the electron population of the methyl group is equal to the decrease in electron population of the methylene group². These observations account for the additivity observed for these molecules. In propane where the single methylene group is bonded to two methyls, its energy is equal to $B - 2\Delta E$, and its decrease in population is $2\Delta N$. The methylene group in butane is bonded to only one methyl and its energy is $B - \Delta E$ with the corresponding change in electron population being ΔN . Methylene groups in pentane and hexane which are bonded to a single methyl have the same properties as those in butane. Thus the central methylene group in pentane and the two such groups in hexane, those that are bonded only to other methylene groups, should have an energy equal to B and a zero net charge. This is what is found to within the uncertainties of the integrated values. Therefore, methylene groups bonded only to other methylenes, as found in pentane and all succeeding members of the series, possess zero net charge and contribute the standard energy increment B to the total energy of the molecule.

The group additivity scheme for the energy in hydrocarbons is thus not a result of the methyl and methylene groups contributing the same amount in each molecule. In fact, the energies of the methyl and methylene groups do change with the changes in their environment, even though these are small changes. The different environments make for a possibility of two types of methyl groups and three types of methylene groups. The two types of methyl groups are those which are directly bonded to a methyl or directly bonded to a methylene, while the three types of methylene groups are those which are bonded to two other methylene groups, one methylene and one methyl group and finally, to

two methyl groups. Environmental changes are damped by a single intervening methylene group thereby limiting the number of distinct methylene groups to three. The reason for the additivity found in these hydrocarbons is the fact that the ratio of the change in energy for an accompanying change in population, $\Delta E/\Delta N$, is the same for both methyl and methylene groups. A shift of electronic charge from one group to the other results in the same change in the energy. From the values listed in Table IV.1, one observes that these changes both in the population and the energy are restricted to the carbon atoms of the methyl and methylene groups. Properties of the associated hydrogen atoms remain essentially constant. This effect is to be anticipated as the carbons are the atoms which are directly bonded in the two groups. Through this bonding, they share a common interatomic surface. Charge transfer from one group to the other is reflected in a shift in the surface towards the carbon from which charge is withdrawn. A shift in the surface results in a shift of the bond critical point between the two carbons and this shift is typically on the order of 0.003 or 0.004Å in the opposite direction to the charge transfer. Since the charge transfer occurs between chemically similar atoms, the resulting change in energy is zero. It is also necessary that the change in the correlation energy for a change in the population be the same for both groups if one is to account for the experimental observation of group additivity of the energy.³ One now has a 'building blocks' approach to predicting the

³In density functional theory the correlation energy is expressed as a functional of the charge density. Thus, when ρ remains unchanged for a given group in different molecules, the group's contribution to the correlation energy will also remain unchanged. Various correlation energy density functionals have since been studied (Carroll 1988) with a non-local

energy of a member of the $\text{CH}_3(\text{CH}_2)_m\text{CH}_3$ homologous series of hydrocarbons. This capability may have been utilized by chemists in the past, but the theory is now able to relate this empirical observation to real physical changes in the charge density distribution and consequently the energies of the functional groups.

Reference to Table IV.1 indicates that the energy of a hydrogen atom decreases as its average population increases. In general, this is not true for carbon atoms which have a more complex electronic structure. Take for example the carbon atom of the standard methylene group in pentane or hexane. This carbon has a smaller average population than that of the repeating methylene groups but is more stable by 5 kcal/mol. The charge density is slightly more contracted in the carbon of CH_2 than that in CH_3 , as is reflected in the values of the charge density at the nuclei, $\rho(0)$ from Table IV.1.

The data listed in Table IV.5 illustrates the basis for the observation of group properties in chemistry. The properties of a group are determined only by the total force acting on it and not by the individual components of that force (Bader and Beddall 1972. Bader and Nguyen-Dang 1981). The atoms considered to exemplify this property are the hydrogens and carbons of the methyl groups in the series propane to hexane. All quantities are referenced to the hexane molecule. Total atomic populations and the kinetic energies, which are equal to the negative of the atomic energy, are all remarkably constant for each type of atom. If the distribution of charge is the same for each type of atom

gradient corrected expression giving the best agreement with experiment. However, these functionals are not of sufficient chemical accuracy for energy additivity schemes.

then the potential energy of interaction of the nucleus of atom Ω with its own charge distribution, the quantity $V_{neo}(\Omega)$, should also be the same. Indeed, this is the case. The largest difference is 0.4 kcal/mol for hydrogen and the carbon atoms exhibit a variation of ± 2.6 kcal/mol about the mean value. The interaction of all the nuclei in the molecule with the electronic charge of atom Ω , the quantity $V_{ne}(\Omega)$ increases by very large amounts with each removal of a CH_2 group. The value $V_{ne}(\Omega)$ changes by 1.5×10^3 kcal/mol for the hydrogen atom and by 9.2×10^3 kcal/mol for the carbon atom on changing from hexane to propane. The electron-electron repulsion, that is the repulsion of the electrons of atom Ω by all the other electrons in the molecule, denoted $V_{ee}(\Omega)$, and the effects on the nuclear-nuclear repulsion, $V_{nn}(\Omega)$, on the other hand also decreases by dramatic amounts upon removal of each CH_2 group.⁴ The sum of the three contributions, $V_{ne}(\Omega)$, $V_{ee}(\Omega)$ and $V_{nn}(\Omega)$, to give the total potential energy of the system $V(\Omega)$ yields however the same value for each kind of atom through the series. This must be the case as $V(\Omega)$ is by the virial theorem, twice the total energy of the atom. One recognises that $V(\Omega)$ is the virial of the total forces acting on the atom. These include the nuclear-electron, electron-electron and nuclear-nuclear interactions for the atom Ω . This quantity is conserved along with the kinetic energy when the distribution of charge of the atom Ω remains unchanged.

The total virial remains unchanged even though there are significant changes in the individual components that make up that virial. On

⁴The nuclear-nuclear repulsion energy for atom Ω is the virial of the Hellmann-Feynmann forces exerted on the charge density in the atom by all of the nuclei in the molecule.

examination of these individual changes, one sees that the change in the electron-electron repulsion and the nuclear-nuclear repulsion are individually one half of the magnitude of the change in the electron-nuclear attraction. Therefore, the removal of successive CH_2 groups causes changes in increasing magnitude, as the changes occur closer to the methyl group with each successive removal, to all the components of the total potential energy $V(\Omega)$ for each atom of the methyl group but the changes sum to zero for each atom. For example, the sums of the incremental changes in $\frac{1}{2}V_{en}$, V_{nn} and V_{ee} for one of the two equivalent hydrogens in the methyl group for the removal of all three methylene groups to change hexane into propane are found to be +1.2018, -1.2018 and -1.2010au respectively.

The branched molecules isobutane and neopentane are more stable than their normal isomers by 1.9 and 5.1 kcal/mol respectively in terms of their ΔH_f° values at 25°C. In their vibrationless state at 0 K they are 1.6 and 3.8 kcal/mol more stable than their normal isomers respectively (Fliszar 1983). Calculated energies at the 6-31G^{*}/6-31G^{*} level of approximation predict increased stabilities of only 0.4 and 0.5 kcal/mol respectively. This indicates that the change in the correlation energy for a change in the population of the CH and C groups is different than that for the CH_3 and CH_2 groups. From the order of electron withdrawing power ($\text{CH}_3 > \text{CH}_2 > \text{CH} > \text{C}$) the charges on methyl groups in the branched isomers are greater than those found in the normal isomers, therefore they are correspondingly more stable. Comparing these methyl groups to that in ethane, the methyl group in isobutane is more stable by $\Delta E = -21.6$ kcal/mol and the population is increased by $\Delta N = -0.028e$. In

neopentane, the methyl is more stable than that in ethane by $\Delta E = -28.8$ kcal/mol and $\Delta N = -0.034e$. Nearly all of the increase in stability of the methyl group on both isobutane and neopentane reside in the carbon atoms. The carbon atoms of these methyl groups are more stable than the carbon atom of the methyl group in ethane by 20.1 kcal/mol and 25.8 kcal/mol for isobutane and neopentane respectively. On the other hand, the carbon atom at which the branching occurs is less stable than the carbon in the methyl group of ethane by 17.9 kcal/mol and 23.1 kcal/mol for isobutane and neopentane respectively. It follows then that the actual energies of the CH and C groups in the branched molecules are less than the values assigned to them in the additivity scheme.

G. Strain Energy

The effects of increased geometric strain on electronegativity and ultimately on the energy of a methyl or methylene group has been discussed above. Experimentalists used heats of formation for the cyclic, bicyclic and propellane molecules to quantify the strain energy. One can define strain energy using the theory of atoms in molecules by subtracting from the energy of the group of interest the energy of the corresponding standard group. It is noted here that this definition for group energy is in the same manner as is done by using heats of formation, except that they do not reference the standard state of the constituent atoms. The standard group energies for the methyl group have been reported above. They are $E(\text{CH}_3) = A = -39.61438$ au and $E(\text{CH}_2) = B = -39.03478$ au. To obtain the standard values for the methyne (CH) and carbon groups one subtracts three and four times the

value of A from the total energies of isobutane and neopentane respectively. This gives the standard energy for the methyne group as $E(\text{CH}) = -38.45582$ au and $E(\text{C}) = -37.87630$ au. The standard energies obtained in this way do not take into account the effects of charge transfer to the attached methyl groups. This effect makes the standard methyne and carbon group more stable than the actual group by 64.7 kcal/mol and 113.1 kcal/mol respectively. Strain energies calculated in this manner are given alongside their corresponding group in Figure IV.1. The strain energies are given in units of kcal/mol with the group strain energy, listed as E , followed by the total strain energy of the molecule, listed as SE , and finally the experimental strain energy given in parenthesis. The experimental strain energies (Wiberg 1986) are determined by using the Franklin group equivalents (Franklin 1949). From the values listed in Figure IV.1, one notes that the theoretical and experimental values are in fairly good agreement with the largest errors found in [1.1.1]- and [2.2.2]propellane. One should include electron-electron correlation to properly handle highly strained molecules.

H. Cyclic Molecules

It has been noted previously that the electron-withdrawing power of hydrogen and carbon are reversed as the carbon atom is subjected to increasing geometric strain. This change in the electronegativity of the carbon can be explained by the increasing s character of the C-H bonds. Relative to the standard methylene group, each hydrogen transfers 0.048e to carbon in cyclopropane. Accompanying this charge transfer is an increase in the stability of the carbon of 15.5 kcal/mol and a decrease in

the stability of each of the two hydrogens by 12.6 kcal/mol. Overall, the transfer of charge from the hydrogens to the carbon leads to a 9.6 kcal/mol decrease in the stability of the methylene group. The total strain energy for cyclopropane therefore is three times 9.6 kcal/mol or 28.8 kcal/mol which is in good agreement of the generally accepted value. The methylene group in cyclopropane is only 2.3 kcal/mol more stable than the same group in ethylene and in terms of charge transfer within the group and its energy, it resembles the ethylene fragment more than the standard methylene group.

Using the 6-31G** basis set for these calculations, the same group charges and same transfers of charge within a group are found. This leads to the same changes in energy relative to the standard groups and is true not only for the methyl and methylene groups in the acyclic molecules as noted above but also true for the strained systems. The use of the 6-31G** basis sets for the calculations yields a charge transfer of 0.044e from hydrogen to carbon beyond that found in the standard methylene group and a contribution to the total strain energy of cyclopropane of 9.2 kcal/mol.

If one considers the hybridization on the carbon in the C-H bonds to the carbon of the standard methylene group, ethylene and acetylene, the hybridization changes from sp^3 to sp^2 to sp respectively. This change in hybridization would correspond to a change in the percent s character of the C-H bonds to be from 25% to 33.3% to 50% respectively. The change in energy accompanying this change in percent s character behaves in a linear manner with the energy decreasing by 3.0 kcal/mol with each percentage increase. In all three of these molecules the charge transfer

is between the carbon and the hydrogen and the functional group has no net charge. The population of the carbon atom in cyclopropane is slightly higher than that of the carbon in ethylene and its energy is correspondingly greater by 7.9 kcal/mol. Using the relationship above, this would correspond to a percent s character for the C-H bonds to be approximately 31%. Even though the carbon atom in ethylene is more stable than the carbon atom of the standard CH_2 group, the CH_2 fragment of ethylene overall is less stable than the standard methylene group. The same is true for the methylene fragment of cyclopropane. In both ethylene and cyclopropane, stabilization of the carbon atom is through the effects of charge transfer between the carbon and the hydrogen. This charge transfer stabilizes the carbon atom at the expense of destabilizing the hydrogens. In both ethylene and cyclopropane, the destabilization of the hydrogen atoms is greater than the stabilization of the carbon atom, making the methylene groups in these molecules less stable overall than the standard methylene group.

As the amount of geometric strain is reduced, as it is in cyclobutane, the charge transfer that occurs between the carbon and the hydrogen is reduced. In the example of cyclobutane, this charge transfer is reduced to 0.014e. The carbon atom has a correspondingly slightly lower energy than the carbon of the standard methylene group. In terms of the above relationship, the C-H bonds have a 26% s character. Evidence to support this comes from the value of the C-H coupling constant (Levy 1980) of 134 Hz which is only slightly greater than the value of 123 Hz for the methylene group in cyclohexane. The relationship between percent s character and the coupling constant gives a percent s character of 27%

for the C-H bonds. Similarly, the bond length, the stretching force constant and the HCH bond angle for the methylene group in cyclobutane all suggest only a small increase in the percent s character increase of the C-H bonds over that in the standard methylene group. The stability of the carbon atom in cyclobutane is increased by 1.0 kcal/mol over the carbon of the standard methylene group but the stability of the hydrogens is decreased by 3.9 kcal/mol each. Overall the methylene group in cyclobutane is 6.7 kcal/mol less stable than the standard methylene group and the total strain energy of the molecule is calculated to be 26.8 kcal/mol compared to the experimental value of 26.5 kcal/mol.

This analysis of the strain energy agrees with and substantiates the observations made in the preceding chapter regarding the greater stability of the carbon atoms in cyclopropane as compared to those of cyclobutane. This increased stabilization is the result of the delocalized concentration of charge over the interior of the three membered ring where it is shared by and binds all three ring nuclei. The value of $V_{\text{neo}}(\text{C})$, the potential energy of attraction of the nucleus for its own charge density, is 127 kcal/mol more negative for the carbon atom in cyclopropane than that in cyclobutane. The greater charge and stability of the carbon atom in cyclopropane are a result of the increased s character in the C-H bonds. This increase in stability appears in a relatively large C-H bond dissociation energy for cyclopropane of 106 kcal/mol which is only 2 kcal/mol less than that for ethylene (Baghal-Vayjooee and Benson 1979).

The relative degree of geometric strain in the cyclic, bicyclic and propellane molecules can be measured by the difference of the C-C-C bond path angle from the tetrahedral angle. These values are listed in

Table III.2. As the carbon atom experiences increased strain as measured by this deviation from the tetrahedral angle an increasing amount of electronic charge is transferred from the hydrogens to the carbon of the methylene group using the populations in the standard methylene group for comparison. This redistribution of the charge density leads to a stabilization of the carbon atom but leads to an even greater destabilization of the hydrogen atoms. Overall, the strain energy of the molecule is equal to the increase in energy of the methylene groups relative to the standard methylene. These observations may be rationalized by orbital theory by assuming that the s character of the C-H bonds increases as the geometric strain on the carbon atom increases. This rationalization can be carried into a discussion of the bicyclic molecules.

J. The Bicyclic Molecules

Of all the bicyclic molecules, bicyclo[1.1.0]butane, structure 13, is the most strained. The magnitude of the net charge of $-0.121e$ on the bridgehead carbon in this molecule is exceeded only by that found in [2.1.1]- and [2.2.1]propellane. The bridgehead carbon in bicyclo[1.1.0]butane which has an inverted geometry, withdraws charge from the hydrogen directly bonded to it as well as from the methylene groups. Its energy is only 9.5 kcal/mol greater than that for carbon in acetylene suggesting a considerable degree of s character in its bonds. Orbital analyses indicate that the bridgehead bond in this molecule is pure p (Newton and Schulman 1972. Finkelmeier and Luttko 1978) therefore all the s character is in the hybrid orbitals used in bonding to the groups from which the carbon withdraws charge. Using the coupling

constant relationship, the observed $J(^{13}\text{C-H})$ coupling constant yields a percent s character of 41% which leaves an approximate percent s character of 30% for each of the bonds to the methylenes. Coupling constants for the C-H bonds in the attached methylene groups average to the same value as the coupling constant in cyclopropane which gives a 32% s character. This implies that the hybrid orbitals on the carbon of the attached methylene group which are directed towards the bridgehead carbon have only 18% s character, considerably less than those directed from the bridgehead. This approximate analysis seems to suggest that there is more s character from the bridgehead carbon than from the methylenic carbon atom in the carbon-carbon bonds. One expects then that the bridgehead carbon will withdraw charge from the methylenic carbon as well as from the hydrogen. Therefore, what at first seems an anomaly where the most strained carbon atom in the molecule possess the most negative total energy can be rationalized by orbital theory. This rationalization predicts a high s character contribution from the hybrid orbitals of the bridgehead carbons leading to the most electronegative and consequently the most stable atom of the molecule.

As was discussed earlier, in assigning the group energy to CH, it is assumed that there is no charge transfer from this CH group to the three attached methyl groups. However, in isobutane, the CH group bears a charge of +0.084e and as a result the group energy for the standard CH group is 60 kcal/mol more stable than the same group in isobutane. In bicyclo[1.1.0]butane, because of the very high electronegativity of the bridgehead carbon and its similarity with the energy of the carbon in acetylene, the energy of the bridgehead CH group differs from the

standard value by only 1.6 kcal/mol. Therefore essentially all of the strain energy originates from the methylene groups and their charge density. For these methylenic hydrogens, the charge, energy and ^{13}C coupling constants for the C-H bond are very similar to those of cyclopropane. Thus, the increase in strain energy in bicyclo[1.1.0]butane beyond that found in cyclopropane is a result of the additional charge transfer that occurs in this molecule. Each methylene group has a net charge of +0.068e and is calculated to be 32.7 kcal/mol less stable than the electrically neutral standard methylene group. The total calculated strain energy is 68.6 kcal/mol as compared to the experimental value of 63.9 kcal/mol.

As one progresses through the series of bicyclic molecules from the most strained bicyclo[1.1.0]butane, structure 13, to the least strained bicyclo[2.2.2]octane, structure 19, the populations of the bridgehead carbons experience a continuous decrease and the CH group becomes positively charged. The bridging methylene groups on the other hand experience an increase in the population until they become negatively charged through this series of molecules. Parallelling these changes in populations is the group energy where there is a near linear relationship with the methylene groups becoming more stable as the methine group with its charge approaching that of the methine group in isobutane becomes less stable and also the principal source of strain energy. Thus as the strain energy at the bridgehead carbon is decreased, its hybrid orbital scheme has decreased s character directed at the hydrogen and at the methylene carbons. As the electronegativity decreases along with this decrease in s character the relative electron-withdrawing power reverts to

the normal order with the methylene group withdrawing charge from the methyne groups.

These observations are further illustrated by the molecule bicyclo[1.1.1]pentane, structure 16, for which the C-H coupling constants are known. This molecule displays the maximum total strain energy and corresponding maximum contribution from the methyne groups to the strain energy in this series of bicyclic molecules. The C-H coupling constant for the bridgehead carbo-hydrogen bond is 160 Hz (Levy et al 1980) and yields a percent s character of 32% using the percent s character relationship to the coupling constant. This leads to a 23% s character for the two orbitals directed towards the three methylene groups. The C-H coupling constant found in the methylene groups of 144 Hz gives a percent s character of 29%, implying an s character of 21% for those orbitals directed at the bridgehead carbons. In this case, the percent s character between those orbitals used from the methylenic carbon and the bridgehead carbon are quite evenly matched and the two revert to the normal order of electronegativity with methylene withdrawing charge from the bridgehead carbon. Since the methylene groups withdraw charge from the methyne groups they are stabilized relative to the standard electrically neutral methylene group and each of these groups contributes -5.6 kcal/mol each to the strain energy of the molecule.

The methyne group population varies significantly through the series of bicyclic molecules. In bicyclo[1.1.0]butane, it has a large net negative charge. In bicyclo[2.1.0]pentane, structure 14, this net charge is reduced to about half the value in bicyclo[1.1.0]butane while in

bicyclo[2.2.0]hexane, structure 15, it is neutral. The net charge on the methyne group becomes positive in bicyclo[1.1.1]pentane, structure 16. Accompanying this reduction in population, or net negative charge is increased destabilization of the methyne group with the largest contribution to the strain energy in bicyclo[1.1.1]pentane even though the net positive charge continues to increase through the rest of the bicyclic molecules. For the molecule bicyclo[2.2.2]octane, structure 19, the net positive charge on the methyne group is $+0.057e$. Bicyclo[1.1.1]pentane has no bridging bond and this is the reason that there is a sharp increase in the strain energy for the methyne group at this point in the bicyclic series. In terms of the orbital model, the presence of the bridgehead bond which is mostly p in character leaves an increased s character for the remaining bonds. This increase in s character as has been discussed, leads to an increase in the electronegativity of the group and stabilization of the group is observed. In the absence of this bridgehead bond, the bridgehead carbon becomes less electronegative relative to its neighbours of which there are four rather than three. In terms of the potential energy contributions to the atomic energy, there is a sudden relative increase in the repulsive contributions to the energy of the bridgehead carbon of bicyclo[1.1.1]pentane. In structures 16, 18 and 19 the bridgehead carbon atoms all have about the same atomic energies despite a decrease in their electron populations. As a result of this decrease in the atomic population the contribution to the energy of the atom from the attractive interaction of the carbon nucleus with its own charge density is 46 kcal/mol more stable in bicyclo[1.1.1]pentane than in bicyclo[2.2.2]octane. Since the total energies of these two bridgehead

carbon atoms are identical, it means that the repulsive forces must make a larger contribution to the external virial. In other words the contribution from repulsive forces upon interaction with the remainder of the molecule are relatively larger in bicyclo[1.1.1]pentane than in bicyclo[2.2.2]octane. This result is in agreement with the classical idea of a significant non-bonded repulsion between bridgehead atoms which decreases from 16 to 19. This result also shows the significance of an earlier statement that the presence or absence of a bond path between the bridgehead nuclei has direct physical consequences. In the zero-bridged structures 13 through 15 the charge density in the bridgehead internuclear region exerts net attractive forces on the bridgehead nuclei and their virial lowers the energy of the system (Bader and Essen 1984). In those structures where they are not zero-bridged, there is no accumulation of charge density to give the line of maximum charge that links the bridgehead nuclei. In this case, repulsive forces dominate and it is their virial that raises the total energy.

Beyond these observations, there is a further correlation that can be noted. This correlation is between the electronegativity and the energy of the methylenic carbon and the degree of relaxation of the geometric strain as measured by $\Delta\alpha$ where $\Delta\alpha$ is as previously defined in the preceding chapter. The greater the relaxation as measured by $\Delta\alpha$, the greater the stability of the atom. As a comparison, take the carbon atom in the one-carbon-bridge methylene in bicyclo[2.1.0]pentane, 14, and that in bicyclo[1.1.0]butane, 13. While their geometric angles are nearly identical, $\Delta\alpha$ is 5 degrees greater for the carbon in bicyclo[2.1.0]pentane with an accompanying larger population and increased stability than that

of bicyclo[1.1.0]butane. The methylene group in bicyclo[2.1.0]pentane has very similar properties, including the value of $\Delta\alpha$, to those of cyclopropane. The two-carbon-bridge methylene group in bicyclo[2.1.0]pentane is under less strain, its relaxation is smaller and there is a substantial charge transfer between it and the bridgehead carbons in the direction of the bridgehead carbons. This loss of electronic charge leads to a considerably greater strain energy of this methylene group as compared to that in cyclobutane. In bicyclo[2.2.1]heptane where the relative electronegativities have reverted to the normal order (that is $\text{CH}_3 > \text{CH}_2 > \text{CH} > \text{C}$) the one-carbon-bridge methylene has a larger population and hence is more stable than the two-carbon-bridge methylenes. In addition to having a larger value for $\Delta\alpha$, the one-carbon-bridge carbon can withdraw charge from both bridgehead groups.

In bicyclo[2.2.2]octane, the final member of this series under study, the bond angles are all fairly normal, leading to normal hybridization. As a result, one expects that the methylene groups withdraw charge from the methyne groups. The overall effect should be similar to that in isobutane but not as large since the methylene group is not as electronegative as the methyl group. A methylene group attached to a methyne group in a branched structure used as a reference would give a more direct measure of the source of strain in these types of molecules. Values of the strain energy given here are compared to a standard which is physically unrelated to these molecules. Therefore in bicyclo[2.2.2]octane, the methylene group is found to be more stable than the standard, the standard group bearing no net charge, while the methyne group is

correspondingly less stable. The final strain energy is obtained as a difference rather than as a sum of group contributions.

In the cage structures tetrahedrane and cubane, the electronegativity of the carbon in the methyne groups also parallels the percent s character. In the methyne group of tetrahedrane the percent s character of the group must be considerably larger than that of the methyne group in bicyclo[1.1.0]butane because of the increased geometric strain. Using the previously observed linear relationship between the percent s character and the energy of the carbon atom in electrically neutral methylene and methyne groups gives a value of 42% s character for the carbon in tetrahedrane. The relaxation of the charge density as measured by the quantity $\Delta\alpha$ is also a maximum for this molecule. As a result, the carbon atoms in tetrahedrane are more electronegative than the bridgehead carbons in bicyclo[1.1.0]butane. However, the methyne group of tetrahedrane differs from that found in bicyclo[1.1.0]butane in that it does not carry a net charge. Any charge transfer that occurs necessarily has to be from hydrogen to carbon in tetrahedrane. A charge transfer from hydrogen to carbon in the case of methylene groups as discussed above is accompanied by an overall increase in energy of the group. It is this increase in energy that is the group's contribution to the total strain energy of the molecule. Similarly with the methyne groups being considered here. Each methyne group has a strain energy of 35.2 kcal/mol in tetrahedrane. This value is in fact only 5.9 kcal/mol greater than that of the same group in acetylene. A carbon atom in cubane has an atomic energy that indicates a 36% s character. Using the coupling constant relationship, a 31% s character is predicted. The charge transfer

from hydrogen to carbon is much reduced from that found in tetrahedrane. The strain energy is also reduced to 19.9 kcal/mol for each methyne group to 159.1 kcal/mol compared to 140.8 kcal/mol in tetrahedrane. If one takes into account the $-0.055e$ correction to the population, by using the $6-31G^{**}$ basis instead of the $6-31G^*$ basis set for the calculations, of a hydrogen atom relative to carbon more realistic absolute charges are obtained. In tetrahedrane, the hydrogens around the tetrahedral cage of carbons carry a net charge of $0.056e$ while in cubane the surrounding hydrogens carry a net charge, almost equal in magnitude, of $-0.058e$.

In the molecule spiropentane, structure 26, the percent s character at the central carbon is 25% by symmetry. The methylene groups should be similar to those of cyclopropane which has 32% s character in the C-H bonds and 18% s character in the C-C bonds. These values indicate that the central carbon atom should be more electronegative than the carbon atoms of the methylene groups. The central carbon withdraws charge from the methylene groups and is 12.5 kcal/mol less stable than the standard C group while the methylenes with a net positive charge have a strain energy that is one third again as large as that found in cyclopropane. The energy of the methylene group in spiropentane follows the nearly linear energy vs. net charge relationship observed for this group in the bicyclic molecules.

K. Propellanes

The series of propellane molecules all possess unusual structures and these structures display atomic energies and charges that do not lend

themselves to the percent s character rationalizations used above. It is still possible of course to use the theory to obtain the atomic charges and energies of the constituent atoms. The general observation is that as a carbon atom experiences increased geometric strain, its electronegativity increases. In each of the propellanes, [1.1.1]propellane (20), [2.1.1]propellane (21), [2.2.1]propellane (22), and [2.2.2]propellane (23), the bridgehead carbon atoms have a net negative charge. The magnitude of the charges are the largest for [2.1.1]propellane and [2.2.1]propellane. The smallest magnitude of the net charges is found for [2.2.2]propellane, which is the least strained member of this series. These bridgehead atoms, together with the bridgehead carbon atoms in bicyclo[1.1.0]butane have the lowest energy of all the atoms of the molecules studied here. Strain energies reported in Figure IV.1 for the bridgehead carbons are calculated by comparing their atomic energies to the energy assigned to the standard C group. This standard group is actually considerably more stable than the C group in neopentane as no charge transfer effects are taken into account, which has been previously discussed. Therefore the bridgehead group contributes to the total strain energy of the molecule in two of the propellanes, [2.1.1]propellane and [2.2.1]propellane, despite their large negative charges and low energies. The bridgehead carbon of [2.1.1]propellane whose average electron population exceeds that of the actual C group in neopentane by 0.268e has an energy that is approximately 100 kcal/mol lower. Of all the bridgehead carbons in this series of propellane molecules, those of [1.1.1]propellane are the least stable. Relative to the standard group energy each of the bridgehead carbon atoms contribute 44.0 kcal/mol to the strain energy of the

molecule. The next most stable bridgehead carbon atoms are those found in [2.1.1]propellane. Each of these carbons is 11.4 kcal/mol higher in energy than the standard C group. In this and others of this series of molecules the smallest of the bond angles formed with the bridgehead bond are those with the bonds of the three membered rings. All of these angles are about 60° . The extent of the relaxation of charge density about this angle is about the same for the three such angles found in [1.1.1]propellane as it is for the two such angles in [2.1.1]propellane with $\Delta\alpha$ equal to 10° . In [2.2.1]propellane however the extent of the relaxation of strain is greater as is reflected by the value of $\Delta\alpha$ being 16° . As a consequence, this carbon atom has the largest negative charge and is the most stable of all the bridgehead carbon atoms. Its energy is lower than that of the standard group by 24.3 kcal/mol. In [2.2.2]propellane, the least strained of the propellanes studied here, the bridgehead carbon atoms carry the least net charge of all the bridgehead carbon atoms and the relaxation as measured by $\Delta\alpha$ is correspondingly small. Its energy is 15.1 kcal/mol lower than the energy of the standard C group.

The three- and four-membered ring methylene groups in the propellanes behave in different ways with respect to their charge loss to the bridgehead carbon atoms. Their energies do not correlate with their net charges in the nearly linear fashion found in the bicyclic molecules. They do, however, experience an increase in the electronegativity as increased geometric strain is imposed. Atomic populations decrease in the order bridgehead, one-bridged methylenic carbon atom and two-bridged methylenic carbon atom. Charge is transferred to the bridgehead carbon atoms from both the three-membered-ring methylenic carbon as well as

the hydrogens. The net charge on these methylenic groups is essentially the same in [1.1.1]propellane, [2.1.1]propellane and [2.2.1]propellane with an increasing fraction of the charge residing on the carbon atom. In concert with this increase in positive charge is the increase of the strain energy from 5 to 11 to 14 kcal/mol respectively. It is important to note here that the two middle members of this series of molecules have the largest strain energies. The 6-31G^{*}/6-31G^{*} calculations are in good agreement with the values for these two molecules but they overestimate the strain energies in both [1.1.1]- and [2.2.2]propellane by 6 kcal/mol.⁵

The methylenic carbon in a four-membered ring bears the largest positive charge in these molecules. In both [2.1.1]propellane and [2.2.1]propellane this net charge is about +0.1e but decreases to half this value in the less strained [2.2.2]propellane. The hydrogens are negatively charged in these methylenic groups. Since these carbon atoms lose the largest amount of charge to the bridgehead carbon atoms, they are the least stable carbon atoms in the propellane molecules. These methylenic groups therefore make larger contribution to the overall strain energy compared to the three-membered rings. No matter what standard groups are chosen, the order of stability of carbon atoms in these propellanes will still be bridgehead carbon more stable than the methylenic carbon of a three-membered ring which in turn is more stable than the methylenic carbon of a four-membered ring. This order of stabilities is a result of the flow of charge within the molecules, which is from the methylenic carbon atoms to the bridgehead carbon atom. The largest flow of charge

⁵The 6-31G^{**}/6-31G^{*} results for [1.1.1]propellane are very similar, yielding strain energies for the methylene and C groups of 4.5 and 44.7 kcal/mol, respectively, and a total strain energy of 103 kcal/mol.

to the bridgehead carbon atoms comes from the methylenic carbon of a four-membered ring. This will result in each of the propellanes exhibiting a relatively large quadrupole moment.

The term "unusual" has been used to describe the structure of the propellane molecules. they are unusual in the sense that they do not fit any of the standard hybridization models. In [2.2.2]propellane the bridgehead bond path angles or bond angles predict sp^2 hybridization for the bridgehead carbon, giving a bridgehead bond of pure p which is in agreement with the form of the SCF orbital. However, the energy of the bridgehead carbon atom is 66 kcal/mol more stable than that of the sp^2 carbon in ethylene, but this difference can be understood. In ethylene, the pure p hybrid forms a π -bond while in the propellane the pure p hybrid forms a σ -bond with the second bridgehead carbon with a bond order of 1.26. In [1.1.1]propellane the bond path angles formed at a bridgehead carbon are very close to those required for sp^3 hybrid orbitals to be directed at the bridging methylenes. With this hybridization model then the bridgehead bond arises from the overlap of the tails of two sp^3 hybrid orbitals on the bridgehead carbons. These models account for the bridgehead carbon atoms of [2.2.2]propellane being lower in energy than those of [1.1.1]propellane. It is difficult however to rationalize the larger net charge on the bridgehead carbons in [1.1.1]propellane or to rationalize the charges and energies of the two intermediate members of this series in terms of the orbital model.

III. Summary

The charge distribution of a methyl or methylene group can appear

unchanged as a transferable unit throughout a homologous series of molecules. These methyl and methylene groups behave in this manner if they are defined and bounded by the zero flux surface in the gradient of the charge density. When one of these transferable groups occurs in a molecule, the contribution by the group to the total energy of the molecule is also unchanged. This accounts for the additivity observed for this homologous series. As the electronic charge distribution changes in one of these groups, so too does its contribution to the total energy of the molecule. Changes in the charge distribution induced by the changes in its environment can be related to the change in its energy. The underlying reason for the observation of additivity in this series of molecules is the fact that the change in energy for a change in population, the quantity $\Delta E/\Delta N$, is the same for both the methyl and methylene groups. These observations give further support for the definition of atoms given by the theory. Using this definition it is possible to trace the changes in atomic properties as the form of the atom concerned changes with its bonding environment.

Examples where the methylene group can be transferred with no change, or with little change or with substantial change have been given here. The standard methylene group is identified with the transferable repeating group as found in the central positions of pentane and hexane. The methylene group in cyclohexane is found to be nearly identical and thus the energy of this group in cyclohexane is nearly unchanged from that of the standard. The strain energy of this molecule is therefore zero, which is in agreement with experiment. As the energy of the standard methylene group is independently fixed by the theory, the fact

that the energy of cyclohexane is six times the energy of the standard group is very much a consequence of this atomic theory.

In trying to understand strain one could study the cyclic molecules as has been done here. The methylene group in cyclopropane is dramatically different than the standard methylene group. At first glance, the results obtained in the analysis of this molecules yields what may seem to be surprising. One observes that the atom that is subjected to strain is stabilized at the expense of destabilization of the directly bonded hydrogens. Therefore, when a carbon atom is subjected to strain, its electronegativity relative to hydrogen is increased. This increased electron-withdrawing power of the carbon atom causes an increase in the electron population of the atom and a corresponding increase in its stability. A measure of the amount of geometric strain that the carbon atom is being subjected to is the departure of the bond path angle from the tetrahedral angle, $\Delta\alpha$. The larger the value of $\Delta\alpha$, the more electronegative the carbon atom becomes and hence the more stable. As an example, the bridgehead carbon atom in bicyclo[1.1.0]butane is more stable than the methylenic carbon atom from which it withdraws charge. This reasoning accounts for the relative values of the strain energy calculated the individual groups in the cyclic, bicyclic and propellane molecules. For the cyclics and bicyclic molecule these observations can be rationalized in terms of orbital model. Using hybridization arguments and $J(^{13}\text{C}-\text{H})$ coupling constants, this model is able to predict that the percent s character of the hybrid orbitals from carbon to dissimilar neighboring groups increases as the carbon atom is subjected to an increasing degree of geometric strain. This results in an increase in the

electronic population and an accompanying increase in the stability relative to its bonded neighbours. It should be noted here that the atomic charges defined by the theory have a direct physical and spatial significance. There is therefore a physical flow of charge from the peripheral groups to the bridgehead carbon atoms in both the bicyclic and propellane series of molecules. The magnitude of this charge transfer increases as the bridgehead carbon atom experiences increased geometric strain.

Bader, Henneker and Cade in 1967 proposed that a particular outer contour of the charge density could be used to define the shape of a molecule for its non-bonded interaction with other molecules. This contour was chosen to be the 0.002au contour and it provided a good approximation to the van der Waals' envelope of a molecule (Bader et al 1967, Bader and Preston 1970). This Hartree-Fock based envelope model for the diatomic molecules N_2 , O_2 and F_2 was and still is being used in the elucidation of the crystal structures of the various solid phases of these systems (Barrett and Meyer 1967, Meyer 1969, Mills and Schuch 1969, Schuch and Mills 1970, Raich and Mills 1971, Schiferl et al 1983). From this study, it is clear that good van der Waals' envelopes can be constructed for hydrocarbons of any chain length from the charge distributions of the standard repeating methyl and methylene groups as defined using the theory. Using the theory of atoms in molecules, it is possible to define these groups which account for the additivity observed in the hydrocarbons. Indeed, the atoms of theory can be identified as the atoms of chemistry.

Figure IV.1

Carbon skeletal structures of strained molecules. Opposite each CH_2 , CH , or C group is given the net charge on C , the average net charge on the H atoms, the net charge for the group and the strain energy (E) for the group in kcal/mol. The total strain energy is given below each structure in kcal/mol followed by the experimental value in parenthesis.

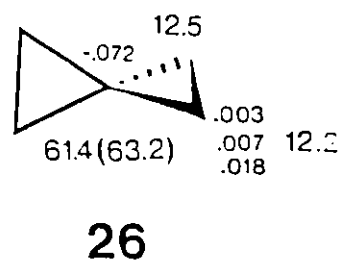
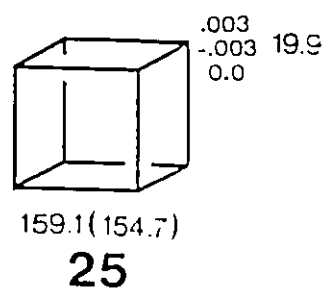
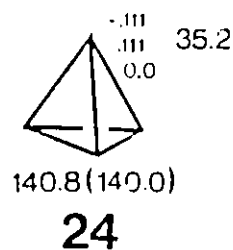
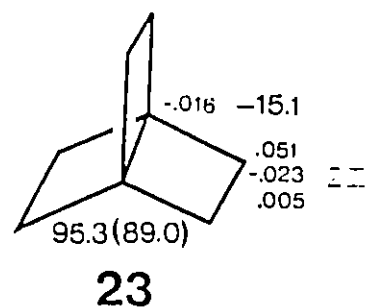
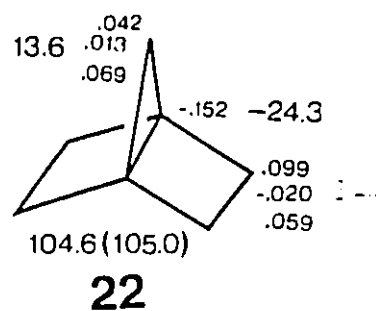
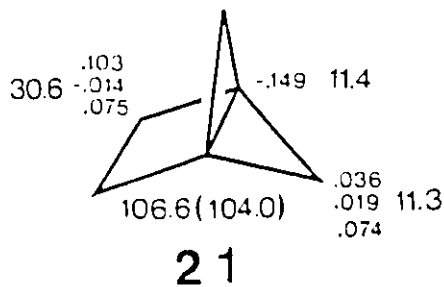
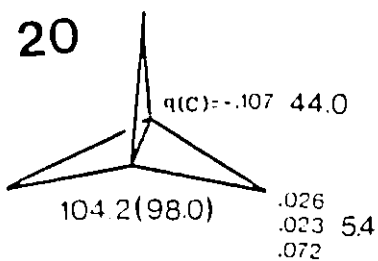
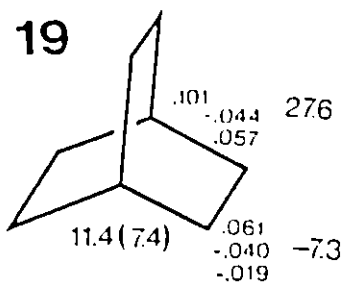
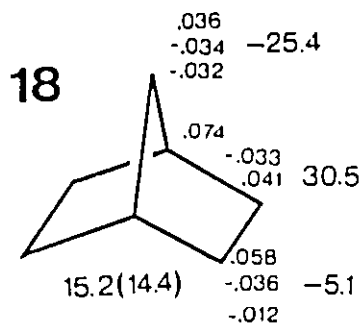
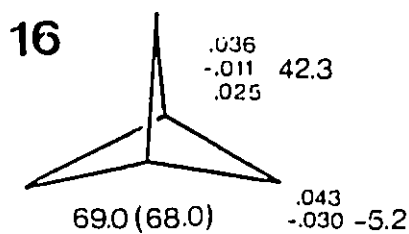
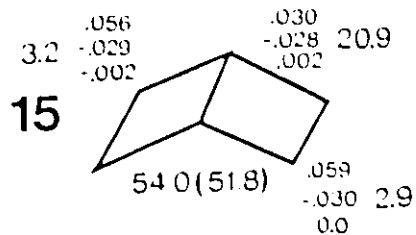
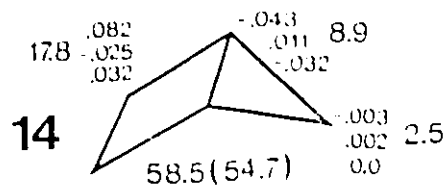
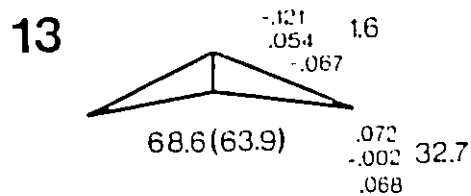
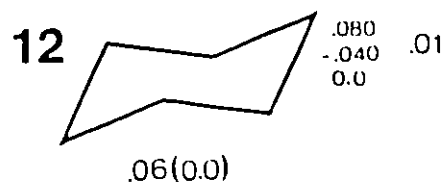
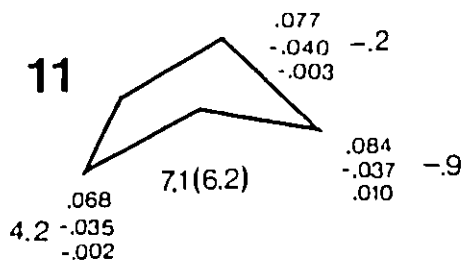
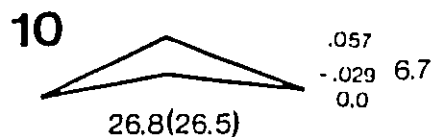
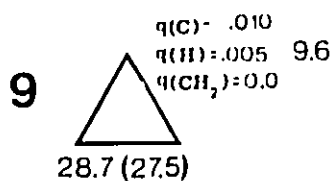


TABLE IV.1
ATOMIC PROPERTIES IN HYDROCARBONS^a

MOLECULE	N(n)	L(n) au	T(n)=-E(n) au	$v_{\text{ncn}}(n)^b$ au	$\rho(0)^c$ au
1. METHANE	C1: 5.9668 H2: 1.0083	-0.00017 0.00007	37.73936 0.61395	-89.55023 -1.29140	117.9958 0.4252
2. ETHANE	C1: 5.9249 H3: 1.0248	0.00040 0.00007	37.73323 0.62711	-89.47475 -1.31048	117.9993 0.4298
3. PROPANE	C1: 5.9373 *C2: 5.8924 H4: 1.0248 H5: 1.0275 H7: 1.0367	-0.00070 -0.00477 -0.00002 0.00013 0.00006	37.75004 37.72485 0.62640 0.62735 0.63826	-89.53348 -89.42062 -1.31006 -1.31202 -1.32562	118.0234 118.0078 0.4294 0.4293 0.4338
4. BUTANE	C1: 5.9350 *C2: 5.9043 H5: 1.0251 H6: 1.0281 H8: 1.0397	-0.00012 0.00053 0.00017 0.00010 0.00020	37.74948 37.73827 0.62734 0.62804 0.63902	-89.52894 -89.46767 -1.31094 -1.31299 -1.32760	118.0218 118.0265 0.4298 0.4297 0.4334
5. ISOBUTANE	*C1: 5.9433 C2: 5.8706 H5: 1.0275 H6: 1.0296 H7: 1.0452	-0.00058 -0.00041 0.00009 0.00010 0.00039	37.76337 37.71128 0.62776 0.62759 0.64825	-89.57491 -89.37296 -1.31251 -1.31290 -1.33740	118.0450 118.0176 0.4295 0.4287 0.4369
6. PENTANE	C1: 5.9343 *C2: 5.9047 C3: 5.9142 H6: 1.0251 H7: 1.0280 H9: 1.0399 H11: 1.0430	0.00024 0.00072 0.00069 0.00008 0.00009 0.00011 0.00011	37.74725 37.74062 37.75732 0.62702 0.62790 0.63884 0.63949	-89.52447 -89.47012 -89.53001 -1.31087 -1.31260 -1.32732 -1.32916	118.0224 118.0262 118.0470 0.4298 0.4295 0.4332 0.4327
7. NEOPENTANE	C1: 5.9460 *C2: 5.8626 H6: 1.0295	0.00005 -0.00163 -0.00008	37.77488 37.69291 0.62845	-89.59899 -89.35801 -1.31412	118.0642 118.0287 0.4294
8. HEXANE	C1: 5.9357 *C2: 5.9044 C3: 5.9136 H7: 1.0249 H8: 1.0280 H10: 1.0400 H12: 1.0427	0.00051 0.00223 0.00086 0.00008 0.00009 0.00010 0.00011	37.74940 37.73837 37.75598 0.62660 0.62775 0.63926 0.63977	-89.52884 -89.46315 -89.52404 -1.31021 -1.31247 -1.32777 -1.32940	118.0196 118.0228 118.0399 0.4294 0.4294 0.4334 0.4329
9. CYCLOPROPANE	*C1: 6.0102 H4: 0.9949	0.00035 0.00009	37.78234 0.61866	-89.76484 -1.28992	117.9648 0.4307

TABLE IV(continued)

MOLECULE		$N(R)$	$L(R)$	$T(R)=-E(R)$	$v_{\text{neo}}(R)^b$	$\rho(0)^c$
			au	au	au	au
10. CYCLOBUTANE	*C1	5.9434	0.00028	37.75930	-89.56237	118.0458
	H5	1.0289	0.00008	0.63220	-1.31694	0.4324
	H9	1.0277	0.00009	0.63252	-1.31613	0.4318
11. CYCLOPENTANE	*C1	5.9160	0.00185	37.75849	-89.54247	118.0532
	C2	5.9241	0.00077	37.75620	-89.53876	118.0506
	C3	5.9308	0.00040	37.74861	-89.53831	118.0435
	H6	1.0326	0.00009	0.63551	-1.32195	0.4333
	H7	1.0416	0.00044	0.64224	-1.33123	0.4348
	H8	1.0407	0.00010	0.64200	-1.33093	0.4350
	H9	1.0386	0.00013	0.63691	-1.32338	0.4339
	H10	1.0338	0.00004	0.63861	-1.32508	0.4344
	H11	1.0369	0.00010	0.64088	-1.32805	0.4349
12. CYCLOHEXANE	*C1	5.9202	0.00024	37.75803	-89.53898	118.0411
	H7	1.0361	0.00009	0.63708	-1.32445	0.4330
	H8	1.0437	0.00010	0.63965	-1.32954	0.4326
13. BICYCLO[1.1.0]BUTANE	C1	6.1210	0.00017	37.86024	-90.15791	117.9854
	*C2	5.9283	0.00208	37.74152	-89.47624	118.0013
	H5	0.9463	0.00006	0.59296	-1.24273	0.4233
	H6	0.9976	0.00008	0.61878	-1.29218	0.4318
	H7	1.0068	0.00011	0.62233	-1.29753	0.4319
14. BICYCLO[2.1.0]PENTANE	C1	6.0433	0.00136	37.82717	-89.92775	118.0263
	*C2	5.9160	0.00464	37.74429	-89.46026	118.0412
	C5	6.0063	-0.00034	37.79396	-89.78073	117.9951
	H6	0.9893	-0.00003	0.61440	-1.28320	0.4296
	H9	1.0288	0.00009	0.63150	-1.31510	0.4324
	H10	1.0211	-0.00007	0.63070	-1.31205	0.4324
	H12	0.9941	0.00007	0.61707	-1.28832	0.4296
	H13	1.0027	0.00009	0.61985	-1.29386	0.4297
15. BICYCLO[2.2.0]HEXANE	C1	5.9696	-0.00123	37.78665	-89.66826	118.1042
	C2	5.9408	0.00100	37.76071	-89.55634	118.0571
	C3	5.9444	-0.00020	37.76075	-89.56513	118.0571
	H7	1.0284	0.00020	0.63593	-1.32088	0.4356
	H8	1.0275	0.00008	0.63420	-1.31812	0.4333
	H9	1.0317	0.00010	0.63527	-1.32133	0.4338
	H10	1.0269	0.00012	0.63391	-1.31764	0.4333
	H11	1.0307	0.00009	0.63506	-1.32055	0.4335
16. BICYCLO[1.1.1]PENTANE	*C1	5.9644	-0.00286	37.76700	-89.60721	118.1198
	C2	5.9570	-0.00002	37.77870	-89.60816	118.1069
	H6	1.0108	0.00006	0.62135	-1.29980	0.4321
	H7	1.0298	0.00009	0.63215	-1.31847	0.4335

TABLE IV (continued)

MOLECULE	N(α)	L(α) au	T(α) = -E(α) au	V _{neα} (α) ^b au	$\rho(0)$ ^c au
17. BICYCLO[2.1.1]HEXANE					
C1					118.1144
C2					118.0573
C5	5.9722	-0.00431	37.78935	-89.66434	118.0999
H7	1.0233	0.00078	0.63224	-1.31672	0.4358
H8	1.0341	0.00010	0.63781	-1.32500	0.4345
H13	1.0365	-0.00004	0.63654	-1.32563	0.4346
H14	1.0257	0.00009	0.63232	-1.31674	0.4329
18. BICYCLO[2.2.1]HEPTANE					
C1	5.9264		37.76991		118.1025
C2	5.9418	0.00120	37.76787	-89.59428	118.0642
C7	5.9641	-0.00174	37.80857	-89.71516	118.1034
H8	1.0326	-0.00008	0.63734	-1.32484	0.4328
H9	1.0356	0.00010	0.63808	-1.32497	0.4334
H10	1.0349	0.00010	0.63690	-1.32395	0.4330
H13	1.0344	0.00011	0.63334	-1.32077	0.4309
19. BICYCLO[2.2.2]OCTANE					
*C1	5.8991	0.00425	37.76559	-89.53394	118.0823
C2	5.9389	-0.00241	37.76453	-89.59438	118.0552
H9	1.0441	0.00011	0.64631	-1.33629	0.4366
H10	1.0400	0.00015	0.64099	-1.32957	0.4341
20. [1.1.1]PROPELLANE					
*C1	6.1076	0.00136	37.80619	-89.70868	118.4066
C2	5.9744	-0.00084	37.79998	-89.87218	118.1019
H6	0.9770	0.00010	0.61313	-1.27767	0.4329
21. [2.1.1]PROPELLANE					
*C1	6.1494	0.00159	37.85821	-90.11457	118.2880
C2	5.8969	-0.00017	37.72970	-89.40991	118.0267
C5	5.9640	-0.00063	37.78928	-89.67126	118.0640
H7	1.0138	0.00007	0.62813	-1.30639	0.4328
H11	0.9835	0.00010	0.61373	-1.27717	0.4311
H12	0.9786	0.00010	0.61376	-1.28079	0.4316
22. [2.2.1]PROPELLANE					
C1	6.1523		37.91503		118.0866
C2	5.9009	0.00044	37.71759	-89.36616	118.0406
C7	5.9584	0.00090	37.77666	-89.62300	118.0122
H8	1.0232	0.00009	0.63198	-1.31418	0.4338
H9	1.0168	0.00010	0.62953	-1.30930	0.4328
H16	0.9867	0.00011	0.61822	-1.28619	0.4323
23. [2.2.2]PROPELLANE					
*C1	6.0156	0.00192	37.90048	-89.98833	118.1432
C2	5.9494	0.00110	37.74431	-89.53655	118.0572
H9	1.0227	0.00009	0.62855	-2.61113	0.4304
24. TETRAHEDRANE					
C1	6.1112	-0.00002	37.83669	-90.06453	117.9035
H5	0.8889	-0.00009	0.56298	-1.18673	0.4138

TABLE IV(continued)

MOLECULE		$N(\Omega)$	$L(\Omega)$ au	$T(\Omega)=-E(\Omega)$ au	$V_{\text{neo}}(\Omega)^b$ au	$\rho(0)^c$ au
25. CUBANE	*C1	5.9966	0.00102	37.80932	-89.73640	118.1552
	H9	1.0034	0.00006	0.61481	-1.28869	0.4266
26. SPIROPENTANE	*C1	5.9969	0.00353	37.78213	-89.71807	117.9752
	C3	6.0718	0.00115	37.85633	-90.11441	117.8755
	H6	0.9926	0.00014	0.61658	-1.28652	0.4296

^a Numbering of structures and of atoms is as given in Table I of part I⁴. Also see Fig. 1 of this paper.

^b $V_{\text{neo}}(\Omega)$ is the potential energy of interaction of the nucleus of atom Ω with the electronic charge of Ω .

^c $\rho(0)$ is the value of the charge density at the nuclear maximum. This is shifted slightly off the nuclear position ($\sim 3 \times 10^{-2}$ au) for a proton for a basis set which does not contain polarizing functions on hydrogen. A Gaussian basis set was used in these calculations and such functions do not satisfy the nuclear cusp condition on ρ .

Table IV.2

Total Energies and Errors in Integrated Atomic Energies and Populations

Molecule	$E(6-31G^*/6-31G^*)^a$ au	$E - \sum_{\Omega} E(\Omega)$ kcal/mole	$N - \sum_{\Omega} N(\Omega)$	$(\tau-1)^c$
1. Methane	-40.19517	-0.02	0.0000	1.000301
2. Ethane	-79.22876	0.22	0.0011	1.000364
3. Propane	-118.26365	-1.97	-0.0033	1.000358
4. Butane	-157.29841	1.06	0.0032	1.000320
5. Isobutane	-157.29896	1.90	-0.0016	1.000314
6. Pentane	-196.33303	2.49	0.0035	1.000261
7. Neopentane	-196.33382	1.81	-0.0001	1.000254
8. Hexane	-235.36779	1.29	0.0065	1.000362
9. Cyclopropane	-117.05886	0.07	0.0022	1.000488
10. Cyclobutane	-156.09703	-0.59	0.0012	1.000347
11. ^a Cyclopentane	-195.16266	1.00	-0.0064	1.000280
12. Cyclohexane	-234.20802	0.34	0.0025	1.000378
13. Bicyclo[1.1.0]butane	-154.87169	-0.02	0.0037	1.000397
14. Bicyclo[2.1.0]pentane	-193.92697	1.65	0.0135	1.000312
15. ^a Bicyclo[2.2.0]hexane	-232.96520	-0.15	0.0001	1.000360
16. Bicyclo[1.1.1]pentane	-193.90568	-1.69	-0.0037	1.000054
17. ^a Bicyclo[2.1.1]hexane ^b	-232.98929			1.000400
18. Bicyclo[2.2.1]heptane ^b	-272.06115			1.000372
19. Bicyclo[2.2.2]octane	-311.10358	-0.54	-0.0021	1.000235
20. [1.1.1]propellane	-192.69110	-2.34	0.0008	0.999810

Table IV.1(continued)

Molecule	$E(6-31G^*/6-31G^*)^a$ au	$E - \sum_{\Omega} E(\Omega)$ kcal/mole	$N - \sum_{\Omega} N(\Omega)$	$(\gamma-1)$
21. [2.1.1]propellane	-231.72188	-1.12	0.0034	1.000054
22. [2.2.1]propellane ^b	-270.75956			1.000544
23. [2.2.2]propellane	-309.80907	1.57	0.0089	1.000396
24. Tetrahedrane	-153.59788	0.48	-0.0005	1.000544
25. Cubane	-307.39370	-0.38	0.0062	1.000293
26. Spiropentane	-193.91753	1.88	0.0158	1.000612

^a Cases marked with a are 6-31G*/4-31G.

^b by difference.

^c $\gamma = -V/T$

^d 1 au = 627.51 kcal/mol

TABLE 1.3

Effect of basis set on atomic populations^a

Molecule	q(C)			q(H)			Δ^b
	STO-3G	6-31G**	6-31G*	STO-3G	6-31G**	6-31G*	
CH ₄	0.250	0.244	.039	-.062	-.061	-.008	-.053
C ₂ H ₆	.228	.237	.075	-.076	-.079	-.025	-.054
CH ₃ CH ₂ CH ₃	.207	.225	.063	-.077	-.079	-.025	-.054
				-.078	-.082	-.028	-.054
CH ₃ CH ₂ CH ₂	.225	.220	.110	-.086	-.092	-.037	-.055
CH ₃ CH(CH ₃) ₂	.187	.218	.057	-.074	-.082	-.028	-.054
				-.075	-.084	-.030	-.054
CH(CH ₃) ₃	.208	.193	.129	-.099	-.102	-.045	-.057
CH ₃ (CH ₂) ₂ CH ₃		.224			-.079	-.025	-.054
					-.082	-.028	-.054
CH ₃ (CH ₂) ₂ CH ₂		.210			-.095	-.040	-.055
CH ₃ (CH ₂) ₃ CH ₃		.227			-.080	-.025	-.055
					-.082	-.028	-.054
CH ₃ CH ₂ (CH ₂) ₂ CH ₃		.209			-.095	-.040	-.055
CH ₃ CH ₂ (CH ₂)CH ₂ CH ₃		.196			-.098	-.043	-.055
C(CH ₃) ₄		.214	.054		-.084	-.030	-.054
C(CH ₃) ₃		.151	.137		-	-	-
C ₃ H ₆	.098	.104	-.010	-.049	-.052	.005	-.057
[1.1.1]propellane							
CH ₂		.137	.026		-.033	.023	-.056
C		-.105	-.107				
C ₂ H ₄		.082	-.035		-.041	.017	-.058
C ₂ H ₂		-.121	-.177		.121	.177	-.056

^a results are from STO-3G/STO-3G, 6-31G**/6-31G* and 6-31G*/6-31G* calculations.^b Δ is the difference in hydrogen populations, double star - single star results.

Table IV.4

Net Charges on Methyl and Methylene Groups
and their Energies Relative to Standard Values^a 6-31G*/6-31G*

Molecule	$q(\text{CH}_3)$	$q(\text{CH}_2)$	$q(\text{CH}_2)^b$	$\Delta E(\text{CH}_3)$	$\Delta E(\text{CH}_2)$	$\Delta E(\text{CH}_2)^b$
	e			kcal/mole		
Methane	+0.032					
Ethane	+0.000					
Propane	-0.017	+0.034		-10.5	+21.0	
Butane	-0.016	+0.016		-11.6	+11.6	
Pentane	-0.016	+0.016	+0.000	-9.9	+10.3	-0.7
Hexane	-0.017	+0.016	+0.001	-10.7	+11.2	-0.5

^a $E(\text{CH}_3)$ in ethane = A = -39.61438 au

$E(\text{CH}_2) = B = -39.03478$ au

^b This CH_2 is bonded only to other methylenes.

Table IV.5

Properties of H and C atoms in CH_3 relative to CH_3 in hexane

Atom	Molecule	$\text{H}(\Omega)$ e	$\text{I}(\Omega) = -E(\Omega)$	$V_{\text{eno}}(\Omega)$	$V_{\text{en}}(\Omega)$	$V_{\text{ee}}(\Omega)$	$V_{\text{nn}}(\Omega)$	$V(\Omega) = 2E(\Omega)$
totals for hexane in au, differences in kcal/mole								
H1	Hexane	1.025	0.6266	-1.3102	-9.3780	4.3442	4.3503	-1.2532
	Pentane	0.000	+0.3	-0.4	356.4	-178.7	-178.5	-0.6
	Butane	0.000	+0.4	-0.4	791.9	-396.5	-396.6	-0.8
	Propane	0.000	-0.1	+0.0	1343.0	-671.7	-671.2	+0.2
H2	Hexane	1.028	0.6276	-1.3125	-10.5354	4.6370	4.6429	-1.2555
	Pentane	0.000	-0.1	-0.1	381.4	-190.8	-190.8	+0.2
	Butane	0.000	+0.1	-0.3	894.1	-445.7	-448.8	-0.2
	Propane	0.000	-0.3	+0.3	1505.3	-754.1	-753.6	+0.6
C	Hexane	5.936	37.7494	-89.5288	-138.1157	37.6551	24.9598	-75.4988
	Pentane	-0.001	-1.3	-2.7	2333.6	-1160.4	-1164.5	+2.7
	Butane	-0.001	+0.1	-0.1	5349.0	-2672.7	-2676.4	-0.2
	Propane	+0.001	+0.4	-2.9	9157.3	-4580.3	-4577.8	-0.8

Chapter V

Models of Molecular Geometry and Reactivity

1. Introduction

It was stated in the introduction to this thesis that the Laplacian of the electronic charge distribution recovers the Lewis model of localized electron pairs. The physical basis of the Lewis models of molecular geometry and chemical reactivity is therefore, contained in the properties of the Laplacian of the charge density. This fundamental property of the Laplacian distribution function is demonstrated here (Bader et al 1984).

The Laplacian distribution function also provides a classification of atomic interactions (Bader and Essen 1984). The local expression of the virial theorem equation (43), relates the sign of the Laplacian of the charge density, $\nabla^2\rho$, to the relative magnitudes of the local contributions of the potential and kinetic energy densities to their virial theorem averages. By mapping those regions where $\nabla^2\rho < 0$, the regions where electronic charge is concentrated, one is mapping the regions where the potential energy density makes its dominant contributions to the lowering of the total energy of the system, equation (43). It is found that such a mapping of the potential energy density defines a spectrum of possible atomic interactions, with those characterized as shared at one extreme, and those characterized as closed-shell at the other (Bader and Essen, 1984).

This classification scheme will be used in an analysis of the bonding in the hydrocarbon molecules, particularly to obtain a deeper understanding of the bridgehead bond in the propellanes. The stability of

the propellanes is also examined from the point of view of how the charge density changes as the nuclei are displaced from their equilibrium positions. This is accomplished by using second-order perturbation theory, a procedure which enables one to identify the most facile nuclear displacement and the accompanying relaxation of the charge density.

2. The role of the Laplacian of the charge density in the quantum theory of molecular structure.

The Laplacian of the charge density in the theory, appears as an energy density in the theory, that is as $L(\underline{r})$, the quantity

$$L(\underline{r}) = -(\hbar^2/4m)\nabla^2\rho(\underline{r}) \quad (69)$$

The integral of $L(\underline{r})$ over an atom Ω to yield the atomic Lagrangian $L(\Omega)$

$$\begin{aligned} L(\Omega) &= \int_{\Omega} L(\underline{r}) d\tau \\ &= (-\hbar^2/4m) \int_{\Omega} \nabla^2 \rho(\underline{r}) d\tau \\ &= (-\hbar^2/4m) \oint dS(\Omega, \underline{r}) \nabla \rho(\underline{r}) \cdot \underline{n}(\underline{r}) = 0 \end{aligned} \quad (70)$$

This integral vanishes because of the zero flux boundary condition, equation (1), which defines an atom in a molecule. The demonstration in Chapter I that an atom is an open quantum subsystem is obtained by a variation of Schrodinger's energy functional $E[\psi, \Omega]$ for a stationary state and by a variation of the action integral for a time dependent system. In each case the zero flux boundary condition is introduced by imposing the variational constraint that

$$\delta L(\Omega) = (\int_{\Omega} \nabla^2 \rho(\underline{r}) d\underline{r}) = 0 \quad (71)$$

at every state of the variation. The possibility of introducing the constraint in this manner is a consequence of the property of the functionals $E[\psi, \Omega]$ and $\mathcal{L}(\psi, \Omega)$, that at the point of variation where the appropriate Schrodinger equation is satisfied, they both reduce to an integral of the density $L(\underline{r})$. The property given in equation (70) is common for an atom and for the total system and it is this property which provides them with similar variational properties, thereby making possible the generalization of the principle of stationary action to an atom in a molecule.

The two forms of the kinetic energy densities $K(\underline{r})$ and $G(\underline{r})$ are defined in terms of the one-density matrix as follows (Bader and Nguyen-Dang 1981a):

$$K(\underline{r}) = (-1/4) \{ (\nabla^2 + \nabla'^2) \Gamma^{(1)}(\underline{r}, \underline{r}') \}_{\underline{r}=\underline{r}'} \quad (71)$$

and

$$G(\underline{r}) = (1/2) (\nabla \cdot \nabla' \Gamma^{(1)}(\underline{r}, \underline{r}'))_{\underline{r}=\underline{r}'} \quad (72)$$

In general, $K(\underline{r})$, the Schrodinger kinetic energy, and $G(\underline{r})$, the gradient kinetic energy, differ by

$$L(\underline{r}) = K(\underline{r}) - G(\underline{r}) = (-1/4) \nabla^2 \rho(\underline{r}) \quad (73)$$

It is because $L(\Omega)$ vanishes for an atom that $T(\Omega)$, the electronic kinetic energy of an atom is well defined, equation (48). It has been demonstrated (Bader and Nguyen-Dang 1981a) that the density $L(\underline{r})$

appears in the local expression for the virial theorem above. This is an important result, since it relates a property of the charge density to the local contributions to the energy, and it is given here as equation (74)

$$(\hbar^2/4m)\nabla^2\rho(\underline{r}) = 2G(\underline{r}) + V(\underline{r}) \quad (74)$$

The electronic potential energy density $V(\underline{r})$, the virial of the forces exerted on the electrons and the electronic kinetic energy density $G(\underline{r})$ define the electronic energy density $E_e(\underline{r})$

$$E_e(\underline{r}) = G(\underline{r}) + V(\underline{r}) \quad (75)$$

Because $L(\Omega)$ vanishes for an atom, integration of equation (75) over the basin of an atom yields the atomic virial theorem

$$2T(\Omega) = -V(\Omega) \quad (76)$$

and as a consequence, the electronic energy of an atom in a molecule satisfies the following identities

$$\begin{aligned} E_e(\Omega) &= \int_{\Omega} E_e(\underline{r}) d\tau \\ &= -T(\Omega) \\ &= (1/2)V(\Omega) \end{aligned} \quad (77)$$

It is a property of the Laplacian of a scalar function such as the

charge density $\rho(\underline{r})$, that it determines where the function is locally concentrated, where $\nabla^2\rho(\underline{r}) < 0$, and locally depleted, where $\nabla^2\rho(\underline{r}) > 0$. Electronic charge is concentrated in those regions of space where the Laplacian of the charge density is negative. The expressions 'local charge concentrations' and 'local charge depletions' will refer to maxima and minima in the function $\nabla^2\rho(\underline{r})$, extrema which are to be distinguished from local maxima and minima in the charge density itself. This property of the Laplacian can be used to determine the dominant contributions to the local energy of the electronic charge distribution using the local expression for the virial theorem.

The potential energy density $V(\underline{r})$ is everywhere negative, while the kinetic energy density is everywhere positive. Thus the sign of the Laplacian of the charge density determines, via equation (74), which of these two contributions to the total energy is in excess over their average virial ratio of 2:1. In regions of space where the Laplacian is negative and electronic charge is concentrated, the potential energy dominates both the local total electronic energy $E_e(\underline{r})$ and the local virial relationship. Where the Laplacian is positive and electronic charge is locally depleted, the kinetic energy is in local excess.

An energy density is dimensionally equivalent to a force per unit area or a pressure. Thus the Laplacian may alternatively be viewed as a measure of the pressure exerted on the electronic charge density relative to the value of zero required to satisfy a local statement of the virial theorem, that is $V(\underline{r}) + 2G(\underline{r}) = 0$. In regions where the Laplacian is negative, the charge density is tightly bound and compressed above its average distribution. In regions where the

Laplacian is positive, the charge density is expanded relative to its average distribution, the pressure is positive and the kinetic energy of the electrons is dominant.

3. The Laplacian of the Charge Density and the Lewis Electron Pair Model.

Neither the electronic charge density nor the electronic pair density offer any evidence of the localized bonded and nonbonded pairs of electrons evoked in the Lewis model of electronic structure. The relatively simple topology exhibited by the charge density has already been described and while it accounts for elements of molecular structure, it does not offer any suggestion of the existence of spatially localized pairs of electrons. The extent to which electrons are spatially localized is determined by the pair density, a distribution function whose properties are dominated by the so-called Fermi hole (Bader and Stephens 1975). An electron can only go where its hole goes and thus an electron is localized to a given region of space only if its Fermi hole is correspondingly localized (Bader and Nguyen-Dang 1981a). The Fermi hole is very localized for motion of an electron in the immediate vicinity of a nucleus. It is possible to define a core radius within which the contained Fermi correlation is maximized for one α and one β electron and the result is a region of space from which essentially all other electrons of both spins are excluded to yield a localized pair of electrons. The fluctuation in the average population of such a region of space is minimized when the contained Fermi correlation is maximized (Bader and Nguyen-Dang, 1981).

Such physical localization of electronic charge is not a general phenomenon, but is found in atomic cores and within the atomic boundaries of ionic systems, such as the Na and Cl atoms in NaCl. In the atoms of these systems, the contained Fermi correlation approaches its limiting value, the negative of the average electron population, and the electrons are in excess of 90% localized within the separate atomic basins (Bader, 1975. Bader and Nguyen-Dang 1981). What one does not find is the pair population to predict are bonded or nonbonded pairs of valence electrons as envisaged by the Lewis model or as represented by individual localized orbitals.

The electron pairs of Lewis and the associated models of geometry and reactivity find physical expression in the topology of the Laplacian of the charge distribution. The Laplacian distribution recovers the electronic shell model of an atom by exhibiting a corresponding number of pairs of shells of charge concentration and charge depletion (Bader et al 1984. Smith and Simas 1988). For a spherical free atom, the outer or valence shell of charge concentration, the VSCC, contains a sphere over whose surface electronic charge is maximally and uniformly concentrated. Upon entering into chemical combination, this valence shell of charge concentration is distorted and maxima, minima and saddles appear on the sphere of charge concentration. The maxima correspond in number, location and in size to the localized pairs of electrons assumed in the Lewis model. The VSEPR model of molecular geometry (Gillespie 1972) is a direct extension of the Lewis model and predicts the geometries of closed-shell molecules about some central atom which contains from two

to seven pairs of electrons in its valence shell. All of the properties postulated in this model for bonded and nonbonded pairs of electrons are recovered by the maxima in the valence shell of charge concentration of the central atom and the Laplacian of the charge density provides a physical basis for this most successful of models of molecular geometry. This mapping of the topology of the $\nabla^2\rho$ onto the Lewis model is illustrated in Figure V.1 for the molecule ClF_3 whose T-shaped geometry can be deduced as a consequence of the behaviour of the maxima in the VSCC of the Cl atom - the most stable geometry being the one which maximized the separations between the maxima. It has been shown that positioning the reference electron at the critical point corresponding to a maximum in the Laplacian distribution maximally localized its Fermi hole (Bader and Stephens 1975).

The discussion so far has focused on the properties of the local charge concentrations of the Laplacian distribution and on how they recover the Lewis and VSEPR models of electron pairs. The Lewis model, however, encompasses chemical reactivity as well, through the concept of a generalized acid-base reaction. Complementary to the local maxima in the VSCC of an atom for the discussion of reactivity are its local minima. A local charge concentration is a Lewis base or a nucleophile, while a local charge depletion is a Lewis acid or an electrophile. A chemical reaction corresponds to the combination of a "lump" in the VSCC of the base combining with the "hole" in the VSCC of the acid. In terms of the local virial theorem, equation (74), the reaction of a nucleophile with an electrophile is a reaction of a region with excess potential energy on the base atom with a region of excess kinetic

energy on the acid atom. The accompanying rearrangement of the charge is such that at every stage of the reaction, $L(\Omega)$ remains equal to zero for each atom. Thus reductions in the magnitudes of the local concentrations or depletions of charge requires opposing changes in other parts of the atom to satisfy the constraint on its charge distribution as given in equation (70).

The positions of the local charge concentration and depletion together with their magnitudes, are determined by the positions of the corresponding critical points in the VSCC's of the respective base and acid atoms. This information enables one to predict positions of attack within a molecule or the geometries of approach of the reactants. For example, a keto oxygen in the formamide molecule has two large nonbonded charge concentrations in the plane of the nuclei ($\nabla^2\rho = -6.25$ and -6.30 au) while the nitrogen atom exhibits two such maxima of less magnitude ($\nabla^2\rho = -2.14$ au) above and below this plane. On the basis of this information one correctly predicts that the formamide molecule will preferentially protonate at the keto oxygen, specifically at the position of the largest of the two charge concentrations and in the plane of the nuclei. There are holes in the VSCC of a carbonyl carbon and they determine the position of nucleophilic attack at this atom. These holes are above and below the plane of the nuclei of the keto grouping and the corresponding critical point for a number of ketones are positioned to form angles of 110 ± 1 with respect to the C=O bond axis. This is the angle of attack predicted for the approach of a nucleophile to a carbonyl carbon (Bader et al 1984)

Similar predictions have been made for the Michael addition reaction, specifically for the nucleophilic attack of an unsaturated carbon in acrylic acid, $\text{CH}_2=\text{CH}-\text{CO}_2\text{H}$ and methyl acrylic acid. The properties of the Laplacian distribution correctly predict that the attack occurs at the terminal carbon of the methylene group, the carbon of the unsubstituted acid being most reactive, and that the approach of the nucleophile will be from above or below the plane of the nuclei along a line forming an angle of 115° with the $\text{C}=\text{C}$ bond axis, the latter prediction being in agreement with calculations of the potential energy surface for this reaction. Bader and Chang (1989) have given a discussion of the use of the Laplacian distribution in the prediction of the sites of electrophilic attack in a series of substituted benzenes.

Electrostatic potential maps have been used to make predictions similar to these. Such maps, however, do not in general reveal the location of the sites of nucleophilic attack, as the maps are determined by only the classical part of the potential. The local virial theorem equation (74), which along with the kinetic energy density, determines the sign of the Laplacian of the charge density, involves the full quantum potential. The potential energy density $V(\underline{r})$ contains the virial of the Ehrenfest force, the force exerted on the electronic charge at a point in space. The classical electrostatic force is one component of this total force.

The Laplacian distribution has since been used to predict the structures of a large number of hydrogen bonded complexes by aligning the $(3,+3)$ critical point, a local charge depletion on the nonbonded side of the proton in the acid HF, with the $(3,-3)$ critical point of the base, a local

concentration of charge, for which $\nabla^2\rho$ attains its large value (Carroll 1989). With only a few exceptions, the geometries of the complexes predicted in the SCF calculations (which agree with experiment where comparison is possible), are those predicted by the properties of the Laplacian as outlined above.

4. The characterization of atomic interactions.

The gradient vector field of the charge density identifies the set of atomic interactions within a molecule. These interactions, which define the molecular structure, can be characterized in terms of the properties of the Laplacian of the charge density. The local expression of the virial theorem equation (74), relates the sign of the Laplacian of the charge density to the relative magnitudes of the local contributions of the potential and kinetic energy densities to their virial theorem averages. By mapping those regions where $\nabla^2\rho < 0$, the regions where electronic charge is concentrated, one is mapping those regions where the potential energy density makes its dominant contributions to the lowering of the total energy of the system.

As discussed in Chapter II the interaction of two atoms leads to the formation of a critical point in the charge density at which the Hessian of ρ has one positive eigenvalue labeled λ_3 and two negative eigenvalues labelled λ_1 and λ_2 , implying that ρ exhibits one positive and two negative curvatures at the point \mathbf{r}_c . Since the two perpendicular curvatures of the charge density, whose eigenvectors define the interatomic surface, are negative, the charge density is a maximum at \mathbf{r}_c in the interatomic surface and charge is locally concentrated there with respect to points in the

surface. The curvature of the electronic charge distribution along the interaction line is positive, charge density is locally depleted at \underline{r}_C relative to neighboring points along the line and the charge density is a minimum at \underline{r}_C along this line. Thus the formation of a chemical bond and its associated interatomic surface is the result of a competition between the perpendicular contractions of the charge density distribution towards the bond path which lead to a concentration or compression of charge along this line, and the parallel expansion of the charge density away from the surface which leads to its separate concentration in each of the atomic basins. The sign of the Laplacian of the charge distribution at the bond critical point, the quantity $\nabla^2\rho(\underline{r}_C)$, determines which of the two competing effects is dominant and because of the appearance of $\nabla^2\rho(\underline{r}_C)$ in the local expression for the virial theorem equation (74), its sign also serves to summarize the essential mechanical characteristics of the interaction which creates the critical point. There is therefore, an intimate link between the topological properties of the charge distribution and its Laplacian, the trace of the Hessian of the charge density, and through the properties of the Laplacian one may begin to bridge the gap between the form of the charge distribution and the mechanics which govern it. The reader is referred to Bader et al (1984) for a full discussion and for numerical and pictorial illustrations.

When $\nabla^2\rho(\underline{r}_C) < 0$ and is large in magnitude, electronic charge is concentrated in the internuclear region as a result of the dominance of the perpendicular contractions of the electronic charge distribution towards the interaction line, or equivalently in these bound systems, towards the bond path. The result is a sharing of electronic charge by both nuclei, as

it is found for interactions usually characterized as covalent or polar and they shall be referred to as shared interactions. In shared interactions, the region of space over which the Laplacian is negative and which contains the interatomic critical point, is contiguous over the valence regions of both atoms and the VSCC's of the two atoms form one continuous region of charge concentration. The interaction is dominated by the lowering of the potential energy associated with the formation of the (3,-1) critical point. In a shared interaction, the nuclei are bound as a consequence of the lowering of the potential energy associated with the concentration of electronic charge between the nuclei, equation (74).

This concentration of electronic charge in the interatomic surface is reflected in relatively large values of $\rho(r_c)$, the value of the charge density at the (3,-1) critical point, for molecules with shared interactions and the ratio of the perpendicular contractions of the charge distribution to its parallel expansion, as measured by the ratio $|\lambda_1/\lambda_3|$, is greater than unity. In cases of tight binding, as evidenced by the large negative values of $\nabla^2\rho(r_c)$ as found in N_2 for example, λ_3 as well as λ_1 and λ_2 is large in magnitude, but the ratio $|\lambda_1/\lambda_3|$ is still greater than unity. Occupation of the antibonding 2π orbital of AB or of the corresponding π_g orbital of A_2 , causes an increase in λ_3 .

The second limiting type of atomic interaction is that occurring between closed-shell systems, such as found in noble gas repulsive states, in ionic bonds, in hydrogen bonds and in van der Waals molecules. One anticipates that such interactions will be dominated by the requirements of the Pauli exclusion principle. Thus for closed-shell interactions, $\rho(r_c)$ is relatively low in value and the value of $\nabla^2\rho(r_c)$ is positive (Bader and

Essen 1984). The sign of the Laplacian is determined by the positive curvature of the charge density along the interaction line, as the exclusion principle leads to a relative depletion of charge in the interatomic surface. These interactions are dominated by the contraction of charge away from the interatomic surface towards each of the nuclei. The Laplacian of the electronic charge distribution is positive over the entire region of interaction and the kinetic energy contribution to the virial from this region is greater than the contribution from the potential energy.

The regions where the Laplacian is negative are, aside from small polarization effects, identical in form to those of a free atom or ion. Thus the spatial regions where the potential energy dominates the kinetic energy are confined to separate each atom, reflecting the contraction of the charge towards each nucleus, away from the region of the interatomic surface. The ratio $|\lambda_1/\lambda_3|$ is less than unity in all the examples of closed-shell interactions (Bader and Essen 1984).

5. Characterization of bonds in Hydrocarbons and Strain Energy

The values of $\nabla^2\rho_b$ for the C-H bonds mirror the behaviour of ρ_b , becoming more negative as ρ_b increases in magnitude. Thus, the relatively large value for ρ_b found in the bridgehead C-H bond, and other hydrogens bonded to strained carbons, is due to the increased contraction of the charge density towards the bond critical point as evidenced by the relatively large negative value of $\nabla^2\rho_b$.

A somewhat different behaviour is observed for the C-C bonds. The values of $\nabla^2\rho_b$ and their constituent components show only small variations for the

majority of these bonds. In the case of the three-membered rings of the bicyclic molecules as well as in cyclopropane, the magnitude of $\nabla^2\rho_b$ for those bonds with significant ellipticities is diminished. This is a result of the reduction in the magnitude of one of the negative curvatures due to delocalization of electronic charge over the ring surface. Examination of contour maps of the Laplacian of cyclopropane in Figure V.2 and of the four-membered ring in [2.2.2]propellane shown in Figure V.3 clearly shows the difference between the concentration of charge in cyclopropane and in a four-membered ring. In cyclopropane, there is essentially a common charge concentration in the interior of the ring that contribute to the bonding of the three nuclei. The four-membered ring of [2.2.2]propellane however, shows charge concentration mainly along the bond, qualitatively different than in cyclopropane. This concentration of charge in the ring surface is due to the significant ellipticities of the ring bonds in cyclopropane. The negative curvature with the ellipticity smaller in magnitude lies in the plane of the ring, hence the charge concentration does not fall off as rapidly as in the direction of the perpendicular negative curvature. This delocalization of charge in the ring interior is reflected in the outward curve of the bond paths making up the ring. These ring bonds also have an unusually short bond length of 1.5069Å (compare to ethane C-C bond length of 1.5274Å). The strain energy resulting from the small bond angles in cyclopropane is offset by this ring delocalization which lowers the potential energy of all three ring carbons (Bader and Essen 1984). This is a unique feature found in three membered rings.

It has been shown (Wiberg 1985) that the enhanced electrophilic reactivity of cyclopropanes over cyclopentanes is not related to the

release of strain energy accompanying C-C bond rupture due to acetolysis. Although cyclopropane and cyclobutane have similar strain energies and enthalpies of acetolysis, cyclopropane has a moderate reactivity while cyclobutane is essentially inert. Susceptibility of cyclopropanes to protonation arises from the same origin as that for olefins, namely bonds with large ellipticities resulting in concentration of less tightly bound electronic charge. It is this loosely bound charge that is responsible for the enhanced electrophilic reactivity of cyclopropanes.

There is observed a trend in $\nabla^2\rho_b$ towards positive values for bonds between atoms of increasing electronegativity (Bader and Essen 1984). As the electronegativity of the individual atoms increases, the bonding between the atoms becomes dominated by the separate localization in the atomic basins. Carbon atoms under angular strain become more electronegative, thus the bridgehead bonds of the propellanes exhibit this trend of $\nabla^2\rho_b$ becoming more positive. From Table III.1, the value of $\nabla^2\rho_b$ for the bridgehead bond in [2.2.2]propellane is negative and large in magnitude. However, the magnitude of $\nabla^2\rho_b$ decreases as more angular strain is introduced into the molecule through the presence of three-membered rings. The value of $\nabla^2\rho_b$ in [2.1.1]propellane approaches zero and finally, $\nabla^2\rho_b$ reverses its sign and is positive in [1.1.1]propellane. Neither the bridgehead bond in [2.2.2]propellane nor those in [2.1.1] and [1.1.1]propellane are usual as compared to the acyclic hydrocarbons. In the case of [2.2.2]propellane, the bridgehead bond has a bond order of 1.26 yet it also possess the largest value of the positive curvature of ρ , $\lambda_3 = 0.3339$. Ethane in comparison has a bond order of unity and $\lambda_3 = 0.2928$. As more charge is concentrated between nuclei λ_3 usually decreases, but in

[2.2.2]propellane there is a tendency to separate the charge in individual atomic basins. For [2.1.1] and [1.1.1]propellane, the contour maps of $\nabla^2\rho$ of these molecules shows that the charge in the bonding regions differs from that of the acyclic hydrocarbons and hence the chemistry of these bridgehead bonds is different.

Since the Laplacian of ρ is a scalar field, it has a topology that can be studied in an analogous manner to that of ρ itself. Maxima in $\nabla^2\rho(\underline{r})$ are linked by lines originating from intervening saddle points. This topology exhibits features such as rings and cages. The total arrangement of maxima linked by lines encompassing local minima in $\nabla^2\rho(\underline{r})$ is called an atomic graph. Carbon atoms in acyclic hydrocarbons such as ethane, have the four bonded maxima arranged in a tetrahedral fashion. A bridgehead carbon of [2.2.2]propellane has a similar arrangement of its bonded maxima. Although there is some slight distortion, the basic pattern remains with the most noticeable difference being the value of $\nabla^2\rho(\underline{r})$ having a slight negative rather than positive value at the center of the face opposite the bridgehead bond. In [1.1.1]propellane however, the inverted geometry of the bridgehead carbon is reflected in the arrangement of the four bonded maxima. The shift of all four of the bonded maxima in the direction of the bridgehead bond causes the three saddle points that connect the bonded maxima other than the bridgehead to coalesce with the local minimum in the face center. This coalescence is not unlike that which is observed when a vertex of a three membered ring is stretched away from the other two vertices. In the case of the three membered ring, the two bond paths associated with the vertex being displaced become longer and their bond critical points get physically closer to each other as well as the ring

critical point. At some specific distance, the two bond critical points and the ring critical point coalesce and form a new but topologically unstable critical point (Bader et al 1981b). A similar scenario occurs in the case of the atomic graph of a carbon under geometric strain. As the bridgehead carbon in the propellanes undergoes increasing strain, the lines joining the bonded maxima get drawn closer together. As a consequence of this, the three saddle points in $\nabla^2\rho(\underline{r})$ defining the face opposite the bridgehead bond and the local minimum in that face come closer together until finally they coalesce, as in [1.1.1]propellane. The result is a broad local maximum, a non-bonded concentration of charge, in $\nabla^2\rho(\underline{r})$. In [1.1.1]propellane then, there are five local maxima in $\nabla^2\rho(\underline{r})$, four bonded and one non-bonded. The magnitude of $\nabla^2\rho(\underline{r})$ is greater for the non-bonded local maximum than for the bonded one associated with the bridgehead bond. This non-bonded maximum is the site of electrophilic attack. As is expected, the chemistry of [1.1.1]propellane reflects this difference in the Laplacian of ρ . [1.1.1]propellane has a pronounced susceptibility to protonation as in acetolysis (Wiberg and Szeimies 1970). If one looks at the plot of the Laplacian of ρ for [1.1.1]propellane after a displacement in the manner of an antisymmetric stretch shown in Figure V.3c, one observes a shortening of the bridgehead bond through concentration of charge between the nuclei and an enhancement of the non-bonded maxima of the bridgehead carbons. Therefore, displacements by way of this intense low frequency motion (Wiberg and Peters 1977. Wiberg and Sturmer 1975. Wiberg et al 1983) serves not only to strengthen the bridgehead bond but also to enhance the electrophilic susceptibility of [1.1.1]propellane.

According to the atomic virial theorem, equation (74), the charge

concentrations for which $\nabla^2\rho(r)$ is least negative will be the least tightly bound. This is observed to correlate spatially to the regions where the HOMO is most concentrated (Bader and MacDougall 1985). In the case of [1.1.1]propellane, the least tightly bound charge concentrations lie along the internuclear axis of the bridgehead bond. Their polarization into the non-bonded regions of the bridgehead atoms mimics the properties of the HOMO. Newton and Schulman (1972) have noted that when the molecular orbitals for [1.1.1]propellane are transformed into an equivalent set, there is a negative overlap population for the orbital localized between the bridgehead nuclei. Jackson and Allen have stressed the extent to which the HOMO accumulates charge in the non-bonding regions. Honegger et al (1985) have determined that the molecular ion formed in the lowest energy photoejection of an electron from [1.1.1]propellane has an equilibrium geometry which differs minutely from that of the parent molecule. This lowest energy photoejection electron comes from the HOMO, according to molecular orbital theory. Honegger et al argue that this lack of structural change can be viewed as a consequence of the non-bonding nature of [1.1.1]propellane. In terms of the properties of the total charge concentration, it has already been observed that there is a line of maximum charge density linking the bridgehead nuclei in the equilibrium geometry where the forces on the nuclei vanish and the bridgehead carbons are bonded. It has also been discussed previously how the nature of this bond differs from typical C-C bonds and within the framework of the orbital model, these differences are a consequence of the density of the HOMO (Newton and Schulman 1972a, Jackson and Allen 1984). In terms of the properties of the total charge density, these differences are most evident

in the Laplacian distribution.

The presence of these non-bonded charge concentrations on the bridgehead carbons does not imply that the net forces exerted on these nuclei by the bridgehead density is anti-binding rather than binding. The atomic dipole $\mu(\Omega)$ is the average of the position vector \underline{r} from the nucleus over the density in the basin of atom Ω . Thus, if the density is spherical, there is no atomic dipole present. In [1.1.1]propellane however, the presence of the non-bonded charge dominates the atomic dipole causing the atomic dipole of the bridgehead nuclei to be directed away from the other bridgehead nucleus. The force exerted on the bridgehead nucleus by its own charge density called the atomic force $F(\Omega)$. This is the average of the vector $\nabla \Omega \underline{r} / r^3$ over the density in the basin of atom Ω . In [1.1.1]propellane this force is directed towards the other bridgehead nucleus and is dominated by the density closer to the nucleus. This pattern of atomic moments, the atomic dipole directed away and the electric field gradient directed towards the bonded nuclei is not unique to these bridgehead carbons but is the normal pattern found in C_2 , N_2 , O_2 and F_2 (see Table V.1). From Table V.1, one notes that the largest atomic moments are for the nitrogens in N_2 which possess an axial "lone pair" and the strongest bond. Thus the bridgehead carbons in [1.1.1]propellane differ not in kind but only in degree of the polarizations. The dipole is larger and the binding force smaller in [1.1.1]propellane as compared to other atoms in molecules that are more strongly bound. In [2.2.2]propellane, this behaviour is reversed and once again, the atomic dipole moment is smaller and the binding force is a little larger. Consequently, the bridgehead carbons in [2.2.2]propellane do not exhibit the special properties they do in

[1.1.1]propellane.

The properties observed for the bridgehead carbons of [1.1.1]propellane are not typical. In [2.1.1]propellane and [1.1.0]butane, the bridgehead carbons also have an inverted geometry. However, on examination of Figure V.2b,d one notices that the non-bonded maxima are not along the internuclear axis of the bridgehead bond. Relative to [1.1.1]propellane, there is a large concentration of charge in the face opposite to the bridgehead bond in these two molecules rather than a depletion. Although these non-bonded maxima are not as accessible as those in [1.1.1]propellane, they should be susceptible to acetolysis. [1.1.0]butane is indeed susceptible to acetolysis (Wiberg et al 1985)

The reactivity and stability of a structure are determined not only by the properties of its equilibrium charge distribution but also by how the charge distribution changes as the nuclei are displaced. Second-order perturbation theory can be used to predict the essential features of the change or relaxation in the charge density for a given displacement of the nuclei (Bader 1960, 1962). This is done by approximating the relaxation in the electronic charge distribution by the transition density obtained by the mixing in of the lowest energy excited state of appropriate symmetry, where the symmetry is determined by the perturbing nuclear displacement. Assuming that the largest relaxation in the charge density is caused by mixing in the excited state of lowest energy, one is able to determine the nuclear displacement that results in the lowest energy increase. By predicting the stretching mode with the lowest force constant, the method may be used to predict the dissociative pathways of unimolecular reactions and the symmetries of equilibrium geometries (Pearson 1976, Bartell 1968).

When used together with the properties of the Laplacian of the charge density in determining the initial approach of the reactants, the method provides a basis for predicting chemical reaction pathways (Bader and Macdougall 1985).

The most strained propellanes and other related compounds such as bicyclo[1.1.0]butane all exhibit a characteristic and intense low-frequency absorption band in the infrared spectrum (Wiberg et al 1985. Wiberg and Peters 1977. Wiberg and Sturmer 1975). This band has been shown to correspond to an antisymmetric stretch of the bridgehead carbons with respect to the rest of the carbon framework. Mixing in of the excited state ψ_k with the ground state ψ_0 yields the transition density ρ_{0k} . This transition density is defined the same way as the ground state charge density except the product $\{\psi_0\}^2$ is replaced by $\{\psi_0\psi_k\}$. The orthogonality of state functions causes ρ_{0k} not to integrate to a finite amount of charge but rather it describes a change in the charge distribution. If ψ_0 is expressed as a single determinant and ψ_k is expressed of the occupied and virtual orbitals of ψ_0 obtained in a calculation of ψ_0 then ρ_{0k} reduces to a simple product of orbitals involving those that are singly occupied in ψ_k . Regions where $\rho_{0k} < 0$, charge is being removed. Conversely, for regions where $\rho_{0k} > 0$ charge is being accumulated. If ψ_0 is totally symmetric, as in the cases here, then ρ_{0k} will have the same symmetry as ψ_k and ρ_{0k} will approximate the relaxation of the charge density for a nuclear mode Q_i of identical symmetry. The charge density, correct to first order, expressed as a function of Q_i , the displacement from equilibrium along coordinate i is

$$\rho(Q_i) = \rho_{00} + C(Q_i)\rho_{0k} \quad (78)$$

which is correct to first order. In the above expression, ρ_{00} is the equilibrium charge density determined by ψ_0 and the coefficient which determines the extent of the relaxation $C(Q_i)$ is given by

$$C(Q_i) = 2(V_{0k}^i / (E_k - E_0))Q_i \quad (79)$$

The quantity V_{0k}^i measures the forces exerted on the nuclei by the transition density. The denominator in equation (79) leads one to anticipate that the largest relaxation will be observed for the mode Q_i of the correct symmetry which will mix in the lowest energy excited states. The transition density ρ_{0k} determines the change in the electric dipole moment, known as the transition dipole, caused by the displacement Q_i . The intensity of the mode Q_i is proportional to the square of the transition dipole. A summary of the symmetries of the highest occupied and lowest unoccupied orbitals of the propellanes is given in Figure V.4. Symmetric orbitals are labelled (S) and antisymmetric ones labelled (A), with symmetric or antisymmetric being referred to the symmetry plane which bisects the bridgehead bond. In each case, the HOMO is S, being primarily the in phase overlap of $p\sigma$ orbitals on the bridgehead carbons. The symmetries of the LUMO and LUMO+1 however switch from being A and S as in [1.1.1]propellane to S and A for [2.2.2]propellane. The antisymmetric lowest energy virtual orbital is in every case the anti-bonding counterpart of the HOMO while the symmetric lowest energy virtual orbital has very large s contributions from each carbon and is anti-bonding between every

carbon and its associated hydrogens.

The energy difference $E_k - E_0$ which appears in the denominator of equation 64 is approximated by the difference in orbital energies of those orbitals appearing in the transition density and is denoted $\Delta\epsilon$. It is observed that the difference in energy between the HOMO and its adjacent occupied orbital is larger than that of the two virtual orbitals. For [1.1.1] and [2.1.1]propellane the lowest energy transition density is for the antisymmetric one, ρ_{AS} . In [2.2.1]propellane, the two virtual orbitals are nearly degenerate and their order is reversed, as they are in [2.2.2]propellane. Thus for [2.2.1] and [2.2.2]propellane, the lowest energy transition density is the symmetric one, ρ_{SS} . Both the symmetric and antisymmetric transition densities for these molecules are shown in Figure V.5 and V.6. The relief maps of the transition density shown in Figure V.6 are all drawn to the same vertical scale, enabling qualitative comparison of their relative intensities. With the exception of [2.1.1]propellane, both ρ_{AS} and ρ_{SS} are most intense in the bridgehead region. Through the series [1.1.1]propellane to [2.2.2]propellane, ρ_{AS} decreases slightly while ρ_{SS} increases dramatically. As is illustrated by [1.1.1]propellane in Figure V.5, the antisymmetric charge relaxation corresponds to a large charge transfer from one bridgehead carbon to the other. This results in atomic dipoles that are similarly directed. Oppositely directed dipoles, smaller in magnitude, are created and centered on the other carbons. This flow of charge exerts forces on the nuclei such that the bridgehead atoms and the rest of the carbon framework move along parallel axes but in opposite directions corresponding to the A_2'' motion for [1.1.1]propellane. The symmetric charge relaxation directly affects

the charge density in the bridgehead bond, either concentrating or depleting charge in that region. This relaxation is illustrated by [2.2.2]propellane in Figure V.5. Concentration of charge in the bridgehead bond occurs for the symmetric motion of the nuclei corresponding to the A_1' symmetric stretch for [2.2.2]propellane, while depletion of charge occurs for the reverse motion of the nuclei.

The antisymmetric transition density ρ_{AS} is predicted to be the most easily induced change in the charge distribution of [1.1.1]propellane. The corresponding transition dipole is very large and is depicted quite well in both Figures V.5 and V.6. Based on these points one expects [1.1.1]propellane to possess a very strong low lying infrared band of A_2'' symmetry, which is indeed the case (Wiberg and Kass 1985). This vibration is predicted and found to be the most facile of the skeletal stretches. Modelling the effects of this vibrational mode can be done by displacing the center of the bridgehead bond by 0.02Å from the σ_h symmetry plane of the equilibrium geometry and re-optimizing the bridgehead separation as well as the distances of the apical carbons from the original center of symmetry. When this was done, it was found that the bridgehead separation decreased by 0.0504Å and the apical distances increased by 0.0162Å. The total energy increases by 9.0 kcal/mol. Therefore the most facile vibrational mode strengthens and shortens the bridgehead bond, increasing the bond order to 0.82. The Laplacian distribution is shown in Figure V.3c where one can observe a significant increase in the extent of charge accumulation in the bridgehead region and an enhancement of the non-bonded charge concentration which alternates between the two bridgehead atoms, as anticipated by the form of ρ_{AS} .

Through the series [1.1.1]propellane to [2.2.2]propellane the symmetric charge relaxation increases in intensity as the symmetric stretch also becomes an increasingly more facile motion. In [2.2.2]propellane, the symmetric stretch has become the most facile motion as shown in Figure V.4. The extension of the bridgehead bond associated with this stretching motion results in a weakening of this bond. The corresponding transition density transfers charge from the binding region to the anti-binding region of the bond. From this observation, one can anticipate that [2.2.2]propellane will be more susceptible to thermal rupture of the bridgehead bond than [1.1.1]propellane even though it has the highest bond order in the static equilibrium geometry. In [2.2.2]propellane the most easily excited thermal stretch coincides with extension of the bridgehead bond. As this stretch increases so does the intensity of the symmetric relaxation of the charge distribution as the energy of the HOMO increases thereby decreasing the $\Delta\epsilon$ for this excitation. In contrast recall that the most easily excited thermal motion for [1.1.1]propellane is the antisymmetric one which shortens and strengthens the bridgehead bond. This in part accounts for the lower susceptibility to thermolysis observed for [1.1.1]propellane as compared to [2.2.2]propellane, the activation energies being 30 and 22 kcal/mol respectively (Eaton and Temme 1973). In addition, both the static and dynamic properties of the charge distribution for [1.1.1]propellane account for the fact that it is susceptible to acetolysis, while the same properties for [2.2.2]propellane dictates that it be unreactive.

In [2.1.1]propellane, the ellipticity of the bridgehead bond is so great and the charge density is so close to the formation of a singularity as evidenced by the value of both $\nabla^2\rho_b$ and λ_2 approaching zero that this

instability in the charge distribution dominates the properties of the molecule. This molecule does not in fact survive above 50K (Wiberg 1983).

[2.2.1]propellane is also thermally unstable. This fact can be rationalized by the observation that the symmetric stretch, which has a moderate intensity, is the lowest thermally excitable mode and coupled with the high ellipticities of the three bonds of the three membered ring leads to the thermal instability.

Also shown in Figure V.4 is the orbital ordering for bicyclo[1.1.0]butane, another molecule that exhibits a high intensity low frequency absorption (Wiberg and Peters 1977). The bonding and antibonding character of the HOMO and of the symmetric and antisymmetric virtual orbitals is similar to the propellanes. The excitation energies for the SS and AS transition densities are close in value with the SS being the lowest. While the symmetric motion is predicted to be the favoured mode in terms of the $\Delta\epsilon$ values, one observes from Figure V.4 that ρ_{SS} will be of low intensity because the dipolar component of this transition density is small and tends to cancel out. However, the antisymmetric bridgehead stretch of B_1 symmetry shows a large transition dipole as depicted in the contour map for ρ_{AS} and therefore should be a very intense band. These predictions are in agreement with experiment (Wiberg and Peters 1977) which shows this molecule to have a weak low lying symmetric stretch at 422 cm^{-1} and a very strong antisymmetric stretch at 735 cm^{-1} . The chemistry of bicyclo[1.1.0]butane, like that of [1.1.1]propellane is dominated by the properties of the charge distribution in the bridgehead region. Both of these molecules exhibit non-bonded concentrations of charge on the two bridgehead carbons which are enhanced by asymmetric

polarization of the bridgehead density induced by the antisymmetric skeletal stretch. This leads to susceptibility to electrophilic attack such as acetolysis.

6. Conclusions

Quantum mechanics predicts the properties of an atom in a molecule in the same way it predicts the properties of the total system. These atomic properties can be measured experimentally and used to verify the predicted values. The atoms of theory were defined in Chapter I. These atoms satisfy the quantum boundary condition, equation (1),

$$\nabla \rho(\underline{r}) \cdot \underline{n}(\underline{r}) = 0 \quad \forall \underline{r} \in S(\Omega, \underline{r}) \quad (1)$$

and as a consequence obey the same quantum mechanics that governs the total system. Properties of these atoms are well defined and the important result that the total value of a property is a sum of the atomic contributions, equation (30),

$$\langle A \rangle = \sum_{\Omega} A(\Omega) \quad (30)$$

This is the principle underlying the cornerstone of chemistry, that atoms and functional groups of atoms make recognizable contributions to the total properties of a system. One recognizes a group and predicts its effect on the static and reactive properties of a system in terms of a set of properties assigned to that group. In the limiting case of a group having essentially the same distribution of electronic charge in two different systems, one obtains a so called additivity scheme for the total properties since in this case the atomic contributions in addition to being additive are also transferable between molecules.

An understanding of the topology of the electronic charge distribution was obtained in Chapter II. In that Chapter, regions of real space that satisfied the quantum boundary condition were identified as the atoms of chemistry. The concepts of bonds, molecular structure and structural stability were then discussed.

Concepts developed in Chapters I and II were applied to a series of molecules in Chapters III and IV. In Chapter III for each member of the series of molecules studied structures were assigned. The existence or absence of a bond between two nuclei is readily identified and the existence of the bridgehead bond in [1.1.1]propellane was discussed in more detail. Bonds were characterized in terms of a bond order, a bond ellipticity. It was also shown that the difference between the bond angle and the angle formed by the bond paths is a measure of the relaxation of the charge density away from the geometrical constraints of the nuclear framework.

In Chapter IV atomic properties were discussed. The constancy and transferability of group properties was shown to be a consequence of the separate transferability of the charge distribution for each separate atom. Standard groups are defined and used to predict total energies with a maximum error of 0.05 kcal/mol when compared to the total energies calculated at the 6-31G^{*}/6-31G^{*} level of approximation. These standard group energies are able to recover the group additivity observed for the homologous series of acyclic hydrocarbons. Changes in the distribution of charge of a group leads to a corresponding change in its energy, an observation that accounts for the origin of the strain energy in cyclic systems. Strain energies can be predicted using the standard groups

defined in this Chapter. The theoretical values for the strain energy are in good agreement with those from experiment.

It was shown in Chapter V how the Laplacian of the charge density recovers the Lewis and VESPR models of electron pairs. Not only does the Laplacian of the charge density recover these models of molecular geometry, but also the chemical reactivity aspects of these models. The Laplacian of the charge density can also be used to classify atomic interactions. In Chapter V this classification scheme was used in an analysis of the bonding in the hydrocarbon molecules, in particular to obtain a deeper understanding of the bridgehead bond in the propellanes. The stability of the propellanes was also examined from the point of view of how the charge density changes as the nuclei are displaced from their equilibrium positions. This was accomplished by using second-order perturbation theory, a procedure which enables one to identify the most facile nuclear displacement and the accompanying relaxation of the charge density.

Figure V.1

Relief maps of the Laplacian of the charge density for ClF_3 . The lower map is the symmetry plane containing all four nuclei. Bonded maxima are observed between Cl and each of the F atoms. The upper relief map is the σ_v symmetry plane showing the separation attained for the two non-bonded maxima of $\nabla^2\rho$ found in the Valence Shell Charge Concentration (VSCC) of the Cl atom. The T-shape geometry of this molecule can be deduced as a consequence of providing the largest separation of the non-bonded maxima in the VSCC of the Cl atom.

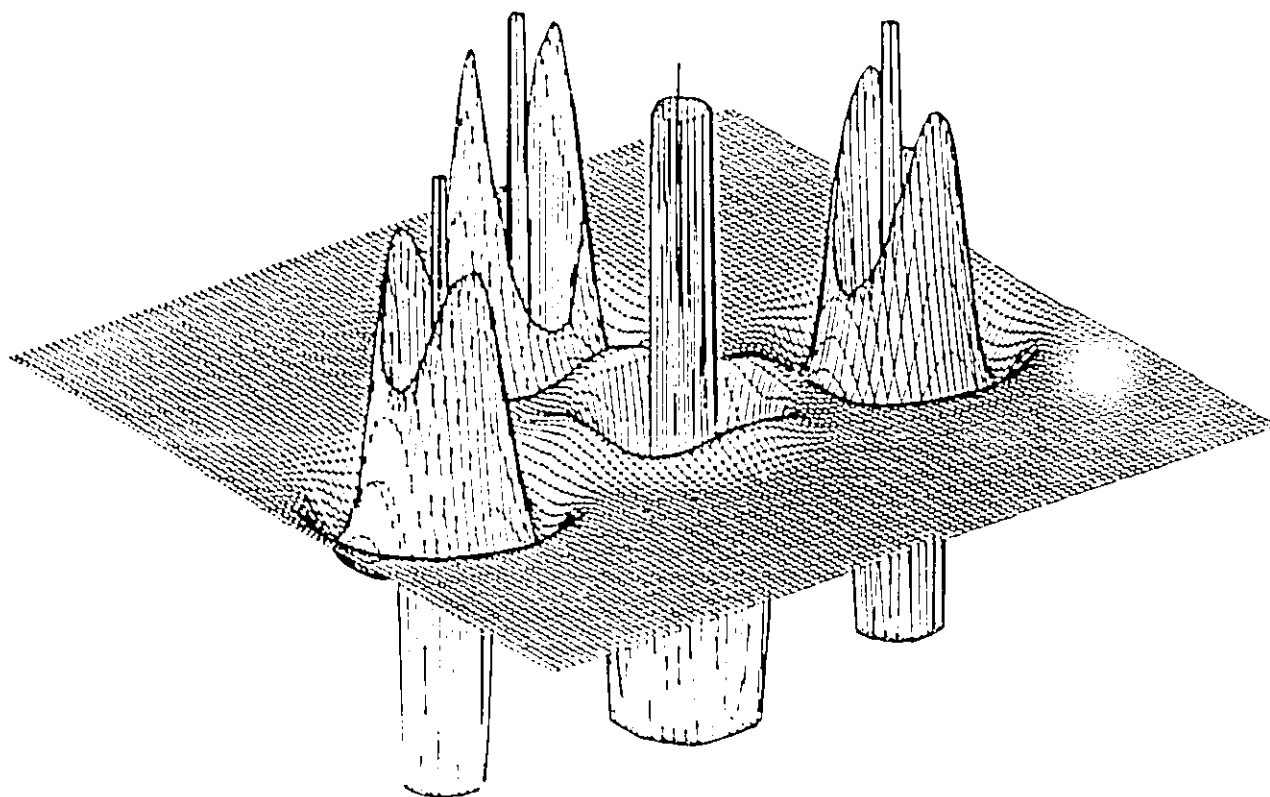
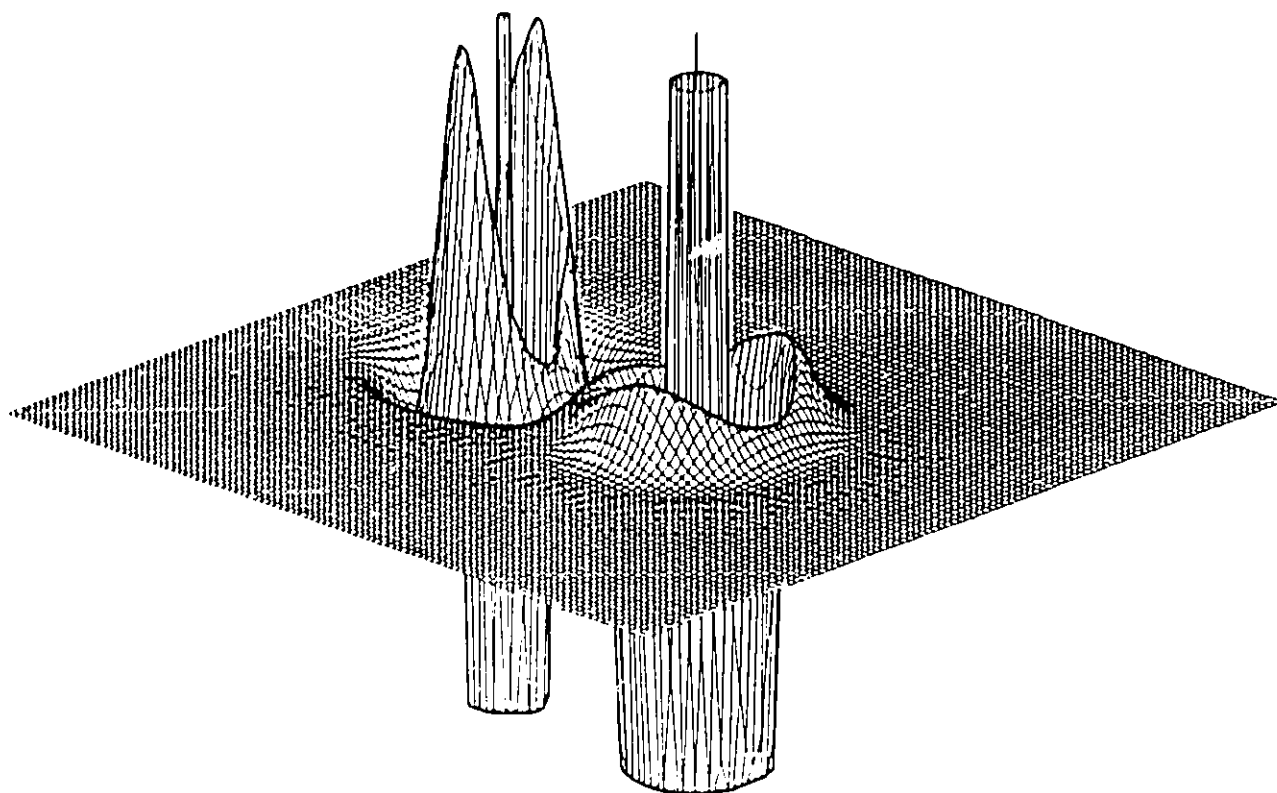
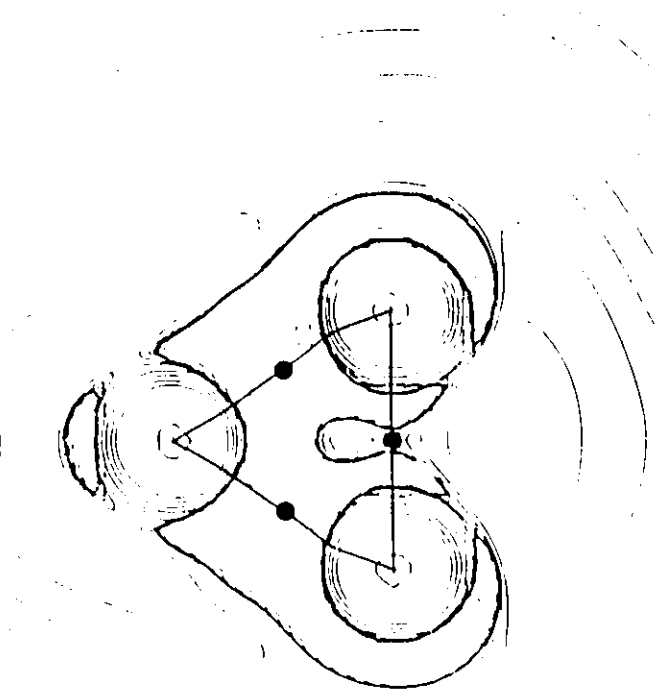


Figure V.2

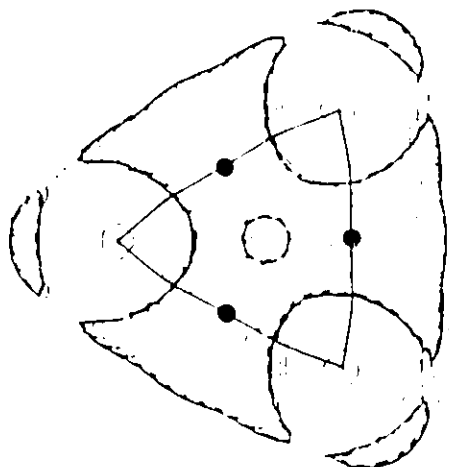
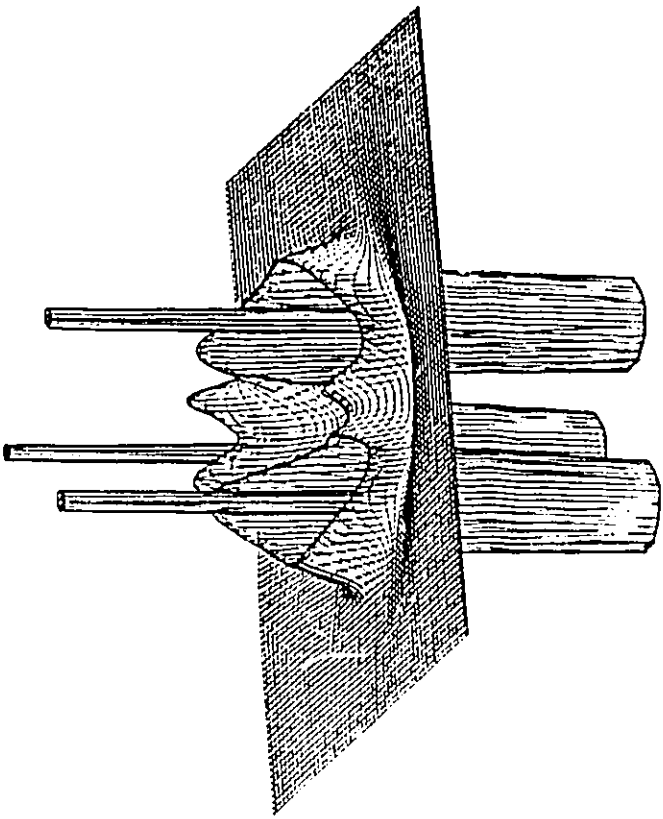
Contour maps of the Laplacian of the charge density overlaid with bond paths, and corresponding relief maps of the negative of this function. Dashed contours denote negative values. The spike like charge concentration at the nuclei has been terminated at -2.0au . Values of $\nabla^2\rho$ at the bond critical points are given in Table V.1.

(a) The symmetry plane of cyclopropane containing the three carbon nuclei. At a bonded maximum between a carbon atom to another carbon atom is -0.89au .

(b) The symmetry plane containing the bridgehead bond in [1.1.1]propellane. The value of $\nabla^2\rho$ at the bridgehead bonded maximum is -0.13au , -0.89au at the bonded maximum with a bridging carbon and -0.40au at the non-bonded charge concentration.



b



a

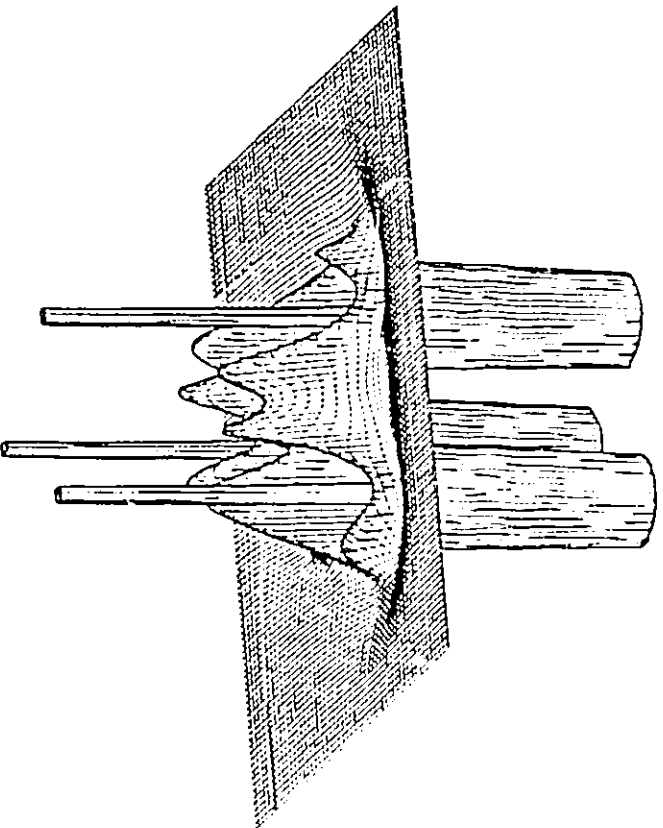
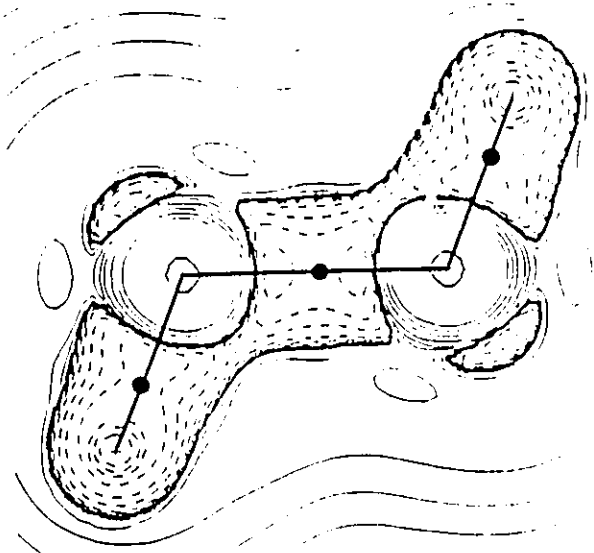


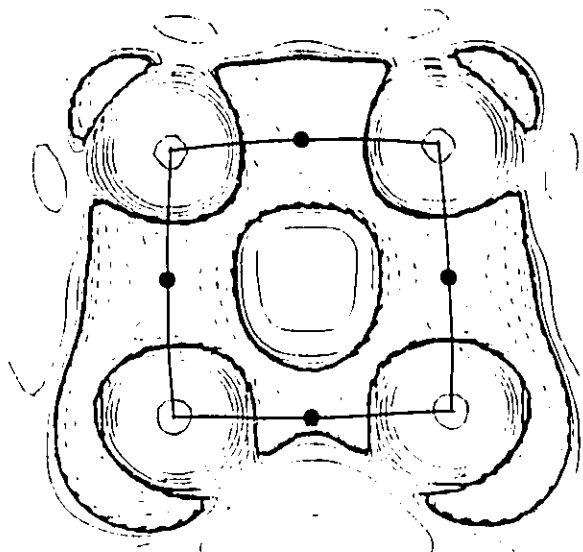
Figure V.3

Contour maps of the Laplacian of the charge density overlaid with bond paths. Values of $\nabla^2\rho$ at the bond critical points are given in Table V.1.

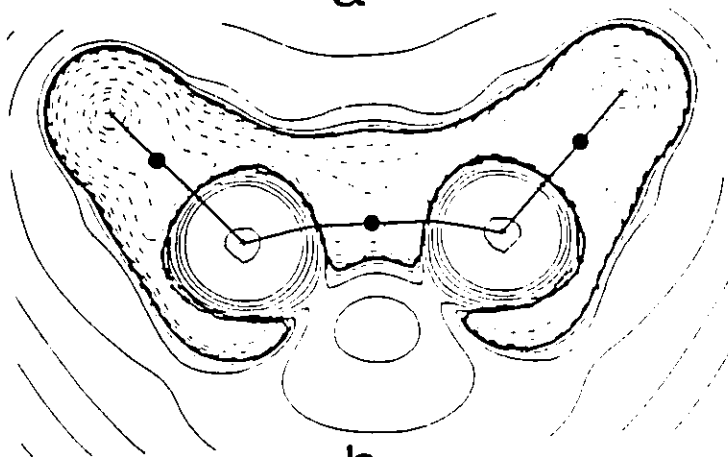
- (a) H-C-C-H plane of ethane. The value of $\nabla^2\rho$ at the bonded maximum along the CC bond axis is -1.03au.
- (b) H-C-C-H symmetry plane containing the bridgehead bond in bicyclo[1.1.0]butane. The value of the non-bonded charge concentration on the bridgehead carbon atom is -0.37au. Along the CC bond axis, the value of the bonded charge concentration is -0.72au.
- (c) Distorted geometry of [1.1.1]propellane in which the bridgehead nuclei are displaced in an opposite direction from the bridging methylene groups.
- (d) Plane of the four membered ring in [2.1.1]propellane. For the bonded maxima of the bridgehead bond, the value of $\nabla^2\rho$ is -0.29au and -1.05au for the second CC bond from the bridgehead carbon.
- (e) Plane of the three membered ring in [2.2.1]propellane. The value of $\nabla^2\rho$ for the bridgehead bond's bonded maxima is -0.86au and -0.84au for the second CC bond from the bridgehead carbon.
- (f) Plane of four membered ring in [2.2.2]propellane. The bridgehead bond's bonded maximum has a $\nabla^2\rho$ value of -1.29au and -0.99au for the bonded maximum of the second bond from the bridgehead carbon.



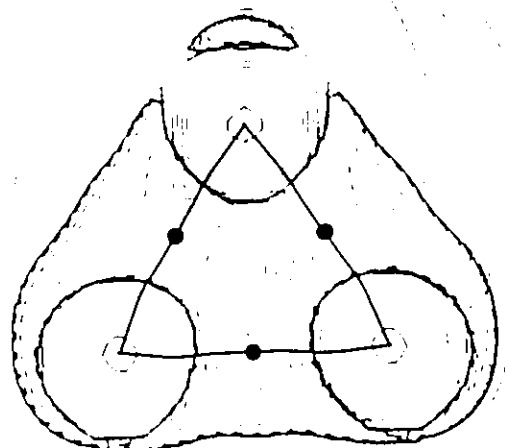
a



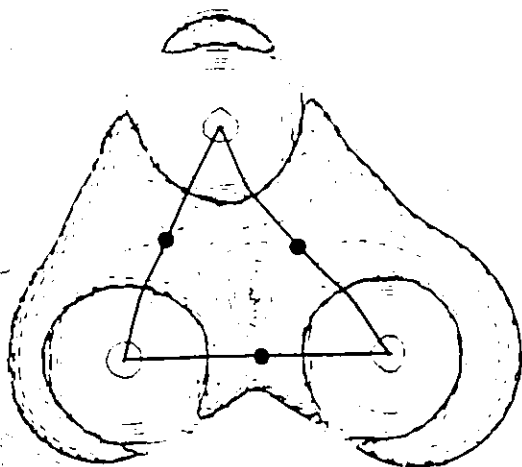
d



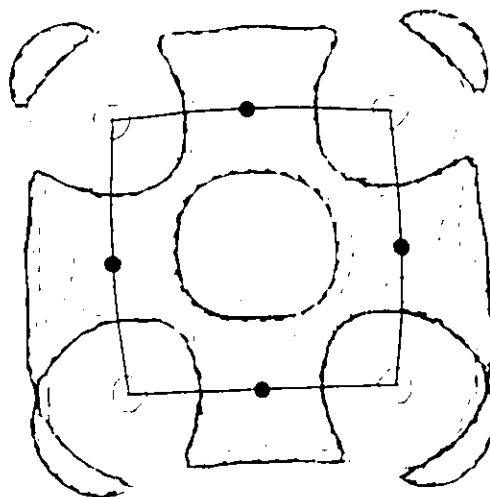
b



e



c



f

Figure V.4

Orbital energy level diagram for propellanes and bicyclobutane. The labels S, symmetric, and A, antisymmetric, denote behaviour with respect to the symmetry plane bisecting the bridgehead bond.

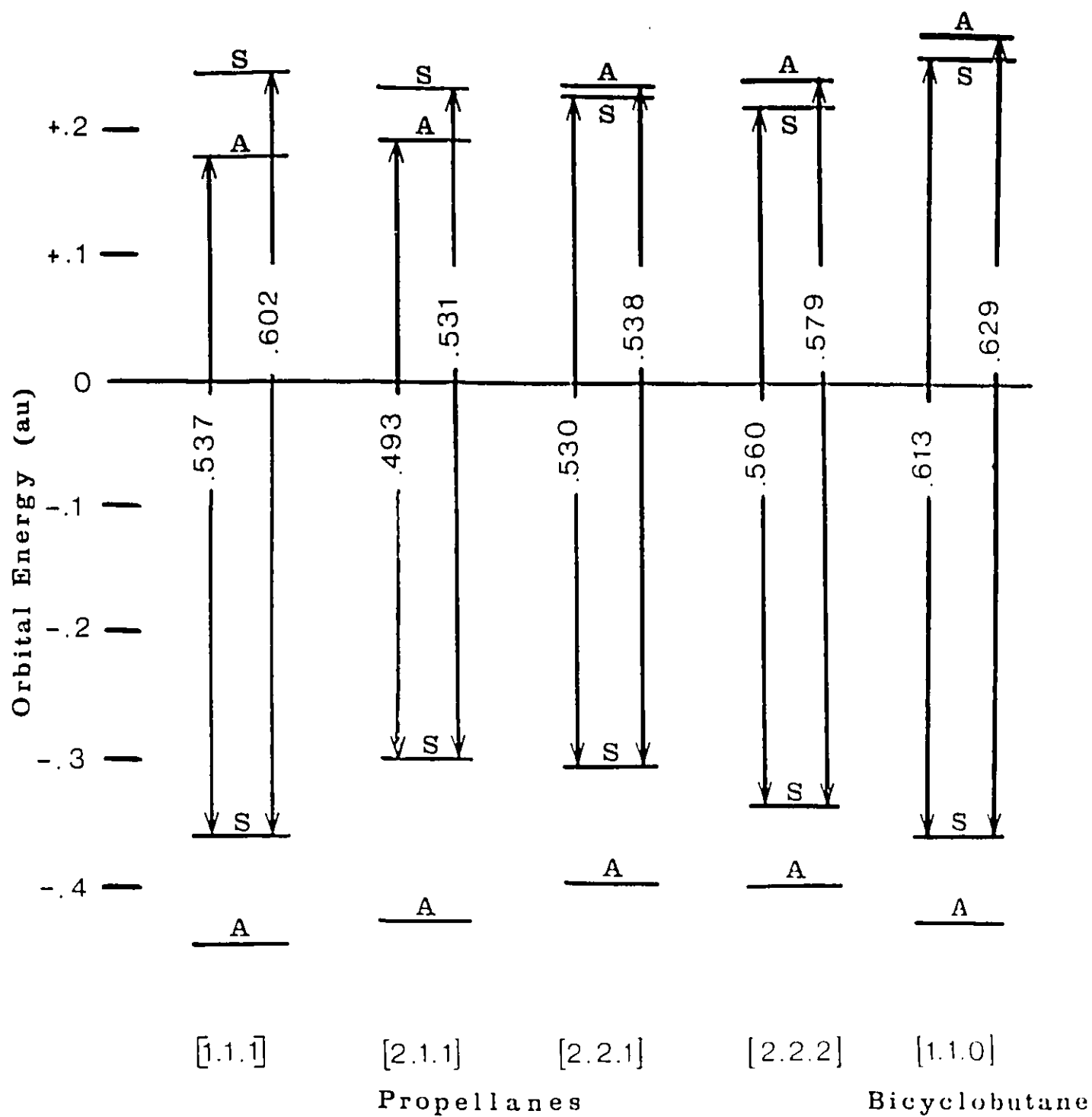
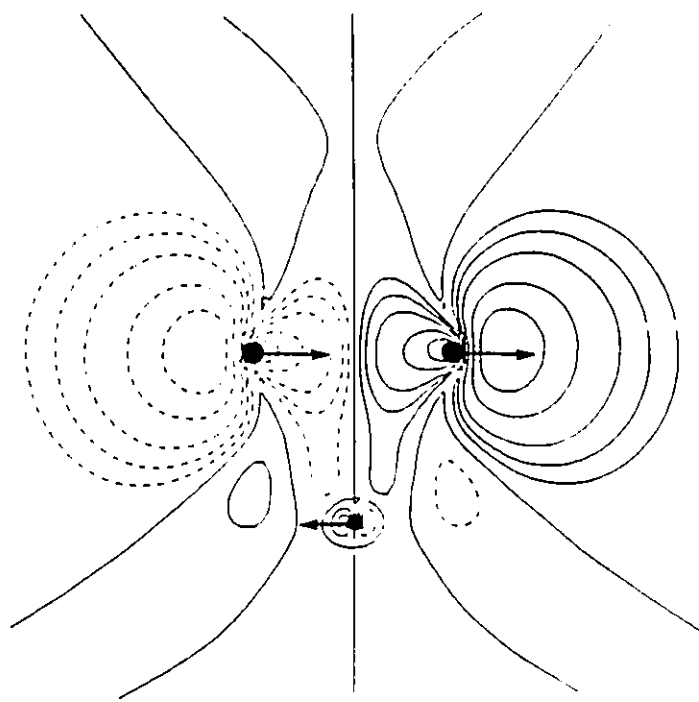


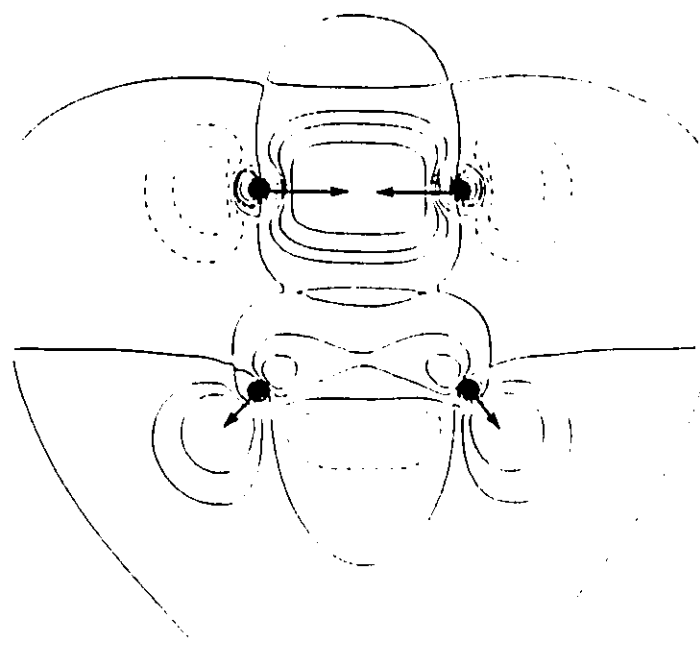
Figure V.5

Contour maps of the transition densities for the bridgehead bonds. The arrows indicate the nuclear motions they induce. Solid contours denote an increase, dashed contours a decrease, in the electronic charge density. Carbon nuclei are denoted by dots, hydrogen nuclei by squares.

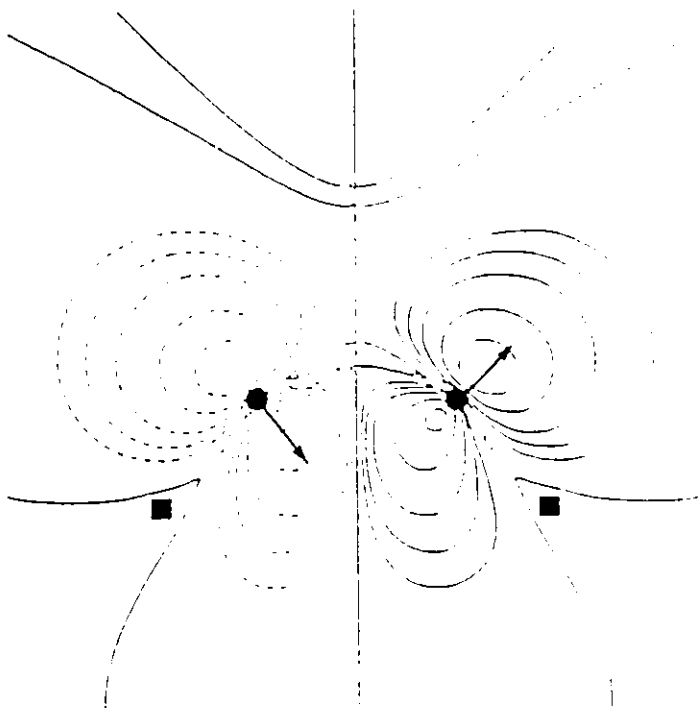


[1.1.1]

PROPELLANE

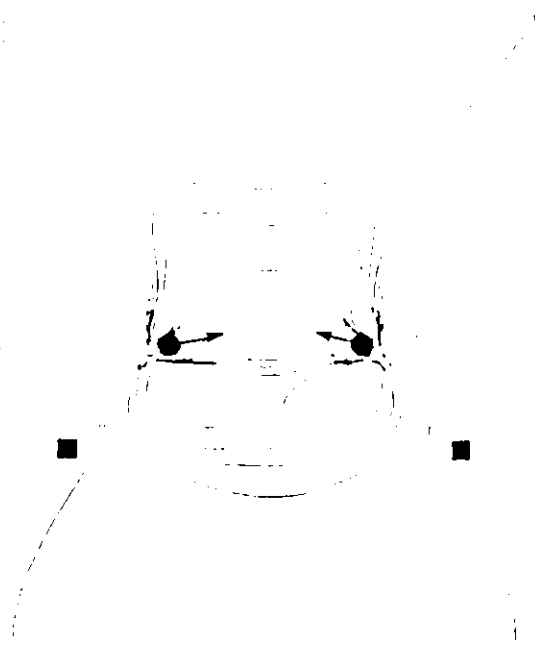


[2.2.2]



ρAS

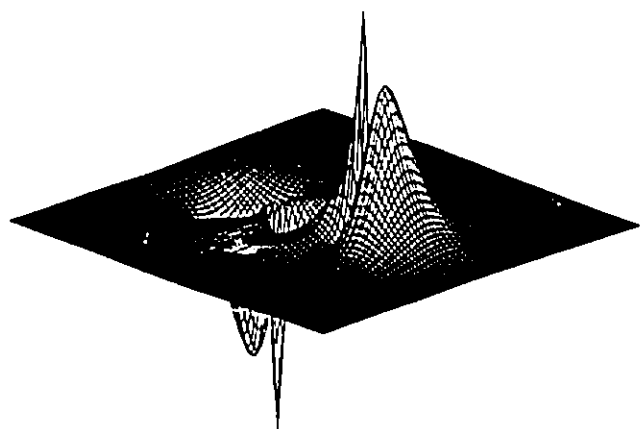
[1.1.0] BICYCLOBUTANE



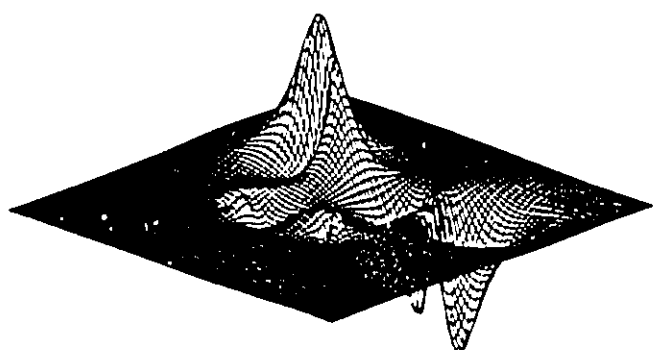
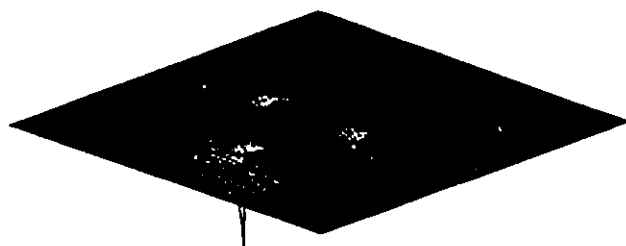
ρSS

Figure V.6

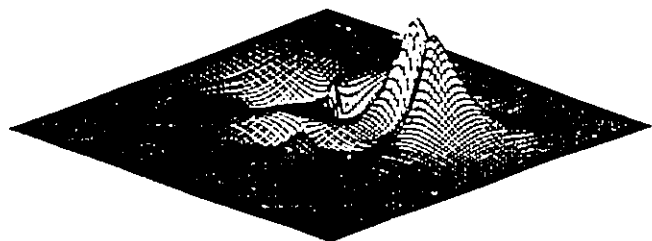
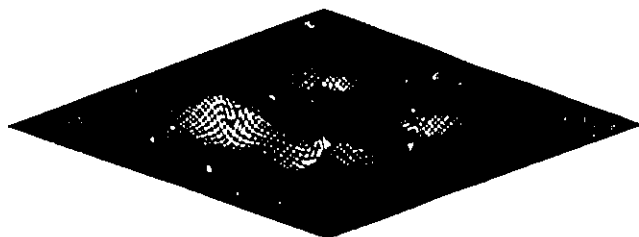
Relief maps of the lowest energy symmetric (rhs) and antisymmetric (lhs) transition densities for the propellanes. A plane of the three membered ring is shown [1.1.1]- and [2.2.1]propellane. For [2.1.1]- and [2.2.2]propellane a plane of the four membered ring is displayed. The antisymmetric density is the most intense for the bridgehead bond in each molecule.



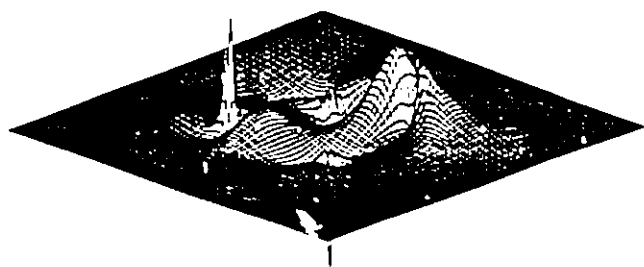
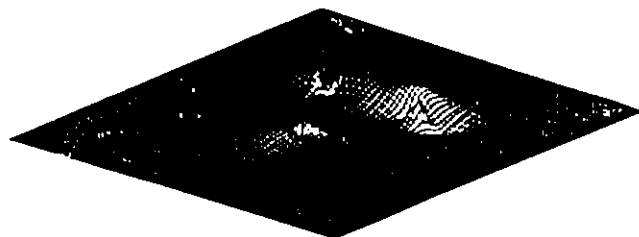
[1.1.1]



[2.1.1]

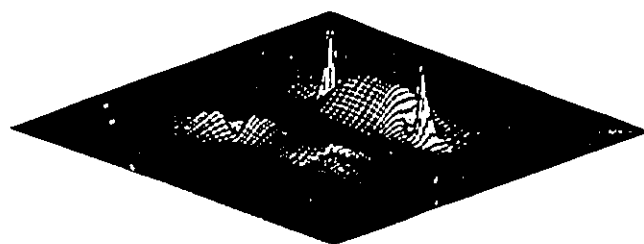


[2.2.1]



ρ_{AS}

[2.2.2]



ρ_{SS}

TABLE V.1

Atomic Dipoles and Forces

Molecule and atom Ω^a	$\vec{\mu}$ (Ω) au	\vec{F} (Ω) au
C in C ₂	-0.172	+0.931
N in N ₂	-0.590	+1.671
F in F ₂	-0.197	+0.520
N in N ₂	-0.623	+1.123
C _b in [1.1.1]propellane	-0.970	+0.435
C _b in [2.2.2]propellane	-0.279	+0.447

^aThe first three sets of results are calculated from functions close to the Hartree-Fock limit. (Cade, P.E.; Wahl, A.C. Atomic Data and Nuclear Data Tables, 1974, 13, 539.) The remaining are from 6-31G*/6-31G* functions, which while quantitatively less accurate than the near Hartree-Fock functions in their description of atomic moments, yield qualitatively similar results. A negative sign for $\vec{\mu}$ or \vec{F} denotes a vector directed away from its bonded partner.

References

- Bader, R.F.W. (1960) Mol. Phys. 3,137
- Bader, R.F.W. (1962) Can. J. Chem. 40,1164
- Bader, R.F.W. (1975) 'MTP International Review of Science. Physical Chemistry Ser. 2 vol 1 Theoretical Chemistry' ed A.D. Buckingham and C.A. Coulson London: Butterworths)
- Bader, R.F.W. (1980) J. Chem. Phys. 73,287
- Bader, R.F.W. (1986) Can. J. Chem. 64,1036
- Bader, R.F.W.; Beddall, P.M. (1972) J. Chem. Phys. 56,3320
- Bader, R.F.W.; Chang, C. (1989) J. Phys. Chem. 93,2946
- Bader, R.F.W.; Essen, H J. (1984) Chem. Phys. 80,1943
- Bader, R.F.W.; Henneker, W.H.; Cade, P.D. (1967) J. Chem. Phys. 46,3341
- Bader, R.F.W.; MacDougall, P.J. (1985) J. Am. Chem. Soc. 107,6788
- Bader, R.F.W.; MacDougall, P.J.; Lau, C.D.H. (1984) J. Am. Chem. Soc. 106,1594
- Bader, R.F.W, Nguyen-Dang, T.T. (1981a) Adv. Quantum Chem. 14,63
- Bader, R.F.W.; Nguyen-Dang, T.T.; Tal, Y. (1981b) Reports on Progress in Physics 44,893
- Bader, R.F.W.; Preston, H.J.T. (1970) Theor. Chim. Acta 17,384
- Bader, R.F.W.; Slee, T.S.; Cremer, D.; Kraka, E. (1983) J. Am. Chem. Soc. 105,5061
- Bader, R.F.W; Srebenik, S; Nguyen-Dang, T.T. (1978) J. Chem. Phys. 68,3680
- Bader, R.F.W and Stephens, M.E. (1975) J. Am. Chem. Soc. 97,7391
- Bader, R.F.W.; Tang, T.H.; Tal, Y.; Biegler-Konig, F.W. (1982) J. Am. Chem. Soc. 104,904
- Baghal-Vayjooee, M.H.; Benson, S.W. (1979) J. Am. Chem. Soc. 101,2838

- Barrett, C.S.; Meyer, L. (1967) Phys. Rev. **160**, 694
- Bartell, L.S. J. (1968) Chem. Educ. **45**, 754
- Biegler-König, F.W.; Bader, R.F.W.; Tang, T.H. (1982) J. Comput. Chem. **3**, 317
- Capon, B.; McManus, S.P. (1976) 'Neighboring Group Participation'; Plenum: New York
- Carroll, M.T. (1989) Ph. D. Thesis McMaster University
- Collard, K.; Hall, G.G. (1977) Int. J. Quantum Chem. **12**, 623
- Coulson, C.A. (1961) 'Valence', 2nd Ed.; Oxford University: Oxford p218
- Coulson, C.A.; Moffit, W.E. (1949) Philos. Mag. **40**, 1
- Dunitz, J. D.; Seiler, P. (1983) J. Am. Chem. Soc. **105**, 7056
- Eaton, P.E.; Temme, G.H., Jr. (1973) J. Am. Chem. Soc. **95**, 7508
- Finkelmeier, H.; Luttke, W. (1978) J. Am. Chem. Soc. **100**, 6261
- Fliszar, S. 1983 'Charge Distribution and Chemical Effects', Springer-Verlag: Berlin
- Franklin, J.L. (1949) Ind. Eng. Chem. **41**, 1070
- Gillespie, R.J. (1972) 'Molecular Geometry'; Van Nostrand-Reinhold: London
- Hariharan, P.C.; Pople, J.A. (1972) Chem. Phys. Lett. **16**, 217
- Hariharan, P.C.; Pople, J.A. (1973) Theor. Chim. Acta **28**, 213
- Hehre, W.J.; Stewart, R.F.; Pople, J.A. (1969) J. Chem. Phys. **51**, 2657
- Honegger, E.; Huber, H.; Heilbronner, E.; Dailey, W.P.; Wiberg, K.B. (1985) J. Am. Chem. Soc. **107**, 7172
- Ibrahim, M.R.; Schleyer, P. V. R. (1985) J. Comput. Chem. **6**, 157
- Jackson, J.E.; Allen, L.C. (1984) J. Am. Chem. Soc. **106**, 591
- Levi, D.A.; Blurock, E.S.; Hehre, W.J. (1979) J. Am. Chem. Soc. **101**, 5537
- Levy, C.G.; Lichter, R.L.; Nelson, G.L. (1980) 'Nuclear Magnetic Resonance Spectroscopy' 2nd ed.; Wiley-Interscience; N.Y.

- Lewis, G.N. (1916) J. Am. Chem. Soc. **38**,762
- March, J. (1985) 'Advanced Organic Chemistry' 3rd ed.; Wiley-Interscience, N.Y. p222
- Messiah, A; (1958) 'Quantum Mechanics' Wiley: New York, Vol. I
- Meyer, L. (1969) Adv. Chem. Phys. **16**,343
- Mills, R.L.; Schuch, A.F. (1969) Phys. Rev. Lett. **23**,1154
- Muller, N; Pritchard, D.E. (1959) J. Chem. Phys. **31**,1471
- Newton, M.D.; Schulman, J.M. (1972a) J. Am. Chem. Soc. **94**,773
- Newton, M.D.; Schulman, J.M. (1972b) J. Am. Chem. Soc. **94**,767
- Pearson, R.G. (1976) 'Symmetry Rules for Chemical reactions' Wiley, N.Y.
- Prosen, E.J.; Johnson, W.H.; Rossini, F.D. (1946) J. Res. Natl. Bur. Stand. (U.S.) **37**,51
- Raich, J.C.; Mills, R.L. (1971) J. Chem. Phys. **55**,1811
- Runtz, G.R.; Bader, R.F.W. and Messer, R.R. (1977) Can. J. Chem. **55**,3040
- Schiferl, D.; Cromer, D.T.; Schwalbe, L.A.; Mills, R.L. (1983) Acta Crystallogr. Sect. B: Struct. Crystallogr. Cryst. Chem. **B39**,153
- Schroedinger, E. (1927) Ann. Phys. (Leipzig) **82**,265
- Schuch, A.F.; Mills, R.L. (1970) J. Chem. Phys. **52**,6000
- Schulman, J.M.; Disch, R.L. (1985) Chem. Phys. Lett. **113**,291
- Schwinger, J (1951) Phys. Rev **82**,914
- Scoolery, J.N. (1959) J. Chem. Phys. **31**,1427.
- Smith, V.H.; Price, P.F.; Absar, I. (1977) Isr. J. Chem. **16**,187
- Sagar, R.P.; Ku, A.C.T.; Smith, V.H.; Simas, A.M. (1988) J. Chem. Phys. **88**, 4367
- Srebenik, S.; Bader, R.F.W.; Ngyen-Dang, T.T. (1978) J. Chem. Phys. **68**,3667

- Staral, J.A.; Yavari, I.; Roberts, J.D.; Prakash, G.K.S.; Donovan, D.J.; Olah, G.A. (1978) J. Am. Chem. Soc. 100,8016
- Thom, R. (1975) 'Structural Stability and Morphogenesis' (Engl. Ed.) Benjamin, Reading, Ma.
- Walsh, A.D. (1947) Nature(London) 159,712
- Walsh, A.D. (1949) Trans. Faraday Soc. 45,179
- Winstein, S. (1967) Spec. Publ. Chem. Soc. 21,5
- Wiberg, K.B. (1983) J. Am. Chem. Soc. 105,1227
- Wiberg, K.B. (1984) J. Comput. Chem. 5,197
- Wiberg, K.B. (1986) Angew. Chem. 98,312
- Wiberg, K.B.; Bonneville, G.; Dempsey, R. (1983) Isr. J. Chem. 23,85
- Wiberg, K.B.; Dailey, W.P.; Walker, F.H.; Waddell, S.T.; Crocker, L.S.; Newton, M.D. (1985) J. Am. Chem. Soc. 107,7247
- Wiberg, K.B.; Kass, S.R. (1985) J. Am. Chem. Soc. 107,988
- Wiberg, K.B.; Peters, K.S. (1977) Spectrochim. Acta. Part A 33A,261
- Wiberg, K.B.; Sturmer, D. (1975) Spectrochim. Acta. Part A 31A,57
- Wiberg, K.B.; Szeimies, G. (1970) J. Am. Chem. Soc. 92,571
- Wiberg, K.B.; Walker, F.H.; Pratt, W.E.; Michl, J. (1983) J. Am. Chem. Soc. 105,3638
- Wiberg, K.B.; Wendoloski, J.J. (1982) J. Am. Chem. Soc. 104,5679
- Wiberg, K.B.; Wendoloski, J.J. (1981) Proc. Natl. Acad. Sci. U.S.A. 78,6561
- Wong, J.S.; MacPhail, R.A.; Moore, C.B.; Strauss, H.L. (1982) J. Phys. Chem. 86,1478